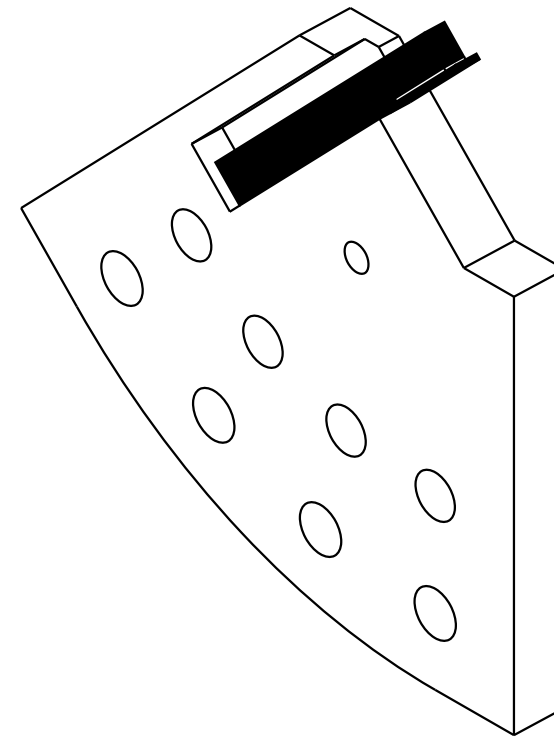


GERD SCHLOTTIG

Reliability at the Chip Interfaces: Delaminating the Silicon Die from Molding Compound



Reliability at the Chip Interfaces: Delaminating Silicon from Molding Compound GERD SCHLOTTIG

Technically this project on the delamination of Si-EMC became reality by the financial and personal efforts of Infineon Technologies AG Munich and Regensburg, Germany, as a collaboration with the Fraunhofer Institute of Reliability and Microintegration in Berlin, Germany, and Delft University of Technology, The Netherlands.

This book was printed by Gildeprint Drukerijen, Enschede, The Netherlands. Its text was typeset using L^AT_EX₂ ϵ and the Tufte-Latex book document class.

Reliability at the Chip Interfaces: Delaminating the Silicon Die from Molding Compound

Proefschrift

ter verkrijging van de graad van doctor
aan de Technische Universiteit Delft,
op gezag van de Rector Magnificus prof. ir. K.C.A.M. Luyben,
voorzitter van het College voor Promoties,
in het openbaar te verdedigen op vrijdag, 30. november 2012 om 10:00 uur
door

Gerd S C H L O T T I G

Diplomingenieur der Elektrotechnik van de Technische Universität Dresden, Duitsland,
geboren te Zschopau, Duitsland.

Dit proefschrift is goedgekeurd door de promotor:

Prof. Dr. Ir. L. J. Ernst

Copromotor: Dr. Ir. K. M. B. Jansen, Technische Universiteit Delft

Samenstelling promotiecommissie:

Rector Magnificus	Voorzitter
Prof. Dr. Ir. L. J. Ernst	Technische Universiteit Delft, promotor
Dr. Ir. K. M. B. Jansen	Technische Universiteit Delft, copromotor
Prof. Dr. Ir. G. Q. Zhang	Technische Universiteit Delft
Prof. Dr. A. Dasgupta	University of Maryland
Prof. Dr. Ing. B. Wunderle	Technische Universiteit Chemnitz
Prof. Dr. D. G. Yang	Guilin University of Electronic Technology
Dipl. Phys. H. Pape	Infineon Technologies AG
Prof. Dr. Ir. F. van Keulen	Technische Universiteit Delft, reservelid

Copyright © 2012 Gerd Schlottig

Some rights reserved. All or part of this book may be reproduced or transmitted in any form or by any means, electronic or mechanical, including photocopying, or by any information storage or retrieval system, without permission in writing from the author, only if proper reference to the original work is made.

ISBN: 978-94-6186-072-9

DOI: 10.4233/uuid:926bb24d-973f-4f1b-93da-4e6cde8fbbda

Summary

This book describes a setup that allows to delaminate the Silicon-to-Molding Compound interface for obtaining interfacial fracture parameters: the Mixed Mode Chisel setup (MMC). With this device for the first time the delamination can be initiated and propagated, while preventing the occurrence of random brittle fracture in one or both of the adjacent materials. This is relevant because of the fact that material interface delamination in electronic components forms a major failure problem. The technology trend to densify components results into more and more interfaces with accompanying growing complexity where thermo-mechanical interactions play a crucial role. Rapidly being able to establish the interfacial properties is crucial for the quantitative design process.

The present work answers questions on how to delaminate Silicon-to-Molding Compound interfaces, how an adequate specimen can be shaped and fabricated, how random fracture can be overcome, what facts are influencing the delamination most, what impact the residual stresses and the viscoelasticity of EMC have, and how the fracture strength compares to that of other interfaces. It describes the setup details, the design choices, the relevant conditions for manufacturing and processing, the choices being made for compression molding and transfer molding and the formation of a starter crack. The delamination experimental procedure and the necessary steps to determine the interface properties are described in detail, including crack length measurements. The results obtained, including the reliability, are discussed. It also describes decisive aspects of interpreting, comparing and applying fracture mechanical results as well as their display. The MMC can be used at elevated temperature and moisture conditions and can be clamped to different loading devices. The Critical Energy Release Rate G_c was found ranging between 50 and 200 J/m² for a Mode Mix range of 15° at room temperature. The practical Mode Mix values depend on a chosen reference length and a measure of the material mismatch as given in the text. The deviation from a polynomial fit of 2nd order reaches a maximum of 20%. In the concluding chapter a multi-specimen approach for future delamination measurements and

further research on mode mix and reference length choices are being advised.

Samenvatting

Dit boek beschrijft een opstelling waarmee "Silicon-to-Molding Compound interfaces" gedelamineerd kunnen worden om de "interface fracture parameters" te bepalen: de "Mixed Mode Chisel" opstelling (MMC). Met deze opstelling kan voor het eerst de delaminatie worden geïnitieerd en voortgezet, zonder dat willekeurige brose breuk zich voordoet in één of in beide van de aansluitende materialen. Dit is relevant omdat de delaminatie van materiaal interfaces in elektronische componenten een belangrijk faalprobleem vormt. De technologische trend naar steeds compactere componenten resulteert in steeds meer interfaces en daarmee gepaard gaande een toenemende complexiteit waarbij thermo-mechanische wisselwerkingen een cruciale rol spelen. Het snel in staat zijn om de interface eigenschappen vast te stellen is van cruciaal belang voor het kwantitatieve ontwerpproces.

Het voorliggende werk beantwoordt hoe "Silicon-to-Molding Compound interfaces" te delamineren, hoe een geschikt proefstuk kan worden vormgegeven en vervaardigd, hoe willekeurige brose breuk voorkomen kan worden, welke factoren de delaminatie het meest beïnvloeden, welke impact de restspanningen en de visco-elasticiteit van EMC hebben, en hoe de breuksterkte zich verhoudt tot die van andere interfaces. Het beschrijft de setup details, de ontwerpkeuzes, de relevante voorwaarden voor productie en verwerking, de keuzes die werden gemaakt voor "compression molding" en "transfer molding" en de formatie van een begin scheurtje. De experimentele delaminatie procedure evenals de benodigde stappen om de interface eigenschappen te bepalen (o.a. scheurlengte metingen) worden in detail beschreven. De resultaten, inclusief de betrouwbaarheid, worden besproken. Het beschrijft ook de doorslaggevende aspecten van het interpreteren, vergelijken en het toepassen van breukmechanische resultaten en hun weergave. De MMC kan bij hoge temperatuur en vochtigheidsgraad gebruikt worden, en kan in diverse trek/druk banken bevestigd worden. De "Critical Energy Release Rate" werd gevonden tussen 50 en 200 J/m², met een "Mode Mix" range van 15° en bij kamertemperatuur. De praktische "Mode Mix"-waarden zijn afhankelijk van een gekozen referentie lengte en een maat voor de "material mismatch"

zoals aangegeven in de tekst. De afwijking van een tweede orde polynoom fit is maximaal 20%. In het afsluitende hoofdstuk wordt een "multi-specimen approach" voor toekomstige delaminatie metingen en verder onderzoek betreffend de "Mode Mix"- en referentie lengte keuzes geadviseerd.

Contents

	<i>Summary</i>	5
1	<i>Fracture at the Interfaces in Electronic Packaging</i>	11
2	<i>Describing Interfacial Fracture — What was Done Before, and Beside</i>	15
	2.1 <i>The Energy Needed to Create New Surface</i>	17
	2.2 <i>The Fracture Mode Mix — Uniqueness for Prediction</i>	19
	2.3 <i>More Than Two Parameters for the Interface</i>	20
	2.4 <i>A Choice of Reference Length</i>	26
	2.5 <i>Numerical Methods for the Fracture Mechanics Analysis</i>	26
	2.6 <i>Delamination of Si-EMC</i>	30
	2.7 <i>Why Si-EMC is difficult to delaminate — Reasons for a New Test</i>	31
3	<i>A Successful Test</i>	33
	3.1 <i>Demands on a Miniaturized Delamination Test</i>	33
	3.2 <i>The Mixed Mode Chisel Setup</i>	39
	3.3 <i>Details of the MMC</i>	42
4	<i>Fabricating Delamination Specimens</i>	45
	4.1 <i>Demands on a Specimen for the MMC</i>	45
	4.2 <i>Two Molding Technologies: The Fabrication Steps</i>	48
	4.3 <i>Assemblies</i>	52

4.4	<i>Materials Involved</i>	53
4.5	<i>Pre-Cracks</i>	54
4.6	<i>Flank Exposure</i>	58
4.7	<i>Design Rules</i>	59
5	<i>From Specimens to Interface Properties</i>	65
5.1	<i>The Delamination Experiment</i>	65
5.2	<i>Model and Simulation</i>	67
5.3	<i>Finding the Crack Tip</i>	70
5.4	<i>Material Properties of the EMCs</i>	75
5.5	<i>Residual Stresses</i>	79
5.6	<i>Fracture Mechanics Results</i>	80
6	<i>Discussion — Relevant Detail to Interpret the Results</i>	89
6.1	<i>Crucial Aspects of the Fracture Mechanics Details</i>	89
6.2	<i>The Largest Impacts and the Uncertainties</i>	93
6.3	<i>Comparing Interface and Bulk Fracture</i>	97
6.4	<i>Limits of the MMC</i>	98
6.5	<i>Data Visualization — A Display of Energy Release Rate</i>	99
7	<i>Conclusions and Recommendations</i>	103
	<i>Acknowledgements</i>	109
	<i>Bibliography</i>	133
	<i>Index</i>	136

Fracture at the Interfaces in Electronic Packaging

Fracture is one of the major obstacles for the functioning of many devices. Materials or their interfaces may break all of a sudden, or after long exposure to adverse conditions, after a static load, or after an oscillating and swelling load. For developing devices engineers are keen to know the materials' limits of fracture since long. At least as early as in the 15th century spawned the interest in why things break, and how that could be avoided. Leonardo da Vinci had described already how moisture induced expansion and contraction causes cracks long before a field of fracture mechanics evolved. The material limits allow to compare materials and to calculate whether one or the other device design is prone to fail under a certain load. Knowing such limits is thus crucial, yet obtaining them can be complex and can demand a multitude of activities. This is especially the case for the limits of material interfaces.

In electronic devices the delamination of interfaces was and is a major fracture problem. The technology trend to densify devices increases the interface number and the complexity of thermo-mechanical interactions in the devices. Therewith increases the need of rapidly knowing interfacial properties. Researchers attribute interface failure to various reasons ranging from steam pressure of uptaken moisture to the mere thermal expansion mismatch of the materials involved. For quantitative design estimates and predictions the interfacial fracture properties tell the crucial limits. To obtain these some standards have been established, such as for the leadframe-to-Epoxy Molding Compound (EMC) interface, for others there is no method successfully tested yet.

Electronic packages include interfaces that realize a certain device function such as electrical and thermal conduction or insulation. Others are specifically designed and chosen for their thermo-mechanical integrity, such as underfills or encapsulation materials as the EMC. Often the interfaces fulfill several purposes. Due to its role and consistence Si-to-EMC is generally regarded as a tough interface, that is

to speak a delamination of the Si-to-EMC demands a high amount of energy. While it fails in some cases, it is thus tricky to intentionally delaminate and therewith test such interfaces. Therefore questions remain about how to delaminate this interface, how a specimen should look like, what influences its delamination most, which influence do residual stresses have, what does the viscoelastic behavior of EMC entail for the delamination, and how does the fracture toughness compare to other interfaces.

This work describes the means to obtain the interfacial properties of the Si-to-EMC interface when using fracture mechanics. It starts out with a fracture mechanics background needed for the calculations, and an overview of previous and parallel studies concluding with the open questions and difficulties of the Si-to-EMC delamination. It then introduces a new delamination test setup, the mixed mode chisel setup (MMC), on pages 33ff and explains its details and design choices. Pages 45ff describe the specimen design, fabrication and processing choices made, as well as some crucial steps and failures to consider when testing a representative interface sample. Pages 65ff detail how a delamination experiment is done, and which steps are necessary to obtain the interfacial properties. The chapter concludes with the obtained results and their accuracy. A last chapter deepens the aspects of interpreting the fracture mechanical results pages 89ff. It includes the influencing measures, the display and comparison of the critical data, the limits of the setup, it names some open questions on the interpretation of any interfacial fracture data, and it looks out on the data application.

Finally, the readers who skip this structure and those who lack the time to read entire chapters may find an index of keywords available at the end of the book.

Describing Interfacial Fracture, What was Done Before, and Beside

Describing interfacial fracture is desired for different reasons. In electronic packaging such matters can be, for instance given two material combinations, which one would fail earlier under a certain load? Or given several different designs using the same material combination, which design offers the lowest risk of damage? Or given a design and material combination, when would it fail? To evaluate these questions I need to model the case to such an extent that I can judge whether failure occurs. In other words, for estimating the reliability of an interface we need a measure of the according critical state, a *criterion of failure*, a criterion that shows us whether the interface fails under the given conditions, whether it de-bonds. The central question is then, how to model it, how to build this criterion?

A criterion of fracture failure can be and has been established in different ways. The earliest were stress based hypotheses applied on the fracture of homogeneous bodies since the late 18th century. But, the stress based criteria failed to predict “rupture” by a factor of two or three in some cases, upon facing problems with materials that contained flaws already. Enough motivation to develop a different criterion for Griffith¹ who did this based on the critical amount of energy needed to create new surface during rupture, and who introduced the concept of critical crack length for ductile materials. (see *page 17*) Various approaches on a fracture mechanical basis followed this early work from the 1950s onwards². Yet flaws are often distributed over an object and before the object fails damage occurs not only in one spot, but progresses in a damage zone or in several zones. This nonlinear behavior in fracture process zones was addressed by cohesive zone modeling³. For fracture process zones that cannot be defined precisely the methods of Continuum Damage Mechanics (CDM) represent an adequate tool.⁴ For purely practical investigations on locations where a crack is most probable to start, very recently the area release

¹ Griffith 1920

² Broek 1982, Anderson 1995, Saxena 1998, Gross and Seelig 2006b

³ Dugdale 1960, Needleman 1987

⁴ For detailed information on such phenomena the reader may study with Ravi-Chandar 2008, Liechti 2008, Sluis et al. 2009b

energy method⁵ was developed. Rather than a quantitative fracture description it allows a sensitivity analysis.

Since the object size (including test specimens) in electronic packaging is continuously decreasing, the above methods become increasingly difficult. Molecular Dynamics (MD) could possibly provide better understanding and prediction of materials and interface properties⁶, looking into the very details of adhesion mechanisms. And finally multi-scale and meso-scale approaches⁷, such as a combination of MD based cohesive zone modeling⁸ or the implementation of scaling effects⁹ try to bridge the gap between the different length scales involved in fracture modeling. Which approach to take?

Cohesive zone (CZ) methods have been extensively used for homogeneous body fracture of well described materials such as silicon¹⁰. But although many studies report its use for delamination problems¹¹, and although CZ methods offer the advantage that no local crack spot has to be assumed in the model, the results have limited fracture mode details, described on *page 20*, and the CZ methods need substantial computation time. The latter argument holds even stronger for molecular dynamics, where computation time increases to unrealistic levels when length scales of roughness are modeled¹². Though assuming a certain crack spot in a model of an electronic package might have its disadvantages, interfacial fracture however initiates in flaws created by the imperfections of processing, be it a mechanical damage, an impurity or absorbed humidity evaporating. Instead of depending on spontaneous crack initiation a predefined crack eases reproducibly inducing delaminations. Thus this thesis concentrates on a fracture mechanical description for a criterion of failure. And the descriptions are restricted to linear elastic fracture mechanics (LEFM), since during the studies on the Si-EMC fracture no inelastic deformations prior to fracture were observed, and the delaminations could be regarded as brittle.

In LEFM a criterion is built on the assumption that for crack growth to occur, a critical load level has to be reached independently from time and inelastic phenomena. Loads below such critical levels would not lead to fracture. In fracture reality the critical load often depends on aspects involving such phenomena. This problem opened own areas of research, such as dynamic and creep fracture mechanics.¹³ Fracture might also appear at load levels that are lower than the ones deemed necessary for a critical stress state, because not all influences on the stress state have been considered. Such influences can be for instance residual stresses, thermo-mechanical cycling loads or the presence of moisture. This happens also if the materials involved show nearly linear elastic behavior.¹⁴ To consider all mechanisms in the analysis is difficult, and some researchers termed such fracture charac-

5 Sluis et al. 2007

6 Ercolessi 1997

7 Sih 2001, Sih and Liu 2001, Auersperg et al. 2008

8 Zhou et al. 2009

9 Sih 2006

10 Mariani et al. 2010

11 Needleman 1990, Ortiz and Pandolfi 1999, Mohammed and Liechti 2000, Chandra 2002, Jin and Sun 2005, Alfano 2006, Jin and Sun 2006, Sun and Jin 2006, Ma et al. 2010

12 Roughness is a major contributor to one of the basic adhesion phenomena, the mechanical interlocking. It affects the sliding in mode II and III fracture components. See Dillard and Pocius 2002

13 Gross and Seelig 2006a

14 Irwin et al. 1967, Ritter et al. 1997

teristics *sub-critical* fracture¹⁵, which contradicts the very definition of the criterion and downplays the importance of residual stresses.

Different approaches have been used to systemize the activities in the field of fracture mechanics. One of them is shown in the margin. However such efforts to classify are taking place after the very activities happened, and such activities always responded to material behavior. Directions of Viscoelastic or Viscoplastic fracture are opened because of a specific material behavior, the fracture mechanics approaches are non-linear.

For a linear elastic fracture mechanics approach the failure model needs a concentrated description of the critical stress state, and this means at least two measures: one for the threshold level leading to fracture, and one for the stress field orientation. Once dealing with interfaces the stress field orientation includes a third measure, an expression of the material property mismatch at the interface. These are parameters that must be identified by practical experience, that is by experiment. Both the failure model and the experiment analysis need numerical simulation. Thus, to introduce the experiment analysis, the following pages show the theoretical background of the parameters and the according numerical methods.

The theory description starts with the energy needed to create new surfaces (see below), continues with the fracture mode mix (page 19), the parameters for interfacial fracture (p. 20), the numerical methods for the fracture mechanics analysis (p. 26), the delamination of the Si-EMC interface (p. 30) and why its delamination is difficult (p. 31).

2.1 The Energy Needed to Create New Surface

To find a clear criterion of failure by fracture, we need to describe two aspects: Which quantity of energy or stress is necessary, and what can describe the uniqueness of the stress situation for failure prediction, for example an orientation angle? This section describes the quantity part. For the orientation problem see the next section on page 19.

Griffith¹⁶ suggested a criterion based on the energy equilibrium in the moment of fracture onset. He assumed the fracture to be hypothetically reversible. In reality fracture is non-reversible, yet assuming it does not alter the fracture criterion. The equilibrium then states that the energy added to an object in order to fracture an infinitesimally small area dA equals the energy that is required to create this area, with Griffith's assumptions the surface energy. The required energy to create new surface by fracture put in relation to the very surface area can be expressed as *energy release rate* G . Once an object receives

15 Singh et al. 2008

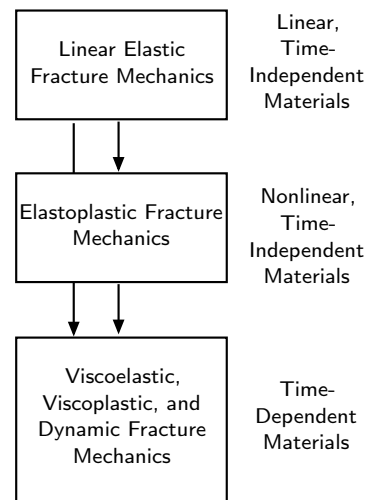


Figure 2.1: Fracture mechanics description approaches, adapted from Anderson 1995

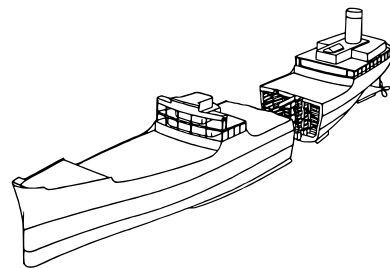


Figure 2.2: Schematic of fracture location in numerous tankers before 1945. A series of large scale fracture incidents during the 1940s led to a rethinking of failure criteria, especially considering the testing costs. Schematic adapted from United States 1947

16 Griffith 1920

a threshold energy per area it fractures. The criterion for expressing whether the object fractures is then G related to the *critical* G_c as

$$G \geq G_c. \quad (2.1)$$

Assuming linear elastic material behavior, and looking at crack initiation only, the related equilibrium can be expressed as

$$\underbrace{d\Pi}_{\text{external work}} = \underbrace{dE_{\text{el}}}_{\text{change in elastic strain energy}} + \underbrace{G \cdot dA}_{\text{released energy through crack growth}} \quad (2.2)$$

or in Griffith's words

... the net reduction in potential energy is equal to the strain energy, and hence the total decrease in potential energy due to the formation of a crack is equal to the increase in strain energy less the increase in surface energy...

Extending the equation to crack propagation and allowing for plastic deformations it can be written as

$$\underbrace{d\Pi}_{\text{external work}} = \underbrace{dE_{\text{el}}}_{\text{elastic strain energy}} + \underbrace{dE_{\text{k}}}_{\text{kinetic energy}} + \underbrace{dE_{\text{p}}}_{\text{plastic deformation energy}} + \underbrace{G \cdot dA}_{\text{released energy through crack growth}} \quad (2.3)$$

But the above extension of the equation was not made at that time, and therefore some of Griffith's basic assumptions, the absence of plasticity and the use of fixed grips in experimentation prevented a broader use of the energy equilibrium concept. After problems with a series of large scale fracture incidents the argument was put into a more "readily useful" form by Irwin who proposed the use of the *force tendency*, and a year later the *stress intensity factor* K ¹⁷

The K concept has been preferred in most applications of fracture mechanics due to its simpler applicability and its transferability of the singular stress field to nonlinear fracture mechanics (LEFM not yet mentioned!). But when it comes to interface fracture mechanics, there are no readily tabulated K_c values available and the comparison of different interfaces is not a straight forward one-parameter approach as in homogeneous bodies. It will be discussed from *page 20* onwards. The stress intensity factor K remains nonetheless a crucial description and is outlined here in brevity for 2-dimensional scenarios.

The stress situation at the geometric singularity of a crack tip, according to the sketch in the margin, can be written in terms of stress intensity factors as¹⁸

$$\sigma_y = \frac{K_I}{\sqrt{2\pi r}}, \quad \sigma_{xy} = \frac{K_{II}}{\sqrt{2\pi r}}, \quad (2.4)$$

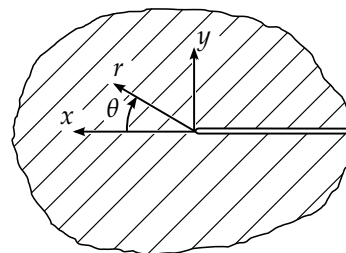


Figure 2.3: Coordinate system at the crack tip in a homogeneous body.

¹⁷ Irwin 1956, 1957, who also suggested a second parameter to describe the critical state of cracking in a 2-dimensional analysis consistently. For the first time the failure criterion was defined by two measures: a quantitative measure, which is an expression of energy or stress intensity, and a representation of the condition's uniqueness, which is a measure of stress field orientation. This concept is detailed in the next section.

¹⁸ Irwin 1968

where the singularity has an inverse \sqrt{r} character and in the critical case of fracture $K \geq K_c$ the values $K_{Ic,IIc}$ represent material properties, namely the *fracture toughness* under the certain load situations I and II. Note that the description involves two coordinate notations in one equation, which allow for expressing tensile and shear stresses and at the same time a certain distance from the singularity pole in any direction.¹⁹ For linear elastic properties K_c can be directly related to G_c through the proportionality of the material's elastic properties, just as Irwin wrote 1957

... the parameter, called the stress intensity factor, is proportional to the square root of the force tending to cause crack extension...

$$G_c = \frac{K_{Ic}^2 + K_{IIc}^2}{E} \text{ for plane stress assumptions, and} \quad (2.5)$$

$$G_c = (1 - \nu^2) \frac{K_{Ic}^2 + K_{IIc}^2}{E} \text{ for plane strain assumptions,} \quad (2.6)$$

where E is the elasticity modulus and ν the Poisson's ratio. The indexes I and II describe the load situation in terms of fracture modes.

The fracture modes are explained below, and the results of Energy Release Rates on page 80. For Interpretation Details on the energy release rates see page 89, and for Data Visualization of energy release rates see page 99.

2.2 The Fracture Mode Mix — Uniqueness for Prediction

To find a clear criterion of failure by fracture, we need to describe two aspects: Which quantity of energy or stress is necessary, and which orientation gives it uniqueness for prediction? This section describes the orientation part. For the quantity problem see page 17

The concept of stress field orientation in the crack tip vicinity is presently known as *fracture modes* and their combination or mix. As shown in the margin these modes are *three* for *one* crack propagation direction under a *three-axes* load situation in *three* spatial dimensions, orthogonal to each other. They describe the different local load orientations in crack tip vicinity relative to the crack propagation face. Why is this important?

The fracture toughness described above is different for different mixes of fracture modes. In other words a different amount of energy is needed to open a crack in a pure tensile mode than in a mix of mode I and II. Furthermore cracks tend to deflect into a mode I orientation even if a mode II or III dominates the remote loading. Thence large parts of fracture mechanical studies report on homogeneous body fracture under mode I loads or normalized to mode I loads²⁰.

Nonetheless a remote mixed loading of a pre-cracked body leads to a mixed stress state at the crack tip, which can be expressed in terms

19 for a detailed description see Hutchinson and Suo 1992

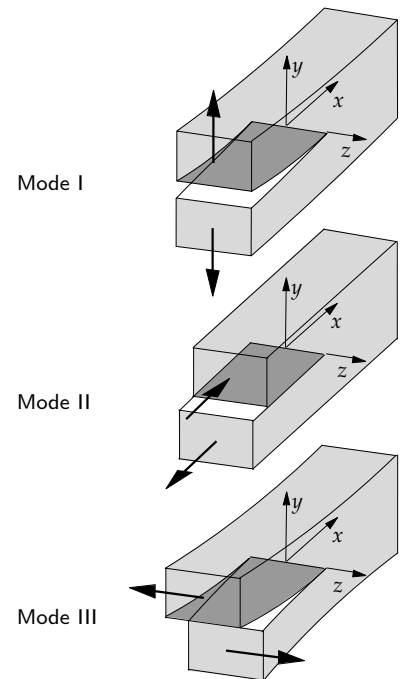


Figure 2.4: Modes of fracture are three, here shown for bulk cracks.

of stress intensity factors. According to equation 2.4 the stress based *mode mix* ψ represents also the relation of the stress intensity factors for homogeneous body fracture, independently from r

$$\tan \psi = \frac{\sigma_{xy}}{\sigma_{yy}} = \frac{K_{II}}{K_I}, \quad (2.7)$$

and thus the angle ψ is the phase of the local stress vector as well as of the remote load vector. This is different at an interface of two materials.

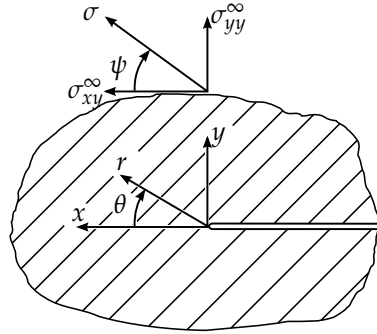


Figure 2.5: Remote loading of a crack in a homogeneous body.

2.3 More Than Two Parameters for the Interface

In order to describe fracture at the interface between two joint materials, the crack's onset and propagation is assumed at that very interface, provided it is weak enough compared to each of the materials – a somewhat *forced* propagation direction unchanged by mixed mode loading. This fact together with the joint of dissimilar material properties complicate the fracture mechanics description of the interface.

Any material interface that is able to transfer loads creates by its very nature one boundary condition in continuum theory: Each point at the interface is shared by two materials and displaces this shared point as one. That is the displacements u_x and u_y across the interface are continuous, they are not suddenly changing when we virtually walk across the material boundary. Additionally the stresses normal to the interface plane σ_{yy} and the shear stresses σ_{xy} are to be continuous across the interface as well, although the materials joining have different elastic properties and strains are bound to stresses by these elastic properties. In addition to a geometric singularity of the crack tip, the interface poses thus a discontinuity, that of material mismatch. Which effects does this have on the fracture description?

The first to describe fracture at such an interface was Williams, who found in 1959 that assuming linear elasticity the stresses

... possess a sharp oscillatory character of the type $r^{-\frac{1}{2}} \sin(b \log r)$, which seems to be confined quite close to the point, as well as a shear stress along the material joint line as long as the materials are different... 21

21 Williams 1959

In other words stresses show a similar singularity in the crack tip vicinity as for homogeneous materials but oscillate with distance from the crack tip, and the stress field orientation is affected by the material property difference alone already. His finding, since it predicted inter-penetrating crack flanks once debonding occurs, provoked various approaches to describe the critical condition (with respect to geometry and loads). Those without further simplifications have *two more aspects* in common, which enter the calculation of K_c and ψ : a dimensionless constant describing the material property mismatch and some definition of a characteristic length scale.

The oscillation was defined by the elastic mismatch of the two materials, and Dundurs²² found that in a 2-dimensional description of a bimaterial body under plane deformation two combinations of the elastic constants describe the stress-dependency on material properties and thus the mismatch sufficiently. Dundurs parameters were an appreciated simplification and are frequently used as α and β with

22 Dundurs 1969

$$\alpha = \frac{\bar{E}_1 - \bar{E}_2}{\bar{E}_1 + \bar{E}_2}, \text{ and } \beta = \frac{\mu_1(\vartheta_2 - 1) - \mu_2(\vartheta_1 - 1)}{\mu_1(\vartheta_2 + 1) + \mu_2(\vartheta_1 + 1)}, \quad (2.8)$$

where $\mu = \frac{E}{2+2\nu}$ is the shear modulus and ϑ and \bar{E} are formed depending on the stress model as follows:

plane strain,	plane stress	
$\vartheta = (3 - 4\nu)$	$\vartheta = \frac{3 - \nu}{1 + \nu}$	(2.9)
$\bar{E} = \frac{E}{1 - \nu^2}$	$\bar{E} = E$	(2.10)

The Dundurs parameters are different in that α expresses the mismatch in the tensile elastic moduli, and to the contrary β expresses the mismatch in compression moduli. Thus α reaches +1 in the case that material 1 is highly elastic compared to material 2, and it vanishes once the moduli are equal. The parameter β becomes 0 when both materials are incompressible. Both α and β become 0 when the materials are equal in all the concerned properties, and they change sign in case the materials are exchanged. One of the parameters commonly serves to describe the oscillation character of the stress and displacement field at the interface using an *oscillatory index* $\epsilon = \epsilon(\beta)$, such that

$$\epsilon = \frac{1}{2\pi} \ln \frac{1 - \beta}{1 + \beta}. \quad (2.11)$$

The oscillatory singularity introduced by Williams is in terms of ϵ

$$r^{i\epsilon} = \cos(\epsilon \ln r) + i \sin(\epsilon \ln r). \quad (2.12)$$

For the second aspect entering the fracture mechanical description, the length scale, it is necessary to take a look at the stress intensity factor, which can be expressed accordingly by

$$(\sigma_{yy} + i\sigma_{xy})_{\theta=0} = \frac{Kr^{i\epsilon}}{\sqrt{2\pi r}}, \quad (2.13)$$

transforming K into a complex²³ measure of interfacial fracture toughness, the complex stress intensity factor $K = k_1 + ik_2$, with its amplitude $|K|$ and a phase angle ϕ . The “forced” crack propagation direction along the interface is expressed by $\theta = 0$.

23 Hutchinson et al. 1987

The stress based mode mix defined earlier for homogeneous body fracture in equation 2.7 now takes the form of

$$\frac{\sigma_{xy}}{\sigma_{yy}} = \tan \psi = \frac{\Im(Kr^{i\epsilon})}{\Re(Kr^{i\epsilon})} \quad (2.14)$$

and does not express the pure relation between the K components anymore. In fact with the phase angle definition above it takes the form of

$$\tan \psi = \phi + \epsilon \ln r \quad (2.15)$$

and thus depends on the distance r from the crack tip. The mode mix ψ therefore represents a local stress orientation *including* a reference to a length measure, in the general formulation of equation 2.15 it refers to a certain distance from the crack tip. For describing a critical stress situation it is now necessary to also give a length measure, a measure that has to be defined however. The two aspects, material mismatch and characteristic length scale have some profound implications for the fracture toughness $K_c(\psi(\epsilon, r))$.

A Different Load Mix for a Different Geometry or Interface For a comparable critical stress state around the crack tip in two bodies of different material pairings $\epsilon_{1,2}$, the $K_{1,2}$ of both situations should be equal when assuming the same characteristic length. But the implication is that a different load angle is required. To achieve a comparable stress field in two different material combinations ϵ_1 and ϵ_2 For instance loading a material combination ϵ_1 in pure tension requires to load a material combination ϵ_2 by a combination of tension and shear. It also means that the separate components of tension and shear cannot be defined unambiguously at the interface. They are inherently bound to each other. Although ψ keeps the mathematical character of an angle, it loses the physical quality of an angle. The

term *mode angle* shall thus be avoided in this work. Likewise the modes cannot be defined unambiguously for the energy release rate components. Yet for an interpretation of the local load situation, the mode mix remains the crucial, the important measure sparked by the oscillatory singularity, and therefore it is crucial how to define the mode mix.

In the seeking of LEFM to concentrate a critical state in a set of parameters, these have to fully account for influences on the crack tip field, and that is from both loads *and* geometry. In the application the same mode mix should represent the same local stress field. If the same field requires a different load angle however, the load angle cannot serve as mode mix.

Asymmetry of the Stress State The different character of an interfacial ψ can be explained in terms of symmetry. In homogeneous bodies the stress field around a crack tip singularity is symmetric to the crack plane under tensile load, and skew-symmetric under shear or mixed loading, as long as the loaded geometry is symmetric. When the geometry is asymmetric the stress field orientation tilts, but lines of constant stress are continuous. In its consequence one angle is sufficient to describe the load *and* the mode orientation.

At the interface this symmetry vanishes due to the different properties of the materials joining. In order to uniquely describe the stress field for comparisons more information must be expressed in the fracture mechanical parameters, such as $K_c(\psi(\epsilon, r))$. The symmetry difference is shown in the plot to the right.

Temperature and the Stress State Since the coupling of modes and the asymmetry are expressed in the elastic mismatch ϵ , the effects are subject to temperature changes or other conditions that change the properties of one material more than the other, such as for the Si-EMC interface. For instance when changing from the glassy to the rubbery state of the EMC the elasticity modulus drops and α increases. Considering the Poisson effect, also β and ϵ change, but quite sensitively to the Poisson value. For instance assuming a change of the Poisson ratio ν_{EMC} from 0.27 to 0.37 changes the mismatch ϵ_{Si-EMC} from 0.073 to 0.064, but if ν_{EMC} changes to 0.44 the mismatch ϵ_{Si-EMC} reaches 0.032, which in turn changes the mode mix ψ accordingly. Additionally the stress state can be subject to changes before fracture. A temperature change creates a state of residual stresses because the material properties change differently in the two concerned materials.

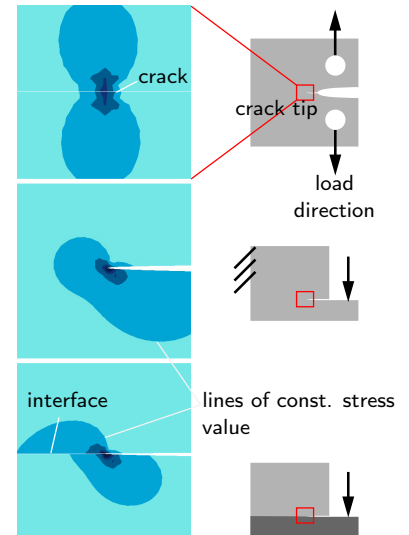


Figure 2.6: Plots of v.Mises equivalent stresses in the crack tip vicinity for tensile bulk fracture with symmetric geometry, tensile bulk fracture with asymmetric geometry, tensile interface fracture with asymmetric geometry (top down).

Coupled Shear and Tension and Unit Changes Another expression that tension and shear components are inherently coupled near the interface crack tip is the unit dependency of complex K and the mode mix defined on its basis. That means the choice of length unit changes the calculated mode mix²⁴. When describing a certain critical state, say of a pure tensile character, by using the length unit of 1 mm, it will have a mixed mode character once expressing the length in terms of 1000 μm . That also indicates that the mode mix remains a measure of stress field orientation at the cost of an intuitive load case angle. As shall be seen in the following paragraph the problem of units can be solved elegantly. The mode mix components are however inherently coupled.

24 Rice 1988

Referring to a Length, a Reference Length As Beuth²⁵ explained the oscillatory conditions in the crack tip vicinity

25 Beuth 1996

... are an artifact of the interfacial fracture model and may have little or no significance related to the physical fracture process. When they occur, however, a direct match of mode mix between ... application and ... tests cannot readily be made. Methods are needed for extracting a mode mix from composite delamination models ...

Such methods have been used out of different ideas, such as

- Assuming a resin rich layer at the interface and letting the crack advance cohesively in this layer,²⁶
- Rejecting the oscillation solution and using a contact model,²⁷
- Recognizing that oscillations are confined to a very close region at the crack tip, and then establishing ψ outside of that region,²⁸
- Minimizing the material mismatch to $\epsilon = 0$ by altering physical properties that do not influence the fracture physics dominantly,²⁹
- Using asymptotic near-tip stress and displacement relations, to define ERR quantities that are separated from oscillatory effects.³⁰

26 Atkinson 1977

27 Comninou 1977, Atkinson 1982, Dundurs and Gautesen 1988

28 Rice 1988

29 He and Hutchinson 1989, Suo and Hutchinson 1989

30 Beuth 1996

Assuming additional layers or changing material mismatch was not observed since the local material properties may have a crucial influence on the local stress field and thus on the result, and the ϵ values concerned are not negligibly small³¹. Following the arguments of Rice the oscillating model is chosen and the approach of Beuth considered for the numerical approach.

31 see page 101 for an extended view on the possible ϵ range.

To explain the use of a reference length demands to start with the energy release rate G , which will be used within the fracture criterion. Keeping the equilibrium definition in equation 2.2, it can be expressed in terms of complex K as³²

32 Hutchinson and Suo 1992

$$G = \frac{1 - \beta^2}{E_*} (k_1^2 + k_2^2) = \frac{1 - \beta^2}{E_*} |K|^2, \quad \forall E_* = \frac{2}{1/\bar{E}_1 + 1/\bar{E}_2}, \quad (2.16)$$

but demands the same unit as for homogeneous body fracture. The stress equation defining a complex K in equation 2.13 does however not allow this. This problem is solved by introducing a stress intensity factor \mathfrak{K} of *classical type*, following the arguments of Rice.³³ He argued, that any complex K to describe the interface always shows dimensions of

33 Rice 1988

$$[K] = (\text{stress}) \sqrt{(\text{length})} \frac{1}{(\text{length})^{i\epsilon}}, \quad (2.17)$$

but to describe any point in the stress or displacement field close to the crack tip, K would *always* appear together with a dependency of the crack tip distance r

$$Kr^{i\epsilon} = (\text{stress}) \sqrt{(\text{length})} \left(\frac{r}{(\text{length})} \right)^{i\epsilon}, \quad (2.18)$$

which allows to define a stress intensity factor of classical type on the basis of a chosen crack tip distance, termed reference length l_{ref}

$$\mathfrak{K} = Kl_{\text{ref}}^{i\epsilon} = |\mathfrak{K}|e^{i\epsilon} = K_I + iK_{II} \neq k_1 + ik_2, \quad (2.19)$$

$$\text{with } K = |\mathfrak{K}| \frac{1}{l_{\text{ref}}^{i\epsilon}} e^{i\psi}. \quad (2.20)$$

This approach gives a convenient solution for both the unit of stress intensity and the characteristic length. Equations 2.13, 2.15, and 2.16 turn into

$$(\sigma_{yy} + i\sigma_{xy})_{\theta=0} = \frac{K}{\sqrt{2\pi r}} r^{i\epsilon} = \frac{\mathfrak{K}}{\sqrt{2\pi r}} \left(\frac{r}{l_{\text{ref}}} \right)^{i\epsilon}, \quad (2.21)$$

$$\tan \psi_{r=l_{\text{ref}}} = \frac{\Im(Kl_{\text{ref}}^{i\epsilon})}{\Re(Kl_{\text{ref}}^{i\epsilon})} = \frac{K_{II}}{K_I} = \tan \phi + \epsilon \ln \frac{r}{l_{\text{ref}}}, \quad (2.22)$$

$$G = \frac{1 - \beta^2}{E_*} |\mathfrak{K}|^2. \quad (2.23)$$

This definition of \mathfrak{K} has been used by various researchers³⁴ but it also has been defined in different ways.³⁵ The reasons for defining and choosing a certain l_{ref} have led to many discussion since the 1960s especially on its physical meaning, and discussions continue today.³⁶ These differences demand attention to the definition. To summarize, the fracture mechanics at the interfacial crack tip needs four descriptors in the form of $G_c(\psi(l_{\text{ref}}, \epsilon))$, all of which have to be named in order to reproduce and to compare data: an energy threshold G_c and an elastic mismatch ϵ with clear definitions, as well as a fracture mode mix ψ and reference length l_{ref} with choices to make in their definition, especially with respect to a reference length.³⁷

³⁴ Liechti and Chai 1991, Hutchinson and Suo 1992, Tay 2006, Ernst et al. 2008, Suo 2010

³⁵ Suga et al. 1988

³⁶ Agrawal and Karlsson 2007, Mantić 2008, Karlsson 2008

³⁷ The author regards the presentation of all *four* parameters as crucial. Rice claimed that \mathfrak{K} characterizes the stress field uniquely, no matter which values l_{ref} or ϵ . This argument could lay the base to a possible toughness comparison without further simulations of complex geometries. However, evidence of comparing data of different interfaces at various stress states is thin. The argument shall be picked up later on page 99.

2.4 A Choice of Reference Length

The measure \mathfrak{K} was introduced with the idea of being

... sensibly independent of r over some range of interest for the application of fracture mechanics methodology...³⁸

38 Rice 1988

The range of interest is the zone dominated by the singularity, that means sufficiently distant from any geometric features such as edges of the concerned object. The range is then restricted at its minimum by being outside of a considerable oscillation zone, for which estimates are available in terms of stresses and displacements.³⁹ The independence of the distance is given as long as

39 Malyshev and Salganik 1965, Rice 1988, Sun and Qian 1997

$$r > l_{\text{ref}}, \quad (2.24)$$

which motivated reference length suggestions between 1 nm ⁴⁰ and $1 \mu\text{m}$ ⁴¹ typical for a material combination on an atomic or at least bonding mechanism scale. Other suggestions follow geometry measures such as the crack length or a layer size. To characterize a local load situation for a reproducible interface property description a non-geometric l_{ref} is preferred over a layer thickness or a crack, since the latter are not interface specific but geometry specific definitions. However, all mode mix measures can be transformed between different reference lengths.

40 Suo 2010

41 Rice 1988

The transformation equals a shifting of the critical data \mathfrak{K}_c or G_c along the mode mix axis, because as the aim is to keep \mathfrak{K} and its amplitude equal for two different $\psi_1 (l_{\text{ref},1})$, $\psi_2 (l_{\text{ref},2})$, equation 2.20 leads to

$$\psi_1 = \psi_2 + \epsilon \log \frac{l_{\text{ref},1}}{l_{\text{ref},2}}. \quad (2.25)$$

Geometry based l_{ref} commonly serve to evaluate analytic solutions as described in more detail by Hutchinson et al.⁴², but as shall be seen in the next section numerical methods are better suited in electronic packaging applications.

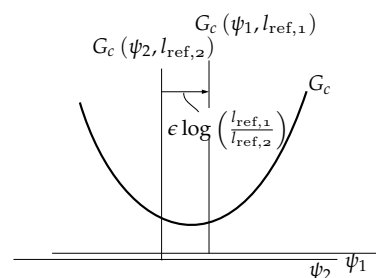


Figure 2.7: Transforming critical fracture data by shifting along the mode mix axis.

42 Hutchinson et al. 1987, Rice 1988, Hutchinson and Suo 1992

2.5 Numerical Methods for the Fracture Mechanics Analysis

Starting from the demand of modeling failure the scenario is rather complex, and complex in two aspects. First the reality of electronic packaging to be modeled is quite detailed in geometry at several length scales. Second the material behavior influencing the stress state is varying through time, temperature, pressure and humidity. In order to calculate the sufficiently accurate thermomechanic reaction of an object to certain boundary conditions, these arguments generally encourage numerical modeling of failure.⁴³ Also, specimens that fit the

43 Auersperg et al. 2005, Driel et al. 2007, Wunderle et al. 2009, Sluis et al. 2009a

simplifications of analytical models are not possible to manufacture while representing the same materials and microstructure of reality.⁴⁴ In both complex reality cases of concern, electronic packages with layer stacks and test specimens representing the microstructure of the former, the assumptions of the simplified analytic descriptions do not apply for the empirically known, global measures. Especially where the specimen's areas of clamping and delamination cannot be separated clearly, and influence each other with respect to the load situation, a numerical model of finite elements or volumes can help. Such models break down the complex case to a high number of simple cases and allow the local establishing of measures that are necessary for a fracture mechanical analysis. Thus a concise overview shall be given here, on the different methods to extract energy release rate values and a measure of mode mix from finite element solutions.

Since an energy release rate defines an energy relative to a cracked area, several methods contain two steps to calculate the energy difference between two immediately successive states of cracking. The finite and virtual crack extension methods give global measures of energy release rates.⁴⁵ Also specific crack tip elements⁴⁶ that draw on analytic solutions can serve to calculate energy release rates. For nonlinear material and fracture behavior different integral approaches have been developed, the first of which was the J-integral as a solution to take plastic material behavior into consideration.⁴⁷ Other approaches consider visco-plasticity or strain-hardening, and are excluded here because the Si-EMC interface does not exhibit such behavior.⁴⁸ A method for energy release rates that are strongly dependent on the mode mix, is the *virtual crack closure technique* (VCCT).⁴⁹ It allows analyzing the fracture in one step only, and includes calculating both the energy release rate and the mode mix. The assumption of the VCCT is that two successive states of cracking are self-similar for an infinitesimally short crack advance. This crack advance, such as $a + \Delta a$ to $a + 2\Delta a$ does not significantly change the stress state at the crack tip.

Once this is given, the forces at the present crack tip can be assumed to be necessary to open the displacements of the next node pair or close the ones that are already open. The elements around the crack tip need equal shape, and a certain size range. They should be bigger than the oscillation zone size and smaller than the area dominated by geometry features, that is the elements should be in the K -dominated region. The components of the energy release rates

⁴⁴ see *page 31* for Si-EMC specific problems and *page 33* for the general problems involved

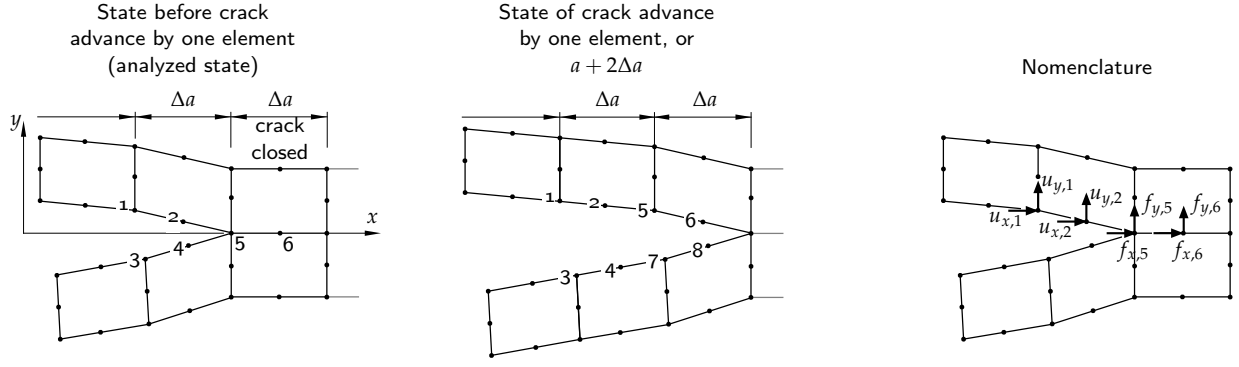
⁴⁵ Hellen 1975, Krueger 2006

⁴⁶ Banks-Sills 1991, Davidson et al. 1995, 2005

⁴⁷ Rice 1967, Cherepanov 1967

⁴⁸ For further integral methods see Anderson 1995 or the works of Goldman and Hutchinson 1975 or Shih and Asaro 1988.

⁴⁹ Rybicki and Kanninen 1977, Krueger 2002, 2004


 Figure 2.8: Nomenclature of the VCCT-based calculation of the G components.

can be calculated according to figure 2.8 by using the following expressions.

$$G_I = -\frac{1}{2\Delta a} [f_{y,5}(\Delta u_{y,1-3}) + f_{y,6}(\Delta u_{y,2-4})] \quad (2.26)$$

$$G_{II} = -\frac{1}{2\Delta a} [f_{x,5}(\Delta u_{x,1-3}) + f_{x,6}(\Delta u_{x,2-4})] \quad (2.27)$$

Raju⁵⁰ found that the G components are dependent on the mesh size. This is especially important to uniquely identify the stress state, that is to calculate a mode mix ψ . There are several methods to determine ψ independently from the energy release rate, for instance by using the displacements of nodes in the crack tip vicinity: Crack surface displacement (CSD)⁵¹, Crack tip opening displacement (CTOD)⁵², and Crack surface displacement extrapolation (CSDE)⁵³. The CSDE procedure to extrapolate the nodal displacements is given in equation 2.28, in this case starting from nodes in the third element from the crack tip (the nomenclature is meant different from that of the VCCT, extrapolation starts at node 6, whereas node 1 is the crack tip). Extrapolating nodal displacements of the first two elements introduces substantial deviations.

$$\psi_{CSDE} = \arctan \left(\frac{du_x + 2\epsilon du_y}{du_y - 2\epsilon du_x} \right) - \epsilon \ln \left(\frac{r_n}{l_{ref}} \right), \quad (2.28)$$

$$\forall r_n : n = 6 \dots 27, \text{ and} \quad (2.29)$$

$$\forall du : du = du(r_n) \quad (2.30)$$

Despite these methods it is desirable to directly extract the mode mix from the finite element results, without defining additional measures such as a crack tip opening displacement, or a crack surface length for an extrapolation. The extraction of the mode mix from VCCT results is however not straight forward, as the components were observed to be non-convergent with distance when approaching the crack tip.

50 Raju 1987, Raju et al. 1988

51 Matos et al. 1989

52 Wells 1961, Newman et al. 2003

53 Chan et al. 1970, Carpenter 1983, Yuuki and Cho 1989

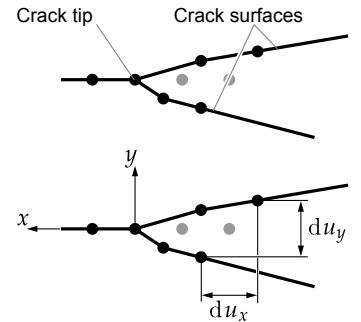


Figure 2.9: The coordinate system for the CSDE method to determine the mode angle.

Raju et al. found that the problem lies in the imaginary part of the G description,⁵⁴ which was approached by different ideas. Hu and Tay modified the VCCT, but the deduction of the calculation remains unpublished since 2004.⁵⁵ Beuth used asymptotic estimates of the G components, separated from their oscillatory character.⁵⁶ His approach for orthogonal anisotropic materials was picked up by Agrawal and Karlsson⁵⁷ and compared to other approaches underlining that the ψ results are only different by an offset angle and can be converted into each other.⁵⁸ Beuth shows a method to calculate a mesh-independent ψ , by modifying the mode mix definition of the original VCCT. The mode mix based on the energy release rate components of the VCCT calculation is, with respect to equation 2.23

$$\psi_{G,VCCT} = \arctan \sqrt{\frac{G_{II}}{G_I}}, \quad (2.31)$$

with the mesh dependency as mentioned for equations 2.26 and 2.27. Agrawal and Karlsson⁵⁹ explicitly show the Δa -dependence of the G components and suggest to redefine them such that they read for the numeric implementation in 8-noded elements

$$\begin{aligned} G'_I &= \frac{G}{2} + \frac{1}{4\Delta a} \left[\cos \left(2\epsilon \ln \frac{l_{\text{norm}}}{\Delta a} \right) (f_{y,5}(\Delta u_{y,1-3}) + f_{y,6}(\Delta u_{y,2-4}) - f_{x,5}(\Delta u_{x,1-3}) - f_{x,6}(\Delta u_{x,2-4})) - \right. \\ &\quad \left. \sin \left(2\epsilon \ln \frac{l_{\text{norm}}}{\Delta a} \right) (f_{x,5}(\Delta u_{y,1-3}) + f_{x,6}(\Delta u_{y,2-4}) + f_{y,5}(\Delta u_{x,1-3}) + f_{y,6}(\Delta u_{x,2-4})) \right], \\ G'_{II} &= \frac{G}{2} - \frac{1}{4\Delta a} \left[\cos \left(2\epsilon \ln \frac{l_{\text{norm}}}{\Delta a} \right) (f_{y,5}(\Delta u_{y,1-3}) + f_{y,6}(\Delta u_{y,2-4}) - f_{x,5}(\Delta u_{x,1-3}) - f_{x,6}(\Delta u_{x,2-4})) - \right. \\ &\quad \left. \sin \left(2\epsilon \ln \frac{l_{\text{norm}}}{\Delta a} \right) (f_{x,5}(\Delta u_{y,1-3}) + f_{x,6}(\Delta u_{y,2-4}) + f_{y,5}(\Delta u_{x,1-3}) + f_{y,6}(\Delta u_{x,2-4})) \right], \end{aligned} \quad (2.32)$$

where $G = G_I + G_{II}$ and the normalizing parameter l_{norm} can conveniently equal the reference length $l_{\text{norm}} = l_{\text{ref}}$. The mode mix definition is accordingly

$$\psi'_{G,VCCT} = \arctan \sqrt{\frac{G'_{II}}{G'_I}}. \quad (2.33)$$

Using the VCCT accordingly, two dimensions have to be considered: the crack extension size Δa and a normalizing parameter, in this case l_{ref} .

The detailed deduction and comparison to other methods, both G and K based are given by Agrawal and Karlsson. More comprehensive reviews of numerical methods are given by Banks-Sills and Krueger⁶⁰. Up to date the methods to mesh-independently calculate a mode mix have not been demonstrated for experimental fracture

54 Raju et al. 1988

55 Hu and Tay 2004, 2005

56 Beuth 1996

57 Agrawal and Karlsson 2006

58 Sun and Jih 1987, Matos et al. 1989, Toya 1992, Bjerken and Persson 2001

59 Agrawal and Karlsson 2006

60 Banks-Sills 1991, Krueger 2006

data of a range of mode mix situations. Therefore the limits of the methods remain unclear, and even for classical fracture application and motivation fields such as aerospace research further development and demonstration is desired.⁶¹

For details on the delamination of the Si-EMC interface see the section below, for the Numerical model and simulation of the experiments see page 67, and for the Fracture mechanical results see p. 80.

2.6 Delamination of Si-EMC

Literature including energy release rates of the Si-EMC interface is thin, although the interface has received much attention since long.⁶² The first to present energy release rate values for such an interface were Wang et al.⁶³, and they remained the only ones being able to successfully monitor a delamination in a specifically fabricated specimen, and the only ones reporting a specimen that did not randomly fracture. They however created specimens of 8 mm EMC thickness, only a rare package dimension, they calculated G_c for only one scenario—one thermal load case that leads to delamination, and their fracture mechanics approach, although drawing from the work of Sun and Qian,⁶⁴ lacks information about the oscillation zone size, or a parameter l_{ref} . During the past decade only few other documents on the Si-EMC interface were published, all of which do not report *critical* energy release rates, that is they did not calculate G_c or K_c values from specific experiments combined with a detailed fracture mechanical analysis.⁶⁵ More reports can be found on the delamination of Si-epoxy, but while some⁶⁶ do report values of G_c , only one group⁶⁷ relates the data to mode mix angles $G_c = G_c(\psi)$. Among the Si-epoxy works there are numerous papers reporting energy release rates based on simulations only⁶⁸ and reporting thus non-critical values $G(\psi)$. They partly give helpful application advice but deduce the findings from simplified models of complex electronic packages and do not verify their results by experiments of isolated fracture load conditions. The situation in the literature raises the question what makes the data so scarce? What is so peculiar in this material combination, what hinders doing the experiments?

A silicon die in an electronic package usually consists of a monocrystalline silicon bulk body, a homogeneous material with anisotropic properties.⁶⁹ This body contains an active area of many layers and a layered backend-of-line stack. Depending on the processing history, also passivation and oxide layers cover the die in different thicknesses. For some packages mainly the oxide layers come in contact with a molding compound throughout the packaging, the type of compound depending on the package technology. There are various types of

61 Krueger 2006

62 Nguyen et al. 1993, Tilgner et al. 1994

63 Wang et al. 1999

64 Sun and Qian 1997

65 Kim 2003, Loke 2009, Hu et al. 2010

66 Widodo et al. 2005, Kim 2007, Nakamura et al. 2007, Hwang et al. 2008, Singh et al. 2008

67 Liechti and Chai 1991

68 Mercado et al. 2001, Nied 2003, Ayhan et al. 2006, Zhang 2007, Hu et al. 2010

paragraph on mixed mode, and shear dominated failure found by. . . , reorganize topic string!

69 Brantley 1973

compounds and this work will concentrate on the combination of one silicon bulk body with one epoxy based mold compound. The compound consists of an epoxy material matrix, cured during processing and filled with a high percentage of silica fillers. For various processing needs and functionality the material also contains different minor substances that influence the properties. The material bulk properties substantially dominate the thermo-mechanical behavior of a package, and they also dominate the global behavior of a bimaterial or sandwich specimen. Depending on temperature and processing history the property mismatch *complicates* experimental procedures as described below.

2.7 *Why Si–EMC is difficult to delaminate — Reasons for a New Test*

The central phenomenon that complicates the delamination of the Si–EMC interface is: Specimens randomly crack before the test finishes. During fabrication the two materials join at an elevated temperature, and during subsequent curing and cooling down the materials shrink to a different extent. Thus the specimen is not stress free after the processing, in fact the samples are highly stressed before loading, a state of so called *residual stresses*. The difference in chemical and thermal shrink of the material layers causes the specimen to warp, and moreover to warp in two dimensions. This effect increases with the specimens size, that is large formats of bimaterials warp more, especially where the thickness of both layers is low compared to length and width. During a loading procedure—be it for handling, preparation, or testing—the specimens are forced to de-warp, and they respond with substantial load reactions. But in an already highly stressed state the specimen needs less additional energy to release bonds. Is the load increased, the specimen reaches a critical stress state and fractures.

To overcome the problem of random fracture before testing, an initial defect at the interface is necessary. Such a *pre-crack* reduces the risk of peak loads before delamination, peak loads that are released suddenly and can break the sample or reduce the observable delamination length. In a state of residual stresses such an intended breaking point also increases the risk of pre-test fracture.

To reduce this pre-test fracture risk, the warpage should be minimized and must at least be restricted to one dimension. Thus specimens should be made of small width compared to height. The then smaller specimens demand a higher precision of the testing equipment than conventional specimens do, an adapted clamping mechanism that allows clamping contacts in a smaller area, especially under tempera-

ture and moisture exposure, and an adequate handling of small volume samples.

Standards do not yet address the above arguments, and as will be shown in the next section standardization might not be the way to go. There are a number of standardized delamination tests, for instance regarding unidirectionally reinforced materials (ISO 15024), fibre reinforced plastics (JIS K 7086 and ASTM D5528-94a), and even leadframe to molding compounds (SEMI G69-0996). Yet for the applied fracture mechanics in electronic packaging scenarios the reasoning contained in the standards is not sufficient. The above named JIS and ASTM standards suggest, for example, to use a 15 μm thick inlay to create an initial defect. We have however seen that inlays of this size introduce further geometric singularities at their edges and do not provide a sufficiently sharp pre-crack for the Si-EMC interface at package scale, instead the crack kinks into the EMC. (*page 54*) Also other tests, such as the peel test (ISO 8510-1) or delamination tests for similar thin film applications⁷⁰ cannot be applied, since the layers concerned are not thin enough and prevent usage of such tests due to the brittleness and high elasticity of the Si and EMC materials.

70 Volinsky et al. 2002

It is thus necessary to look at the demands in detail and to build an adapted test setup around an accordingly designed specimen. This thesis provides these details. It shows

the demands on a delamination test (see below), a test setup to delaminate the interface (page 39), methods to fabricate the specimens (p. 45), it explains the experimental procedure (p. 65), it gives the fracture mechanical results (p. 80) and shows aspects of interpretation (p. 89).

A Successful Test

3.1 Demands on a Miniaturized Delamination Test

As seen above the basic difficulty to overcome is pre-test fracture and random fracture when loading. Assuming this being solved, the test nevertheless has to allow calculating $G_c(\psi)$. The corresponding demands follow below sorted according to different aspects. The list suggests a miniaturized test that is bound to a certain specimen and its fabrication. Thus the reader may consider the arguments on specimen fabrication as well, see *page 45*.

Fracture mechanics aspects include crack monitoring, stress state definition, specimen clamping, load application and microstructure representation. An interface in a real product component life experiences very different loads, which can be described by shear and tensile stresses. The interfacial fracture toughness varies with the ratio of the stresses. If a simulation shall identify whether delamination progresses, it is crucial knowing the interface properties for different stress ratios. A delamination test should therefore allow the testing for such different ratios, and that is testing under different load angles. In a setup for such delamination testing it is difficult to create a precise load situation at the crack tip because of three reasons. Before the very testing the interface toughness is unknown; both the stress state and interface toughness change with load mix and temperature; and the interface intrinsically impacts the stress field orientation. Thus the stress state can only be approximated during designing a setup. The stress state might not only change between differently set experiments but also during an experiment, because the specimen geometry changes. For calculating $G_c(\psi)$ from a numerical model the changing local geometry of the specimen has to be known and therefore to be tracked. The crack tip position at a prescribed load displacement or force defines the local geometry. Because a tracking involves substantial effort a delamination test is desirable that creates an approximately constant

stress state during the experiment. That is crack length independence for both the fracture toughness and the mode mix.

An example for such crack length independence is the edge-cracked bimaterial strip. If mounted in a biaxial loading stage and clamped over the full interface length¹, the stress at the delamination front remains approximately constant during the specimen fracture. Crack length independence conveniently reduces the data and eases studies of crack propagation. But so far no suitable solution for a sufficient clamping has been shown at electronic packaging scale. The material characteristics and test demands prevent the adaption of a Liechti and Chai-type solution.

To ensure clamping, specimens have to be fixed in at least one spot on each side of the crack plane by either force, shape or material based locking. Material based locking could be done by adding an adhesive as clamp for each specimen during fabrication. But the former restricts moisture and temperature exposure and the latter complicates production relevant processing. Such processing also restricts shape based locking in all points due to machining of down-scaled specimens, although it is feasible for ductile material partners, such as leadframe alloys in the works of Xiao et al., and Wunderle et al.² In force based locking the specimen is held in position by a compressive force. The induced compressive stress should be sufficiently big for clamping, but not influence the desired stress state in the region of the crack tip. The ideal way to do this for a brittle tensile specimen with limited shaping options is a serrated wedge. The wedge tacks to the specimen surface and automatically increases a compressive normal force component with an increase of loading force. In the case of *variably mixed* stress states a wedge assisted locking is not possible, because the wedge cannot compensate forces in *different* directions.

Material and interface behavior aspects include elasticity, thermal expansion, brittleness and microstructure. A relatively high elasticity causes substantial load reactions for small load displacements, thereupon storage of elastic energy that can suddenly release during fracture. Being bound to small displacements in a delamination test demands high precision equipment in driving and measuring displacements and monitoring crack opening or length.³

The material mismatch in thermal expansion causes warping of the bimaterial as described on *page 31*. The warpage is unproblematic in crack propagation direction but should be kept small in the other orientations. The suggested change in aspect ratio impacts the specimen's clamping. When reducing one material dimension, accurate support or clamping needs to be adapted to the smaller contact area. The small area clamping creates higher spot pressure at equal clamp

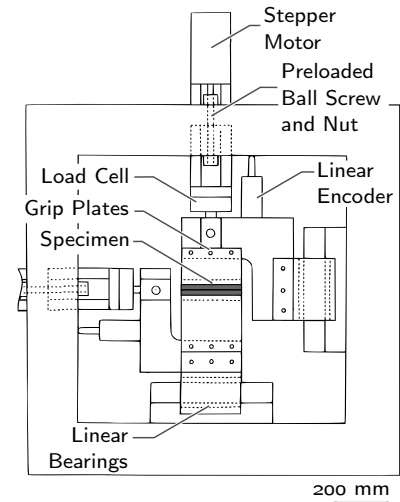


Figure 3.1: A biaxial loading of a edge-cracked bimaterial strip together with a full length clamping ensures a constant stress state during delamination. Adapted from Liechti and Chai 1991.

¹ Liechti and Chai 1991

² Xiao et al. 2007, Wunderle et al. 2012

³ For instance assuming linear elastic behavior, 30 MPa stress in a specimen can represent 1 μm displacement on a length of 1 mm when the materials Emodulus is 30 GPa. The same stress represents 10 μm displacement for an Emodulus of 3 GPa. Observing the specimen with a camera resolution of 5 $\mu\text{m}/\text{pixel}$ gives substantially different errors for the displacement.

force, and thus creates more severe localized stress concentrations in the specimen for a given load magnitude. A feature to not clamp the silicon, which fails easily under peak loads, and a defined load spreading feature that has an alignment support to ease handling of the clamp mechanism can compensate these demands.

While creating a desired stress state at the interface, to isolate a certain fracture behavior, the microstructure of the specimen should represent the product relevant material. When using a Liechti and Chai-type sized specimen the material could not be manufactured under the same conditions such as injection pressure, molding time, or an as homogeneous as possible cooling gradient as shall be seen in section 4 starting on *page 45*. Also residual stresses increase with structure size due to cooling gradients. This demands a miniaturized specimen and test setup in which load application, clamping, actuation, sensing of force and displacement, frame, data acquisition and load control are adequate for miniaturized specimens.

Further not only the joint materials, but also the Si-EMC interface behaves brittle at room temperature. Brittleness leads to sudden fracture without substantial plastic deformations. When using force control to prescribe the delaminating loads this yields abrupt dynamic delamination and thus demands displacement controlled testing. To observe a steady delamination of a brittle interface and to be able to stop the delamination, the displacement must be prescribed. Although the loading machine's frame stiffness and control loop speed limit the linearity of the displacement control, this allows observing a steady delamination.

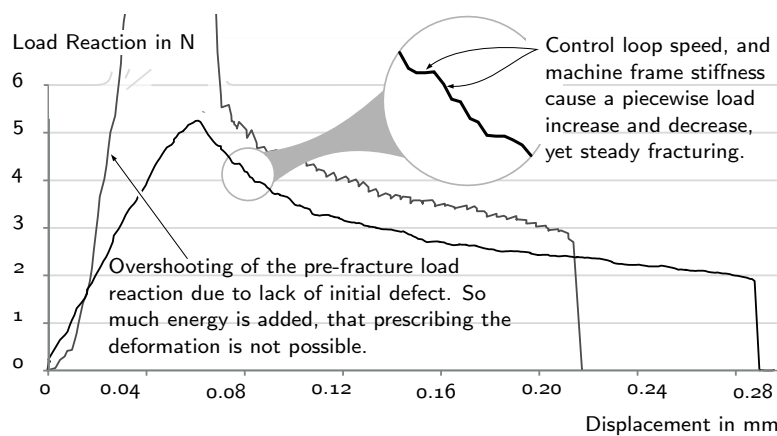


Figure 3.2: Typical overshooting load reaction of a specimen without an initial defect, compared to a specimen reaction with sufficient initial defect. The enlarged part shows the piecewise load increase and decrease typical for brittle fracture, even though a prescribed displacement allows a steady crack propagation.

A setup that involves a decreasing driving load with crack advance or an increasing surface to delaminate (such as in triangle button shear specimens⁴) eases the steady delamination. If the specimen does not show an initial defect so much energy is added to the frame and

specimen that a displacement control is mostly too slow, as can be seen in figure 3.2.

Specimen fabrication aspects are detailed in section 4 starting on page 45. Generally the fabrication restricts the specimen shape and material history, such as the cone-shape of semi-finished molds, residual stresses due to temperature changes or water exposure during dicing and polishing. Additionally the fabrication of a bimaterial geometry at package scale restricts the clamping area.

Specimen handling aspects concern clamping, alignment and repeatable positioning of the specimens. Between tests at high temperatures the specimen should be replaceable rapidly. Thus the test setup must allow a rapid heating and cooling, and the process of clamping and releasing specimens must be ergonomic to prevent a decrease in accurate alignment and repeatability.

Test application aspects concern test costs, test climate conditions, and specimen material structure. The overall testing costs should be low, that is delamination testing plus simulation assisted design is faster than fabricating products and testing those for delaminations in accelerated reliability tests or coarse load impact tests. That means while meeting all demands above, the time and material for fab and operation spent on delamination testing should be as small as possible. Thus specimen fabrication should be simple and as close as possible to production. The handling and operation of specimens and test should be simple. Likewise the analysis of the test should be simple. Besides, testing should be possible at elevated climates also with delamination specimens. The specimens need to be made using relevant production processes, or at least conditions comparable to those, to ensure the microstructure is the same as in products, as pointed out early already.⁵

5 Bennett et al. 1974

Machine compatibility aspects guarantee that the delamination can be run in different loading and analysis machines. This ensures that comparability of toughness results can be tested by copying a comparably cheaper test unit and mounting it into a load device, such as a Microtester 5948 (Instron), an Eplexor DMS (Gabo), or a DMA Q800 (TA Instruments). Advanced crack analysis at micro-scale could be done by mounting the test setup in analysis equipment such as atomic force microscopy (AFM)⁶. These demands have been considered for the concept of a setup's general functional units. Such units are shown in figure 3.3.

6 Keller 2005

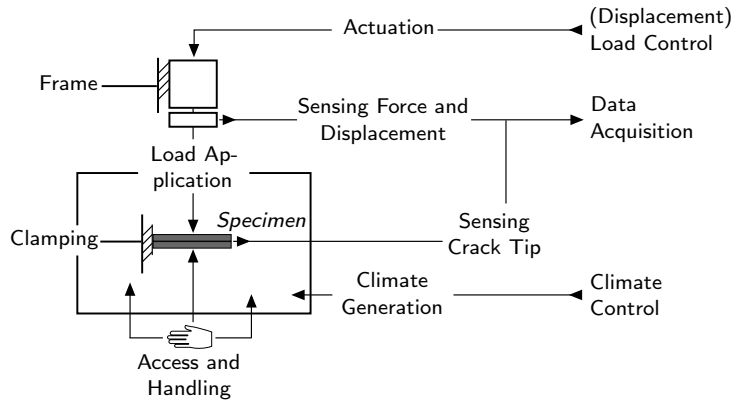


Figure 3.3: The different parts of a general delamination setup.

For the machine compatibility and because of temperature and moisture demands the delamination setup should be disconnected from the force and displacement actuation and sensing, climate control and generation, data acquisition, and machine frame. The remaining functions thus are (displacement) load application, specimen clamping, as well as access and handling as shown in figure 3.4.

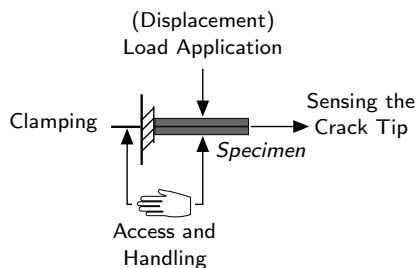


Figure 3.4: Reduced functions to ease compatibility and elevated climate resistance.

These functions shall be discussed in detail. Depending on the concept, the crack tip recognition can be implemented as a mountable feature, and it can be used from outside the loading device as described on *page 70ff.*. But which test setups are available then to fulfill the described demands?

Beside the standards described on *page 32* numerous delamination setups are in use. Most of the setups originate in the composites material research, specifically in aerospace and pipeline structural engineering during 1980s. Many examples are given by Hutchinson and Suo or by Volinsky et al. for thin film fracture.⁷ Table 3.1 gives a selection of delamination and fracture setups dating from the 1950s to the present day:

⁷ Hutchinson and Suo 1992, Volinsky et al. 2002

Name of test or specimen	Abbrev.	First Publisher	
peel test	–	Spies	1953
blister specimen	–	Dannenberg	1961
sandwich strip blister specimens	SSBS	Liechti	1962–1991
free-edge delamination coupon	FEDc	Pagano and Pipes	1973
cone test	–	Anderson et al.	1974
end loaded split	ELS	Vanderkley	1981
double cantilever beam	DCB	Whitney et al.	1982
end notch flexure	ENF	Russell	1982
brazil nut / crack brazilian disk	BN/CBD	Atkinson et al.	1982
edge-delamination tension	EDT	O'Brien	1984
asymmetric double cantilever beam	aDCB	Bradley et al.	1985
cracked-lap shear	CLS	Bradley et al.	1985
modified free-edge delamination	mEDT	Whitney and Knight	1985
mixed mode flexure	MMF	Russell and Street	1985
short beam shear	SBS	Adams	1986
variable mixed mode	vMM	Hashemi et al.	1987
mixed mode bending	MMB	Crews and Reeder	1988
four point bending	4PB	Charalambides et al.	1989
symmetric center crack beam	sCCB	Charalambides et al.	1989
microindentation	–	Ritter et al.	1989
single leg bending	SLB	Davidson and Sundararaman	1996
fixed ratio mixed mode	FRMM	Kinloch et al.	1993
prestressed end-notched flexure	PENF	Szekrényes	2006
modified mixed mode bending	mMMB	Xiao et al.	2007
over-leg bending	OLB	Szekrényes and Uj	2007
triangle button shear specimen	TBSS	Durix	2010
side clamped beam	SCB	Renart et al.	2010
advanced mixed mode bending	AMB	Wunderle et al.	2012
further individual biaxial loadings	–	Mulville	1978
		Liechti and Knauss	1982

Table 3.1: Selection of specimens to obtain interfacial fracture mechanical parameters, this list is by no means complete, as there is a vast number of tests.

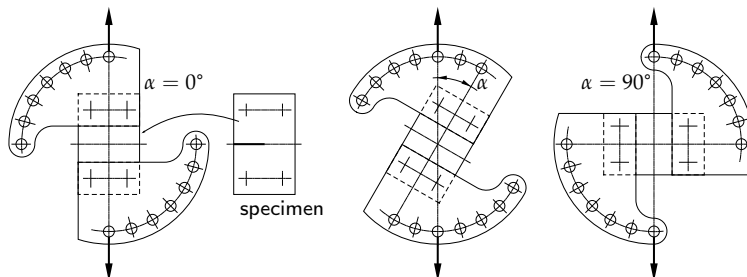
The first and widely used adhesion tests were the lap shear test,⁸ the peel test,⁹ the blister method,¹⁰ and the cone test¹¹. None of these tests however is suitable for a variable mode mix testing of the material pairing Si-EMC.

The ones most relevant to mode mix conditions desired for the Si-EMC interface are the Mixed Mode Bending (MMB), the Compact Tension Shear (CTS) or Arcan specimen, the adapted test of Liechti and Chai, the brazil nut, and the classic Double Cantilever Beam (DCB), End Notch Flexure (ENF) and Four Point Bending (4PB) specimens.¹² The latter three are constrained in their individual mode mix range and might be combined for an optimal use.¹³ The related specimens are however not at package scale and risk pre-test fracture for the Si-EMC interface. The MMB, CTS, brazil nut and Liechti type specimens offer a wide mode mix range. But a sufficient clamping mechanism of brittle materials at package scale that can withstand elevated climates has not been demonstrated yet. The only package scale specimens apart from thin film delamination have been used by Xiao et al. and Durix et al.¹⁴ Their contributions have been parallel works to the MMC development.

Renart et al. explain the the clamping difficulties in detail, including the specific geometric solutions when using two hinges, operator skills, and the additional joints failure when exposing to test conditions.¹⁵ Partly this was addressed by Xiao et al.¹⁶, who modified the MMB and drilled hole features through one of the bonded materials to circumvent the clamping – processing that is time costly and difficult in accuracy for the Si-EMC interface.

3.2 The Mixed Mode Chisel Setup

The mixed mode chisel setup combines the fracture mechanics idea of the CTS concept with the ball or die shear test¹⁷ clamping. In the CTS test a specimen is revolved relative to the load axis of a one-directional loading device.



A bulk fracture specimen is fixed on both sides of the expected crack plane such that the achieved angle setting is invariant during

8 the lap shear was first used for bolts in aerospace engineering by Volkersen 1938, then described for adhesion using fracture mechanics by Ripling et al. and later modified to a pre-cracked version by Brussat et al. 1977, see also the review of Lai et al. 1996

9 the peel test is mentioned in several patents before Spies who described his works in 1953. It was then analyzed in detail by Bikerman, Yurenka, Gardon, more details can be found in the related reviews of Kinloch et al., Wei and Hutchinson, Dillard and Pocius

10 the blister test was an early test for color adhesion, and first pressure actuated by Dannenberg 1961

11 Anderson et al. 1974

12 Crews and Reeder 1988, Richard 1985, Liechti and Chai 1992, Atkinson et al. 1982, Whitney et al. 1982, Russell 1982, Nishimura et al. 1992, Charalambides et al. 1989

13 Shirangi 2010

14 Xiao et al. 2007, Durix et al. 2012

15 Renart et al. 2010

16 Xiao et al. 2007

17 The CTS specimen was introduced by Richard 1985. The ball shear test entered microelectronics industry in 1967, see Arleth and Demenus 1967, Gill and Workmann 1967. Figure 3.5: Examples of CTS positions relative to the load axis. Adapted from Richard 1985.

one experiment as shown in the figure below. A CTS type fixation on both sides of a specimen's interface brings the enormous disadvantages of bigger clamping areas far from relevant material geometries, attaching additional materials subject to moisture uptake or a distorted stress state – be it for force, form or material locking. Thus the fixation concept of the CTS was changed to combining a force locking with a form locking and to compressive instead of tensile operation. The figure below shows the different load angle settings of the concept. The MMC specimen has a clamping face for force locking one side and a notch for form locking the other side. This combination ensures a force application into the specimen's testing part.

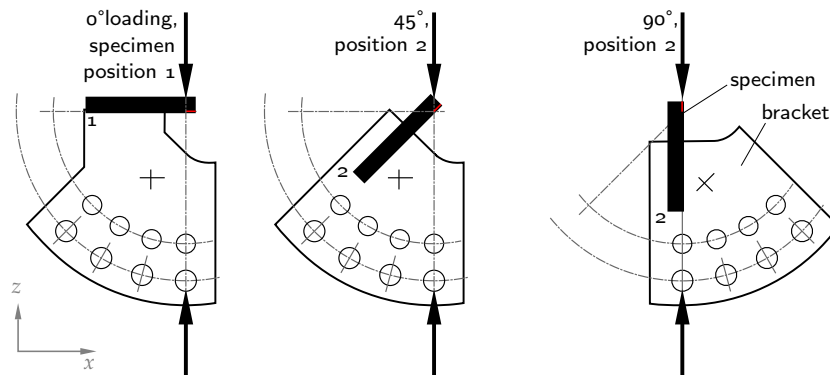
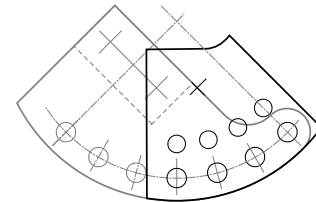


Figure 3.6: The concept of the MMC setup (left). The size of the clamp was reduced to half of the CTS angle range to fit smaller experimental spaces (below). The 90° range is realized by two specimen clamping positions.



This clamping combination is similar to a ball or die shear test but uses the revolving bracket of the CTS. While in bulk fracture specimen of the CTS the remote load angle directly translates to mode mix at the crack tip, the mode mix in an interface specimen loaded accordingly can only be a roughly estimated, as described in the fracture mechanics demands on *page 33*. The ball shear test is conceptually restricted to pure shear loading and usually does not involve pre-cracks. The interfacial mode mix is strongly influenced by the chisel height during delamination. This has been used in recent work by Dreßler et al. and Durix et al.¹⁸ They ran shear tests for fracture mechanical analysis and addressed both issues by prescribing the shear chisel height and by adding a material layer as initial defect.

Using a revolving bracket the stress state can be changed without introducing an additional degree of freedom to the loading device. In both the CTS and the ball or die shear test the loading device actuates *one* translational degree of freedom during the delamination. This concept is resumed in the MMC to maintain device compatibility, and because each added actuation axis affects the stiffness and accuracy of the device. The remaining five degrees of freedom have the tolerances shown below, which can lower the test accuracy.

¹⁸ Dreßler et al. 2009, Dreßler 2010, Durix et al. 2012

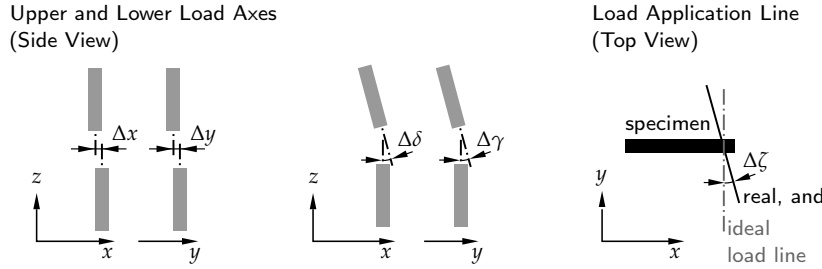


Figure 3.7: The five degrees of freedom due to machine tolerances: two translational and three angular offsets.

The tolerances in figure 3.7 have their largest impact on the point or line of load transfer into the specimen. Thus the realization of the contact point, the point of load application as a part of the clamping solution is described first. Since this feature is crucial for the accuracy, it was varied in three basic cases: a chisel, a pendulum loaded in compression and a leaf spring loaded in tension.

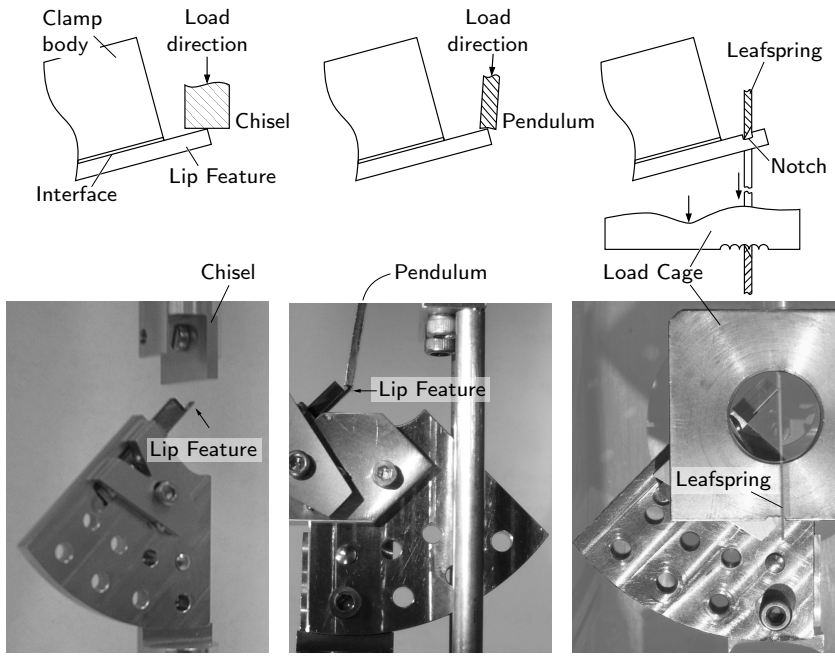
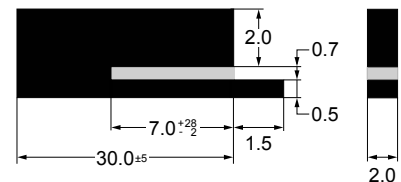


Figure 3.8: Close-Up of the load application point for the three variations: chisel, pendulum, and leaf spring (left to right).

The Chisel consists in a steel block of a width that covers the horizontal specimen movement during the delamination. Since a beam type feature of the specimen¹⁹ bends during the delamination and thus creates a relative movement of the contact point, sliding at the contact point was allowed in the chisel concept. To reduced the friction between specimen and chisel, different steel blocks were compared: A milled stainless steel surface, a polished stainless steel surface, and a

19 see page 59ff. for details of the specimen geometry. Sandwich type specimens allowed the interface testing with the MMC, and they were about 33 mm long, 2 mm wide, and 4 mm high.



polished hardened tool steel. Although promising for handling, the friction impact on the load reaction demands individual testing before each new specimen material to chisel combination. This implies a substantial effort when changing material pairings and test climates.

The Pendulum as a way to transfer load replaces the sliding concept to a beam component with two knife-edge joints. The pendulum therefore at one end has a blade feature that is rounded to ease positioning in the yz -plane. The other pendulum end touches the specimen load lip, and uses the load lip as a blade. To ease the placement on the specimen the pendulum is thus equipped with a groove. Due to the nature of the joints, the pendulum rotates when displaced during loading. The rotation must be accounted for unless it is so long that a horizontal component of the load can be neglected. The pendulum is not fixed to a bracket or device clamp, but manually placed between the specimen and a notched block connected to the machine each time before the test. This procedure slows the specimen replacement and adjustment.

The Leaf Spring follows the pendulum idea of knife-edge joints but instead can be hung to the specimen before the test. Instead of using the leaf spring in a bending manner it is loaded in tension. The leaf spring needed two changes: a notch feature in the specimen's load lip to create the cutting joint, and a reversal of load direction. The latter was achieved by a load cage that can be mounted to the loading device. The cage is equipped with notches and an observation window for crack monitoring. The notches provide the knife-edge bearings together with the leaf spring. They lead to a similar rotation behavior as with the pendulum, and thus the leaf spring must be sufficiently long to neglect horizontal load components. The leaf spring reverses a compressive load movement on the load cage, experiences a tensile load and avoids any buckling in the load transfer.

The MMC specimen design reduces the number of clamping points to one load line and a clamping area. Due to the high elasticity of the silicon and EMC the load line is brought slightly out of the interface area to a *load lip* feature.

3.3 Details of the MMC

Clamping The specimen is clamped from its side in out-of-plane direction. A free movement of the specimen's binding partners is necessary to study different loading modes between tension and shear. Therefore a *groove* in the bracket enables the specimen to not touch the bracket in the interface area. Secondly, inserting a spacer beneath

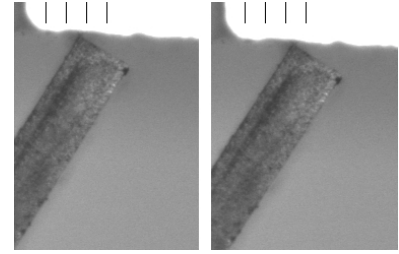


Figure 3.9: Using a chisel to load the specimen is bound to a relative horizontal movement between specimen and chisel. The seemingly rough line of the chisel (white) is an optical artefact due to different focus depth of chisel and specimen.

the specimen hinders the latter to touch the bracket below. The spacer is removed after clamping. And thirdly, a force spreader between specimen clamp and specimen avoids point loading of the specimen body, and thus EMC breakage caused by clamping. The force spreader contains a groove as well and is guided by a clearance in the bracket for positioning. A clamp fixes the force spreader to the specimen and bracket using a screw. The following figure shows the steps to clamp a specimen to the MMC setup and set the load angle.

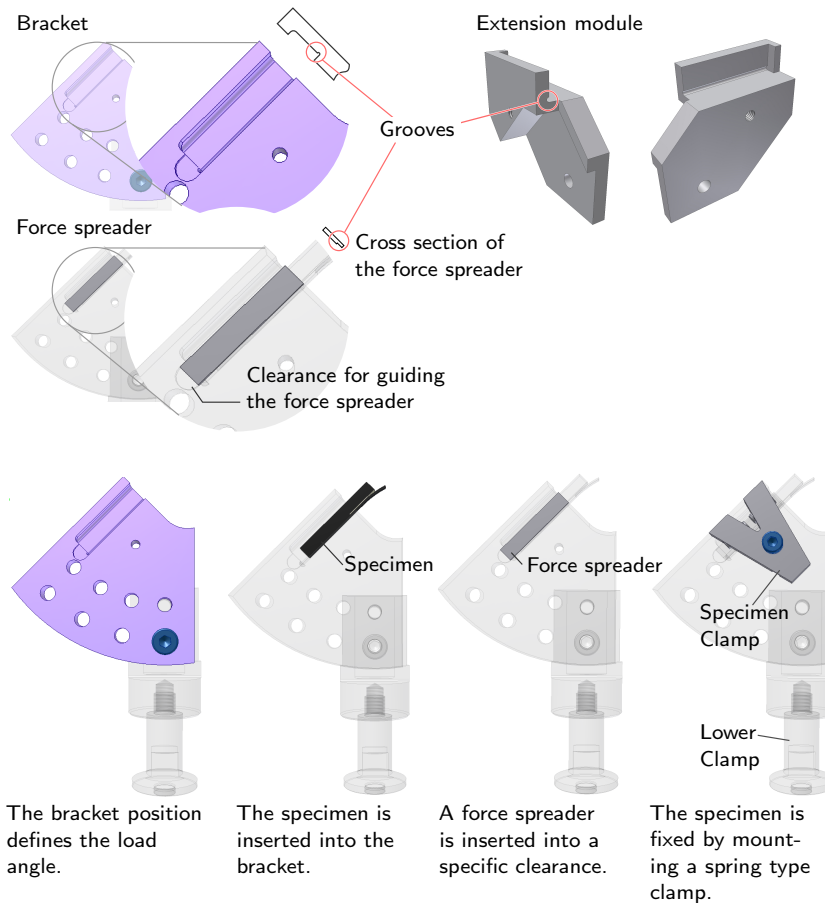


Figure 3.10: Details of the MMC bracket, which serves to set the load angle and hold the specimen. Grooves prevent a clamping of the interface area. The figure row at the bottom shows the steps of clamping a specimen in the MMC setup from left to right. The lower clamp, here only shown shaded, is mounted and aligned to the loading device before specimens are clamped.

The bracket can be fixed in 15° steps and consists of a base plate with four angle positions and specimen recess. An extension bracket allows three more angle settings with an own specimen recess. The combination of both bracket parts allows to set load angles between 0° and 90° . To define the positions well a circumferential support with the bracket's radius constrains the setting. Combined with a guidance pin, the position of the bracket can be uniquely defined at the fixhole positions.

To support a stable crack growth, the center of rotation is the approximate position of the pre-crack. After the onset of delamination the crack propagates away from the load axis, and can be observed from the flank side.

Tolerances are connected to all load device dimensions as of figure 3.7. The load direction's tolerance is bound to the accuracy of the loading device. The other five degrees of freedom are listed below.

Δx always occurs *during* delamination due to bending of the load lip.

The ideal constructive solution leaves an x degree of freedom in the contact line, such as the chisel with minimal friction. The load cage of the leaf spring loading carries notches to keep the leaf spring as vertical as possible independent of any Δx . A long leaf spring provides a small angular error but introduces a double rotation of the load transfer feature, which constrains the movement and thus mode mix range. In the simulations it is about 2deg. of mode mix. During the calibration of the loading device the Δx should be minimized.

Δy was considered in the width definition of the chisel, pendulum and leaf spring, which are at least five times wider than the specimen.

$\Delta \delta$ adds or subtracts a load angle increment. It can be kept small using a long pendulum or leaf spring. For the chisel this angle tolerance is absolute. Although it can be monitored through the crack recognition tools and compensated in the calculations, the load cell sensing might be inaccurate due to the side component.

$\Delta \gamma$ should be calibrated through the loading device. It was not compensated by constructive means in the MMC.

$\Delta \zeta$ is manually aligned during clamping before the delamination test.

The relative positions of specimens load lip and pendulum or leaf spring are definite during the experiment. For the chisel concept ζ is a degree of freedom at the contact point.

The corresponding specimen fabrication is described in the next chapter (page 45), afterwards the settings for running the experiment with the MMC setup (p. 65), the fracture mechanical results (p. 80) and aspects of interpretation (p. 89).

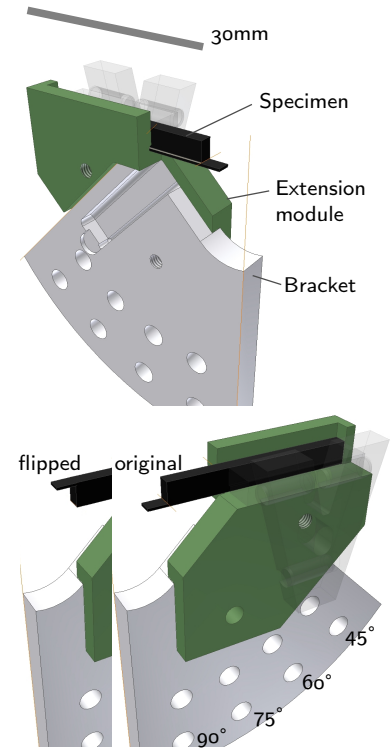


Figure 3.11: A bracket extension allows load angles of 0° to 90° and decreases the size of the bracket for device compatibility. Flipping the specimen and loading direction can extend the load angles beyond the 90° range.

4

Fabricating Delamination Specimens

The specifics of the Si-EMC interface were listed on *page 30*, and the problems to be overcome on *page 31*. This chapter shows that it *is* feasible to make such delamination specimens. It discusses the demands for a specimen (*below*), the fabrication steps (*page 48ff.*), and design rules (*page 59*).

4.1 Demands on a Specimen for the MMC

Design and processing are restricted¹ by various aspects, namely risking accidental fracture, clamping, predicting mode mix, the material properties, the ease and accuracy of use, the applicability of the investigations, the device load range, fracture mechanics, and the processing itself. These aspects influence the specimen layer composition, the layer dimensions ($h \times l \times w$), the clamping zone, the loading zone, the constituents processing, and the specimen preparation.

Layer Composition

Every specimen needs the interface to delaminate and zones to clamp and apply the load at. If two layers of material form the specimen – simpler to mold than three or more layers – two ways of clamping may be considered. Either the silicon layer is clamped and the EMC layer is loaded, or vice versa. But due to flaws from silicon processing the brittle silicon might fracture before any delamination with the slightest mis-alignment or mis-orientation. Consequently either the delamination setup needs the highest accuracy in alignment and orientation, or the clamping and load application zones should be made of EMC, and due to their very definition be separate zones. In other words the specimen should consist in three layers, two layers of EMC embedding one layer of silicon. And there is another motive for a three-layer design.

Three layers can be designed symmetrically or close to symmetry. And although stresses are then higher than in a two-layer configu-

¹ The demands on specimens are closely tied to demands on the delamination setup (see *page 33*). Since the listed items depend on each other, the following pages are mostly prose.

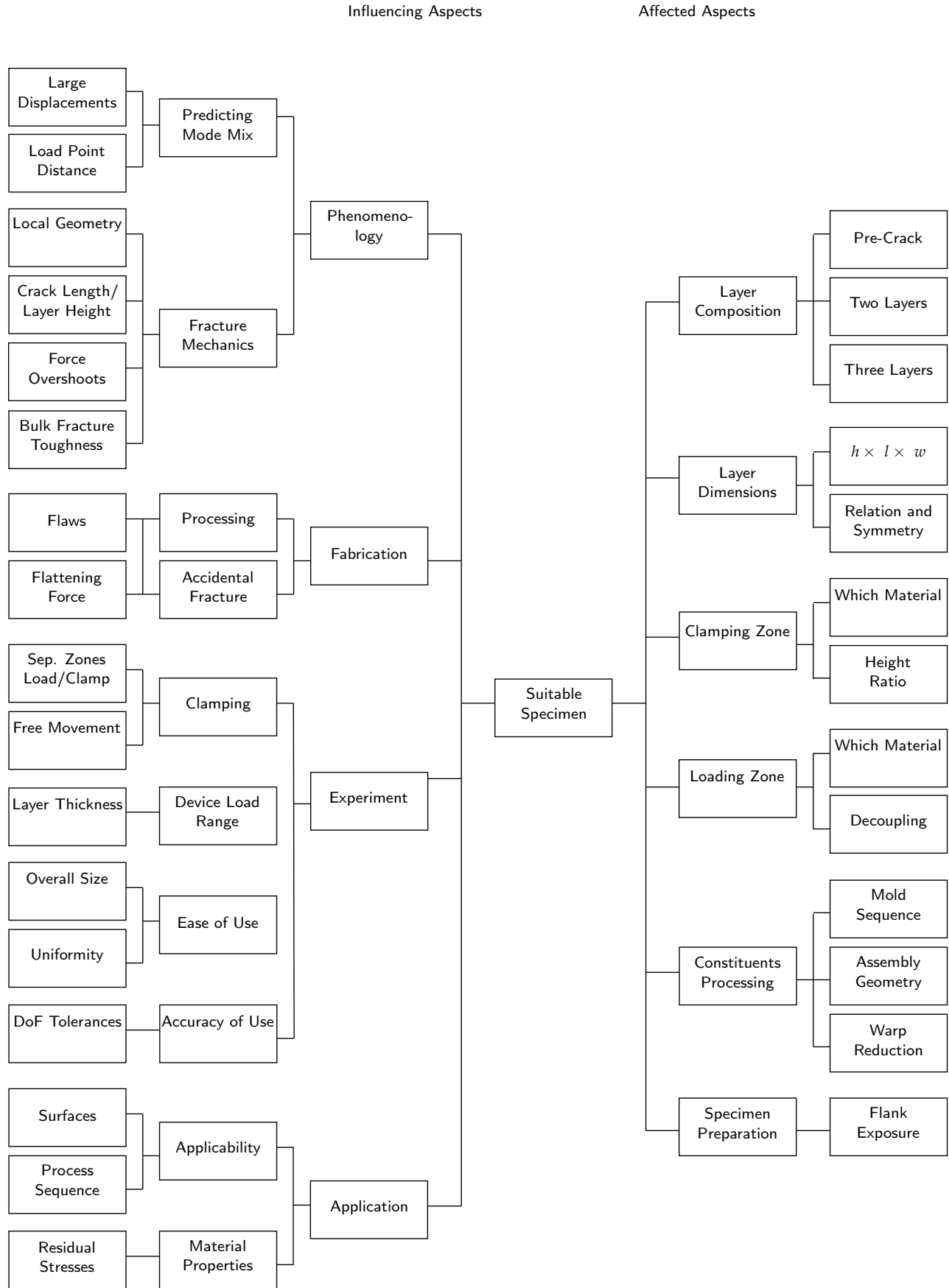


Figure 4.1: Various demands on specimen design and processing.

ration, the semi-finished parts become flat for processing and need not to be forced flat – a major reduction of accidental fracture risk. This does not keep the residual stresses low, as described on *page 31*, and they must not be reduced by changing processing conditions, because the specimens are thought to model such conditions. The CTE mismatch and cure shrink of the EMC must be equivalent to fabrication conditioned products. Yet the stress effects in warpage *can* be minimized, and additional stresses can be kept low in later processing such as singulation on a dicing chuck. Just molding and shaping three layers however will not guarantee a delamination, especially since the very materials and processing were originally chosen to not delaminate.

If there is no weak point, no pre-crack, the load force will overshoot. It is then not given that the interface fractures at the designed singularity, or even that the *interface* fractures. Secondly an initial reference state is not well-defined because the crack initiation is then flaw dependent, that is each specimen cracks at a different initial load. A pre-crack layer must thus be included (see *page 54*) in the fabrication process.

Layer Dimensions

Load Lip The load lip dimensions, given that a specimen had a load lip feature, have an impact on accidental fracture, on the mode mix and the load range. They should be chosen such that the load lip stays intact during the experiment. With increased lip length and bending the horizontal tension at the top side of the lip increases, and with it the shear load at the crack tip increases. Simultaneously this represents a tensile load on a potential bulk crack running into the lip. If the load lip is too thin, the lip bulk material cracks instead of the interface. If the load lip is too thick, the layer to delaminate bends with the load lip in realistic force ranges. Before the cracks occur, the actuator reaches its load maximum or the control loop is at its limit.

Height, Length, and Width If the specimen is flat, that is low in z -orientation, it has two negative consequences. Any loading results in substantial bending of the whole specimen, because the area moment of inertia is small. Such bending dominates the mode mix at the crack tip because of an increasing horizontal load component, and thus diminishes the impact of the load angle setting. Secondly a then necessary clamping is normal to the interface, and limits a free movement of the load lip. To prevent both, the specimens clamping body must be designed higher than the load lip feature.

The specimen should be as wide as possible for the alignment of the loading feature, since the angle γ becomes difficult to control the

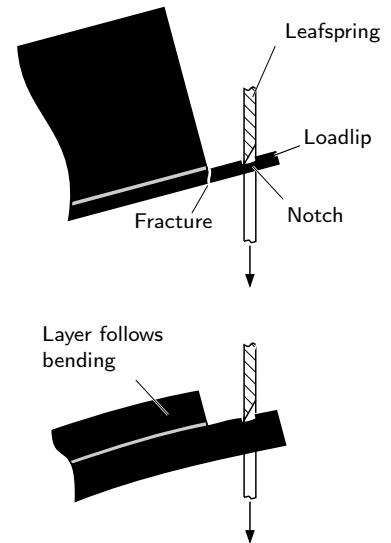


Figure 4.2: Risk of bulk fracture in too thin load lips, and no delamination in too thick load lips

thinner the specimen is. It should be kept as thin as possible for lowering the risk of pre-test fracture due to an increased residual stress curve. The loaded point or line should be close to the crack tip because longer distances create additional shear stresses in the crack tip. Due to the different material properties, loads can be transferred parallel to the interface through the EMC at high shear loads. This should be avoided because the desired loading of the interface decreases as a share of the total loading.

The layers should be uniformly high to simplify the geometry for numerical modeling, and to provide equal conditions for different stages of one delamination. This includes maintaining a straight placement of silicon during all steps of molding.

Specimen Preparation

If the load setup requires a crack monitoring such as the MMC setup (page 33), and if not using through-layer methods, such as infrared interferometry,² the specimen interface needs to be observable, that is exposed to the monitoring system and cleaned from any fabrication residuals. Both the exposure and the cleaning should be done without additionally stressing the interface. (see page 58)

4.2 Two Molding Technologies: The Fabrication Steps

Fabrication Costs The cost of a specific mold tool are easy to justify for an established specimen, for which the experimental procedure is clear, and for which the vicinity to fabrication conditions can be guaranteed. The situation for the Si-EMC is different. Before this work it was unclear in which way the interface can be successfully delaminated. Designing, Failing and Re-designing several mold tools would have devastated the project financially. Thus, to achieve a running specimen, the existing fabrication tools had to be modified in minor ways and accompanied by processing that would not alter the material properties. Another motivation to choose this path was to provide a method that can be copied without a lot of effort, since the data on such interfaces is scarce.

The MMC delamination specimens were fabricated in two ways, using the major package molding process – *transfer molding*, and the somewhat younger *compression molding*, which is used in the embedded wafer level ballgrid array package (eWLB).³ In both methods a defined quantity of EMC is inserted into the tool before the very molding step.

Compression molding For compression molding dies are placed on a taped carrier in a desired reconstituted pitch. The carrier is put in



Figure 4.3: A notch below the interface decouples the load lip from the clamping body.

² Liechti 1993

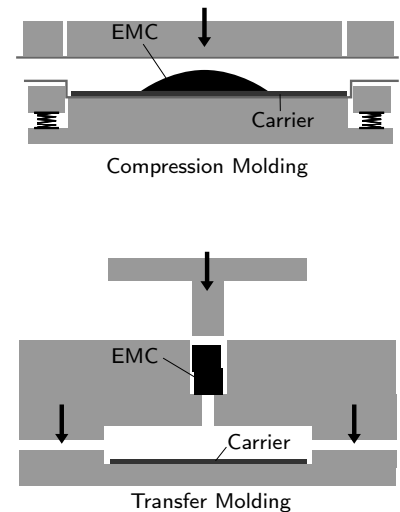


Figure 4.4: Two ways of molding delamination specimens. Partly adapted from Ohori 2010.

³ Brunnbauer et al. 2006a, Meyer 2007

a cavity, and for molding a liquid or powder compound is applied or injected depending on the chosen process. The resulting mold wafer containing dies can be handled in further wafer processing steps for instance to build up a redistribution layer. For this work a liquid compound was applied on the carriers before closing the tool, and only dicing followed the molding step.

Two aspects deserve more attention before detailing the individual steps. Two parts around the silicon must be free of molding compound during the experiment: the flank and the front. Yet the silicon is completely surrounded by EMC after molding and the mere position of dies is invisible then. Flank exposure is detailed in an own paragraph on page 58 and serves crack monitoring. The flanks of the compression molding specimens were exposed by dicing through inlays and molding the specimens at the desired width respectively. The front of the die needs to be exposed because the pre-crack layer is only applied on one of six die surfaces. In the compression molding specimens such a gap for exposing the load lip is also created by dicing, and by dicing a finger structure concluded by an inlay. All these inlays consist of a double layer of the adhesive tape used to stick the silicon dies on the carrier. The final thickness of the inlays was 200 μm . Using the compression molding demands to apply another mold layer by a second mold step, or to rotate the dies during pick & place by 90° and mold the specimens directly to desired width. Both the two-step-molding and the die-rotation require considerable more effort than in eWLB molding. For this reason the silicon should be surrounded by EMC after one molding step only, which was tried using a transfer molding process, and which is described in the next section.

The process sequence for compression molding was thus as shown in Figure 4.5 The dies were placed in a 10×4 pattern using a flip chip bonder.⁴ The molding at 120°C took 600 seconds.⁵ After the second mold step the body was post mold cured (PMC) for 1 hour at 150°C under non-conditioned ventilation.

4 Datacon 8800 FC Quantum

5 Molded using a Yamada MZ 625

Transfer molding Unlike in compression molding the die carrier used in transfer molding remains in the final package. The EMC is transferred from a pot under high pressure by a plunger into the tool cavity through a sprue. But a die carrier made of a third material was to avoid in interface specimens. All specimens molded with an additional carrier material failed before the very testing. Figure 4.6 shows the approach to make such a specimen. In this case copper foils were added as a silicon carrying structure.

To obtain Si-EMC specimens bearings were made from cured EMC to carry the silicon and hold it in place. Dicing them from EMC ensured the same material properties and did not demand reuse. A

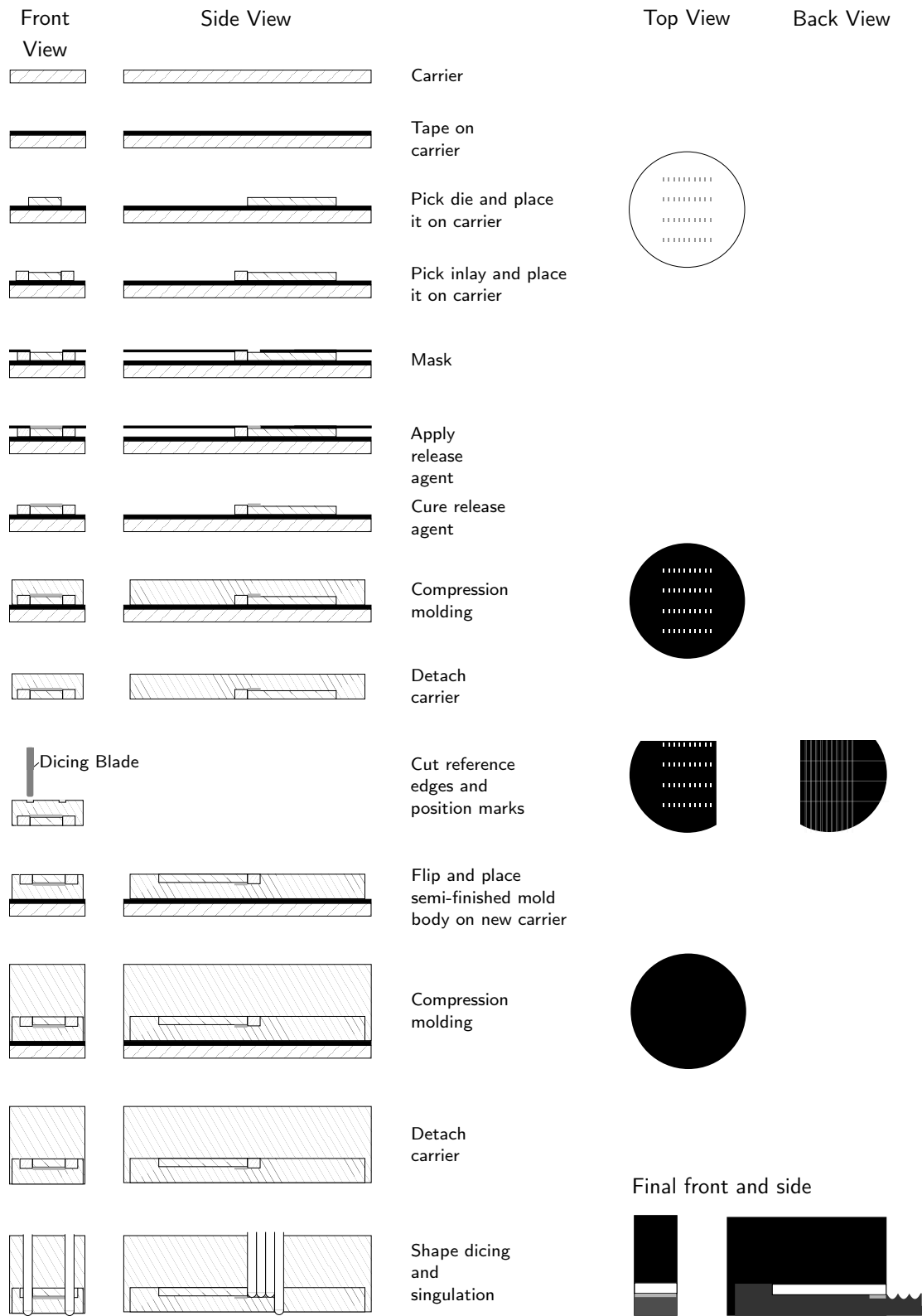


Figure 4.5: Fabrication steps in compression molding. (Not to scale)

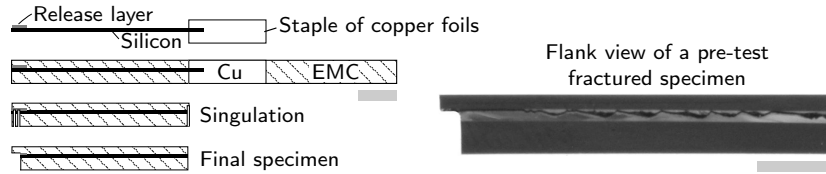


Figure 4.6: Adding a carrier material was tried with staples of copper foils. The specimens fractured however before dicing. The gray bars are 5 mm.

$3 \times 100 \times 100 \text{ mm}^3$ mold cavity with a top central transfer sprue ensured appropriate dimensions. The molding at 180°C and a pressure of 200 bars, took 180 seconds. After releasing the molded body from the tool it was post mold cured (PMC) for 4 hours at 175°C under non-conditioned ventilation.

Because the bearings had to be made before molding, the process steps were as follows.

- molding of bulk EMC bodies
- shape dicing the bearings
- applying local release agent to silicon
- assembly of silicon strips to bearings
- molding
- grinding and polishing
- shape dicing and singulation

During transfer molding the silicon strips cannot be held in place without covering part of the silicon. Longer strips prevent the bearings from masking large parts of the silicon. They cause larger absolute warpage, which is a problem for sawing depending on the chosen orientation. This effect is increased by curvature of the strips due to asymmetric spread of the liquid EMC. When entering the cavities on one side of the silicon, the EMC bend the strips the other cavity side. Because the bent state is frozen into place during curing and cool down, this increases residual stresses substantially and renders later separation of the specimens difficult.

Among the two options to position the silicon strips in the cavity – flat and standing – the one-side sprue suggests a perpendicular orientation of the silicon as follows. The orientation prevents the mold flow to enter one sample side earlier than the other. The bearings made from cured EMC material hold silicon strips in place as can be seen in Figure 4.7. Above and below the silicon remains a gap of 0.5 mm allowing the mold flow to pass. The cross section of the assembly shows double symmetry and therefore avoids warpage due to CTE mismatch and cure shrink.

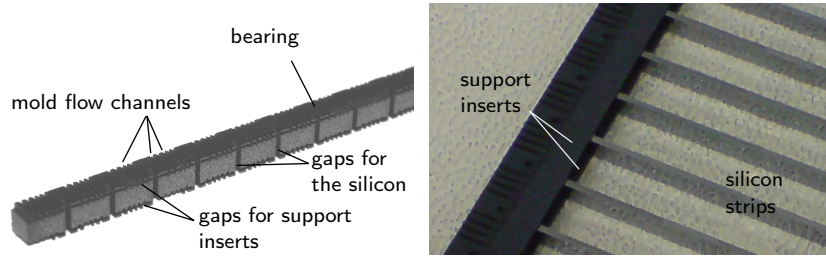


Figure 4.7: The silicon strips are held in place by bearings shape diced from cured EMC.

Because the liquid EMC is transferred with considerable pressure, the bearings should be fit well into place. The impulse of the EMC can displace the bearings and let the silicon strips flow out of place. The strips can also break and affect other samples that were still in place, as shows Figure 4.8.

The bearings are sized to the nominal height of the mold cavity, so that the thermal expansion at mold temperature oversizes and traps the bearings.

Both sides of the semi-finished mold body are ground before singulation. One surface was protected with an adhering foil before grinding the second side. The foil prevented micro cracks in the already exposed interface. To further reduce this risk the grinding grain size was reduced when reaching a height above silicon of about maximum EMC filler size. The subsequent dicing steps defined the final geometry of the specimens.

4.3 Assemblies

Silicon Placement A symmetric cross section creates a flat body for further processing, which reduces additional stresses. The symmetry can be achieved by placing the silicon strips in the vertical center with the help of bearings instead of direct placement into the cavity.

From a top view perspective, a symmetrically silicon filled cavity leads to a uniform mold flow. No channel is preferred and filled first, just as in the design of productive lead frames. Thus the silicon strips are not bent by an overpressure from a first-filled channel.

In compression molding, the silicon strips need to be sufficiently small for an automated pick & place process. This concerns also the aspect ratio of the die sides, long strips are difficult to assemble. When fabricating die flank interfaces, the silicon strips had to be flipped *after* placement, because the standard nozzles cannot pick up silicon dies from their flanks.

Bearings design The most essential function of the bearings is to hold silicon strips in place during a transfer mold process. Thus such

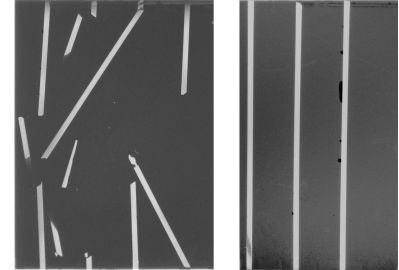


Figure 4.8: Silicon strips broken by the mold flow during molding (left) and intact (right). The molded body is shown in top view after grinding and shows the full length of the 25 mm silicon strips. The intact body (right) shows some voids at the interface of the third silicon strip.

bearings must constrain the vertical and horizontal movement of the strips. Vertical gaps take up silicon strips in a defined distance to each other. The distance is given by the layer height plus the singulation kerf. Horizontal grooves keep the silicon strips in vertical center of the assembly, that is a little above the bottom and a little below the ceiling of the cavity. Into these grooves inserts were placed to let the silicon strips rest on and limit their movement to the top.

Mold flow channels were introduced in three areas: parallel to the silicon strips at the bottom and top of the bearings, and at the perpendicular edges of the bearings that face the corners of the mold cavity. Together they open a flow path between sprue towards the suction channels in the eight outer corners where air is constantly removed during molding. Distance strips of mold compound were glued in the outer gaps of each pair of bearings to maintain the distance during silicon strip assembly. They finish their task after placing the assembly in the already hot mold cavity. Afterwards the properties are not fit to take up any additional loading and protect the silicon strip assembly. But once the cavity closes for injection, the bottom and ceiling of the cavity hold the bearings in place. Once the bearings reach the mold temperature fully they would deform under the pressure exerted by the cavity ceiling.

The bearings had the following dimensions: One bearing strip contained 21 vertical gaps for the silicon strips, which reached 1 mm into the bearing. The silicon pitch was 4.2 mm. Two horizontal grooves for 300 μm thick supports started from the same side as the gaps. The supports secured the vertical Si position above and below. Between the silicon strips in each clearance, 1 mm deep mold flow channels were introduced on four gates, that is above and below the bearing. The silicon strips were diced to $2 \times 26 \text{ mm}^2$. The strips define the distance between the bearings in an assembly, as shown in Figure 4.9.

4.4 *Materials Involved*

Wafers The silicon wafers used were $\langle 100 \rangle$ orientation and 500 μm thickness to investigate die backside adhesion and $\langle 110 \rangle$ orientation and 900 μm thickness to investigate the die flank adhesion to EMC. The $\langle 100 \rangle$ oriented wafers were chosen for they are most commonly used for electronic chips. The $\langle 110 \rangle$ orientation was chosen because it was rapidly available in a thickness of more than 750 μm . The wafers had a native oxide layer of below 6 nm thickness measured in an ellipsometer. The wafers were treated for pre-cracks as described on page 54 onwards.



Figure 4.9: Assembly of silicon strips placed between two bearings. Here shown for a gold release layer at the center of each strip, for 4PB use.

Molding Compounds For each of the two molding technologies a specific compound was used. The transfer molding compound was of the CEL 92xx series⁶, and the compression molding compound was a liquid compound of the T69x series.⁷ Both compounds are highly filled thermosets, with more than 80 vol% spherical SiO₂ fillers. The viscoelastic and thermal expansion properties were measured using DMA, TMA, and PVT equipment. (Dynamic Mechanical Analyzer, Q800 TA Instruments and Eplexor GABO Qualimeter, Thermo Mechanical Analyzer, Q400 TA Instruments and Netzsch TMA 202, Pressure Volume Temperature measurements, Gnomix high pressure dilatometer) The measurements were carried out in laboratories of Delft University of Technology, The Netherlands and Fraunhofer Institute of Reliability and Micro-Integration Berlin, Germany. Partly these experiments were done and reported by colleagues in parallel projects or requests.⁸ The cure shrink was estimated elsewhere⁹, and neglected throughout this work for all data analyses because no significant influence on the fracture properties were expected.

4.5 Pre-Cracks

Sharp and Reproducible Pre-Cracks

A *sharp* pre-crack knows six qualities: the release of previously bonded materials, uniformity across the interface, a tiny point of intersection, a low slope towards the opening, and reproducibility.

Ideally the pre-crack is an existent crack at the very interface to delaminate. This means the now cracked area was a bonded area before – a closed interface. Therefore ideally the pre-crack should form by opening a closed interface. If the interface toughness is low, such a release of bonds can be achieved by loading under tension while forcing the part to investigate closed in place. This method is most suitable for ductile materials and rough surfaces.

When bending a ductile material partner, such as copper alloys, the displacement can be driven so as to reach plastic deformation of the layer without fracture. Silicon and EMC show a rather small displacement at considerable load due to their high elastic modulus. Such brittle materials render it hard to arrest a pre-crack, before breaking the sample. Rough surfaces are not fully covered by inlays, and even a perfectly shaped inlay would not create a real pre-crack.

If the interface cannot be easily opened, bonding must be prevented in the first place. This can be done in two ways. Either a preventive layer covers one surface or some sort of non-bonding inlay separates the bonding materials. Examples for the preventive layer are gold or wax in case of epoxy based molding, and an example for an inlay is

6 Hitachi Chemical Co.,Ltd.

7 Nagase ChemteX Corp., specified in the datasheet by Ohori 2010, with reference to Brunnbauer et al. 2006b.

8 Patel et al. 2008, Jansen et al. 2008, Walter and Hartmann 2010

9 Beer 2005, Patel et al. 2008

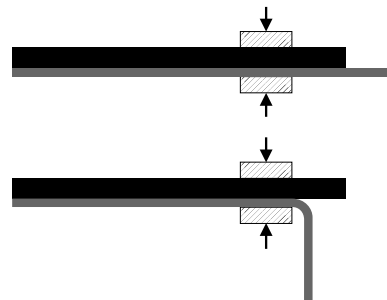


Figure 4.10: Some delamination specimens with one ductile material layer can be clamped and manually pre-cracked, such as done by Xiao et al. 2008b.

PTFE foil. An applied thin film adapts to a given surface roughness and thus mimics a pre-crack best. It also adds a process to fabrication, important to keep in mind for product relevant fabrication conditions.

An inlay prevents a tiny point of intersection between the upper and lower crack flanks. Instead it adds a corner in crack tip vicinity that acts as a stress concentrator. From such corners a bulk crack starts easily, as shown below in Figure 4.11 and in Figure 4.16 on page 57. The pre-crack slope from the crack tip towards the opening should be as low as possible to mimic the singularity of a real pre-crack.

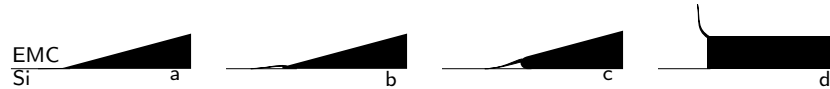


Figure 4.11: Different edge shapes of an inlay or release layer edge: A tip shape (a) creates a stress concentration at the very interface, a slightly rounded tip (b) may lead to an initial bulk crack, but the crack turns to the interface after short crack length, this is true also for larger tip radii (c), but not for inlay tips whose stress concentration points are distant from the interface, such as a two-edge rectangular shape (d).

Reproducible pre-cracks that are uniformly distributed across the interface allow to compare experiments with equal loading slopes and to rapidly extract data for the numeric modeling. If the pre-crack is not well formed, the crack might initiate at a random spot. Figure 4.12 shows an overshooting load reaction that then usually is the result. The slope of force increase differs from other experiments that are carried out under the same conditions.

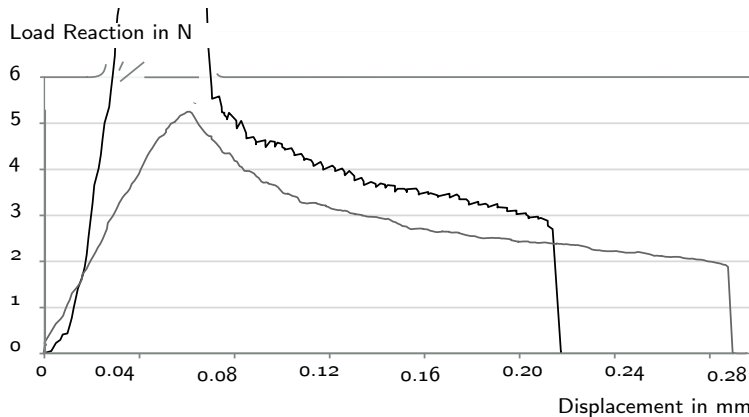


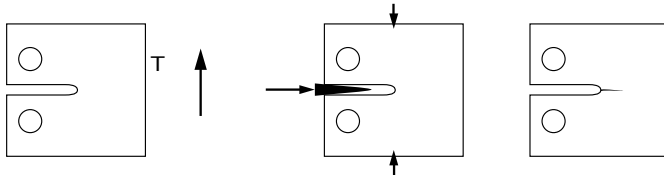
Figure 4.12: Typical overshooting load reaction of a specimen without a pre-crack.

CT-Specimen Pre-Cracks

To study the pre-cracking with less precious samples, different methods were tried using CT-specimens. Table 4.1 shows the pre-cracking methods tried.

Means	Temperature	Pre-crack length	Result
razor blade	ambient	n.a., unsteady	fail
2× razor blade	ambient	250 μm, unsteady	fail
expansion insert of Al	200/150	n.a.	fail
exp. insert Al, razor blade	200/150	n.a.	fail
exp. insert PTFE,	200/150	n.a.	fail
exp. insert PTFE, razor blade	200/150	n.a.	fail
wedge of Al	150	n.a., unsteady	fail
chevron notch + razor blade	ambient	500 μm, unsteady	fail
steel wedge with a low slope	150 precondition.	entry dependent	success
local heating behind notch	loc. 200	n.a.	fail

The CT-specimens were milled from cured EMC molds. Such a large EMC mold, usually made for measuring the cure shrink of the EMC after cool down, is shown in Figure 4.13. Pre-cracking the CT specimens by entering a steel wedge with a low slope allowed repeatable bulk fracture experiments. The figure below shows the principle of driving a wedge in the notch of a CT-specimen. The CT specimen was heated above its glass transition temperature for 20 min. Immediately after taking the sample out of the oven, it was clamped and the steel wedge was driven into it. But the pre-cracks were



not reproducible to a length difference below 1 mm, as can be seen in Figure 4.15. This experience from pre-cracking homogeneous EMC specimens, preferably at room temperature when the material is brittle, underlines that the tolerances of reproducible pre-cracks are substantial and lay above the desired measures, when preparing the samples by hand alone, such as done in interface specimens with a ductile material partner and a lower interfacial toughness, where opening is simple. Thus it was important to establish at least a *semi*-automated method to create a reproducible, sufficiently sharp pre-crack.

Different Methods for an Interface

Any attempts to directly pre-crack a clamped specimen derived from a productive sample failed. The following variations of introducing a pre-crack were tried.

Repeating the PTFE positioning turned out to be difficult, because the mold flow displaced the PTFE strips. Despite the problems of

Table 4.1: Pre-crack methods tried in CT-specimens.



Figure 4.13: Four CT specimens milled from an EMC plate. One CT specimen is 25 mm wide. The dimensions followed the geometry defined by Walter 2003.

Figure 4.14: Wedge Pre-Cracking.

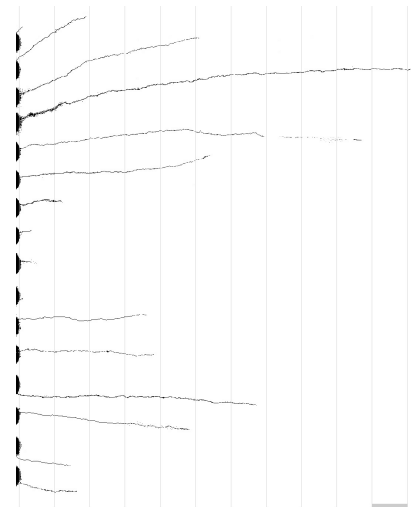


Figure 4.15: Pre-crack lines of 16 CT-specimens sorted by diverging direction. The cracks became visible by means of penetrating fluorescent dyes. To ease comparison the images were cropped, inverted and the notches erased. Cracks ran left to right. Grid pitch 1 mm.

Layer applied	Thickness	Slope of h/l	Result
PTFE foil	20.00 μm	step	EMC crack
release agent, mask+spray	0.50 μm	n.a.	contamination
release agent, brush+cure	0.60 μm	1.33/100	success
gold in Ti-Pd-Au deposition	0.65 μm	0.33/100	partial success

Table 4.2: Pre-Crack methods tried in the interface specimens. All sub-micron layer thicknesses were determined by AFM. The release agents were ACMOS 82-2405, and ACMOSAN 82-6007, ACMOS CHEMIE GmbH & Co.

aligning the non-adherent PTFE foil, those specimens with an acceptable foil insertion still cracked through the EMC layer. The second singularity created by the inlay corner can be seen in the microscopic photos in Figure 4.16. Because the EMC corner is loaded in a close to mode I orientation, instead of delaminating these specimens fracture through the EMC.

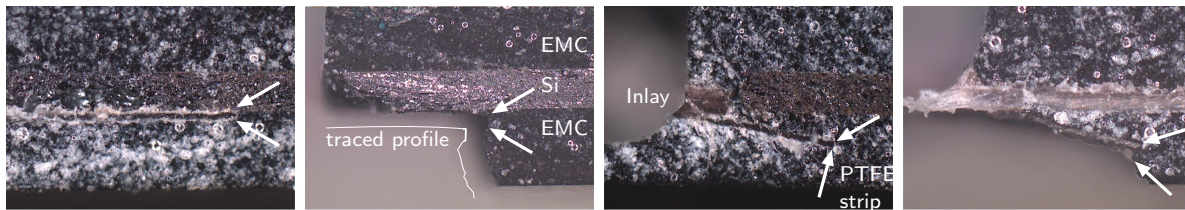


Figure 4.16: Two examples of a EMC crack starting from the edge of a PTFE strip. The arrows indicate the corners and thus singularities formed by the inlay. The additional singularity is most obvious in the second photo from the left, where the PTFE was removed.

The release agent remained the method of choice, although the layer lengths deviated by $\pm 300 \mu\text{m}$ due to the manual application. Using gold as a release layer was tried by a Ti-Pd-Au deposition. As foreseen the layer showed poor adhesion to the EMC, but the crack kinked into the EMC only 200 to 800 μm after the pre-crack layer. Thus in both molding methods a pre-crack layer was formed by applying curable release agent on the silicon strips. Figure 4.17 shows an AFM scan of the cured release layer.

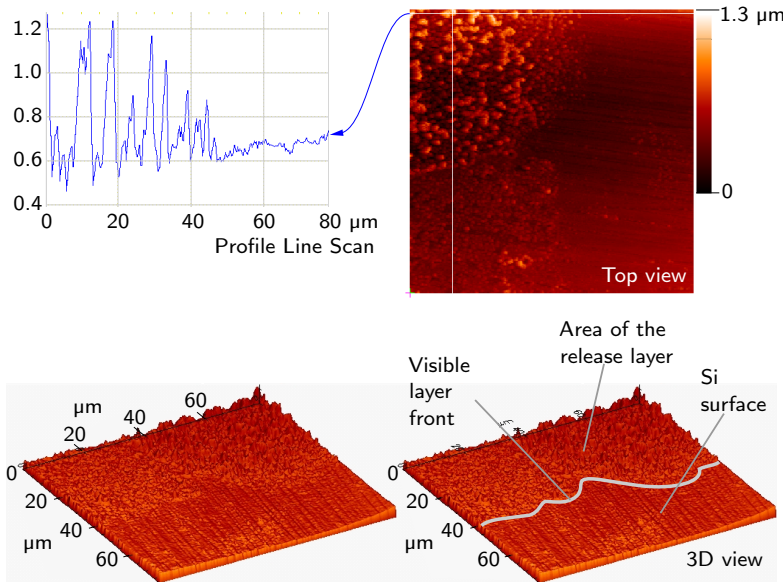


Figure 4.17: AFM scan of the edge of the cured release agent. The top row shows a line profile and its corresponding position in the total scan, the bottom row shows a 3D view twofold, with and without labels.

Pre-Crack Design for Transfer Molding

The bearings that hold the silicon strips in place cover part of the silicon. Because the EMC of the bearings is already cured before assembly, toughness in that region will not be reliable. The interface will either have no bonds but air trapped, or it will have an epoxy-rich flash layer. That region should not be tested for adhesion, and any pre-crack layer should extend to the silicon surface free from bearings.

Adjusting Imperfect Pre-cracks

In some specimens the mold compound could enter a gap between the silicon front and the load lip inlay. Although the pre-crack was there, the interface could not open and was held in position by this tiny amount of EMC in front of the silicon of about 100 to 300 μm . It was possible to remove such a thin layer manually with a serrated razor blade, or if the flash was thin by loading the specimen first in a $\alpha = 0^\circ$ load angle setting, and interrupting the loading immediately after the first force drop.

4.6 Flank Exposure

Exposing the specimen flank for monitoring access was considered in detail because the silicon can be hidden by the EMC, and dicing through two materials at once bears accidental fracture risk.

If the mold cavity holds one specimen a time, few processing is necessary after molding. But because only a *tapered* mold cavity flank allows an appropriate mold release, such specimens would have a tapered flank. Such angles are not negligible in the desirably thin delamination specimens. The flanks could be ground flat, but doing this with a single specimen is time consuming without elaborate instrumentation.

To prevent the tapered flanks, bigger cavities can embody several specimens a time. But the specimen flanks must be re-exposed. The mere exposure process is especially difficult for the compression molding, because the silicon is completely buried and the flanks are perpendicular to the wide mold body planes. For the two-step molded specimens, the position lines were sawn after the first mold step.

Dicing through the attached layers of silicon and EMC at once can introduce flaws and micro cracks into the material partners, foremost the silicon. Dicing can also completely delaminate the specimen, as in the specimen shown in the margin, Figure 4.18. Consequently the silicon is surrounded by EMC at its flanks, which have to be re-exposed.



Figure 4.18: Specimen delaminated from its neighbor during dicing.

We tried three ways of flank exposure: Dicing through protecting inlays (compression molding), grinding the specimens down to silicon width (transfer molding), and arbitrarily molding the specimens at the desired width in the first place (compression molding).

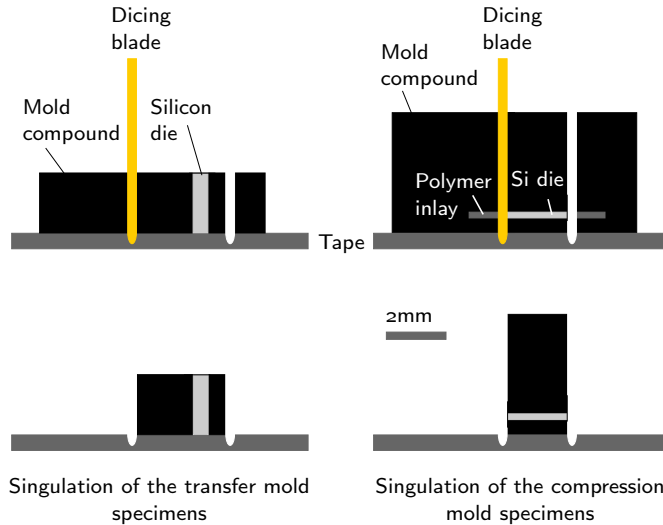


Figure 4.19: After each of both molding technologies the specimens are separated by dicing through one material only.

The inlays touch the die flanks during molding as placeholders, and they are attached to the carrier the same way as the silicon dies. They can easily be removed later and allow a wider tolerance of dicing beside the die, thereby avoiding micro cracks and epoxy residuals. Molding the specimens at the desired width failed for transfer molding, but succeeded for the one-step compression molding to final wafer height with 90° rotated dies.

After the flank exposure by singulation, the specimens were polished, removing eventual epoxy residuals on the surface and providing an optimal surface for crack recognition described on *page 70*. The polishing was generally sufficient for crack recognition, and experiments with additional color coatings (white pattern lacquer) did not improve the results.

4.7 Design Rules

This section describes the limits for the before mentioned demands and processing.

Solution Geometry to the Before Mentioned Demands

The here suggested interface sample consists of a silicon layer, that is embedded in two layers of EMC. The two EMC layers may join at one side behind the silicon layer, where the setup clamps the specimen at

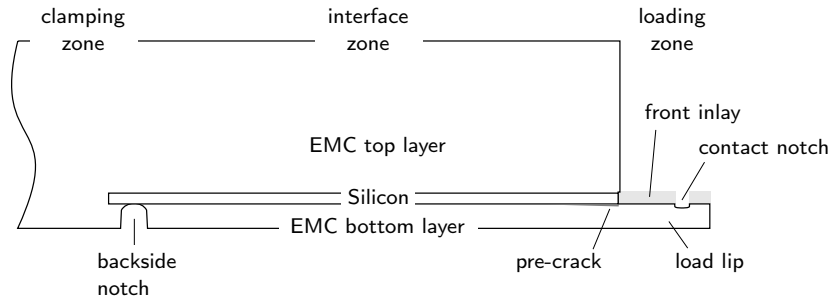


Figure 4.20: The parts of the Si-EMC interface specimen.

the top EMC layer. At the other end, the die front of the specimen the lower EMC layer extends beyond the interface body. At this part of the specimen – the load lip, the setup transfers the load during the experiment.

To avoid EMC fracture and to keep the stress level low, the load lip should be thickened, widened or shortened. We allowed the load lip a length of 0.9 to 1.5 mm beyond the interface. Shorter distances than 0.9 mm restrict the lead spring movement. The lip width consistently matched the silicon width and varied between 0.9 and 2.0 mm. Narrower dies required too extensive handling. Wider samples tend to break before delamination. Further they do not align well with the setup loading parts such as the leaf spring without elaborate changes. The load lip height remained intact between 500 and 900 μm at silicon heights of 185, 500, and 1400 μm . Estimating the minimal thickness from the EMC yield strength gives also about 500 μm .

The interface lengths including the pre-crack were 5 and 7 mm in compression molded specimens, as well as a full 25 mm in transfer molded specimens. For the silicon loading attempts the interface length was 6 of 7 mm.

To prevent the movement of the load lip relative to the loading feature, the load lip contained a contact notch. This feature eases the positioning of the sample in the loading device. A thin chisel in form of a leaf spring inserted in the notch creates a knife-edge joint that reduces the movement and hence friction influences to a minimum. The setup was modified accordingly to maintain the orientation of the sample to the observation camera and the loading actuator. The loading mode of the driving equipment remains compressive.

Another notch was introduced at the lower end of the interface. This release notch avoids a compressive load transfer in the molding compound that occurs at higher shear load components at progressed delamination. The position of the notches can be seen in Figures 4.20 and 4.21.

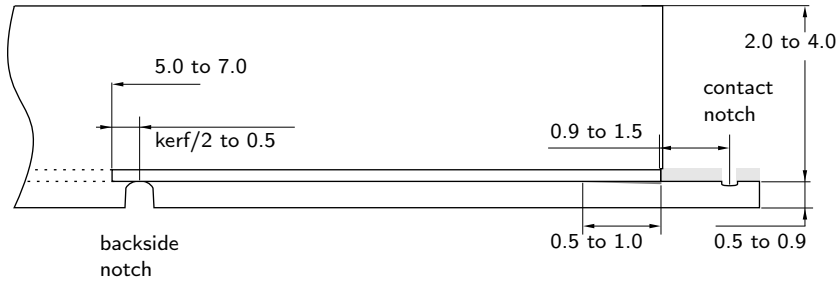


Figure 4.21: The measures of the Si-EMC interface specimen.

Figure 4.22 shows the difference in load reaction. The missing increase of force during the final delamination stage allows the interpretation of a larger load reaction section. Also the linear force increase before the load lip fractures is not present in the lower graph. Since the notch replaces the molding compound below the interface end, only a very thin bulk layer remains. Its loading before fracture does not cause a substantial force increase.

The relation between lip height and body height above the chip is a compromise: The body above the silicon demands sufficient height for clamping and for resisting a pure bending that would avoid any delamination. A lateral clamping allows the interface vicinity region to move freely. The height was at least 2 mm and max. 4 mm. Higher specimens demand different clamp designs and different dicing equipment.

The length of the interface can reach the specimen length but should be at least 5 mm. This leaves enough space for pre-crack and notches, and gives enough data points to analyze. For sufficient clamping space all compression molded specimens were 30 ± 5 mm long and all transfer molded specimens were 25 ± 1 mm long. The die thickness and the interface area of the specimens remain at package scale.

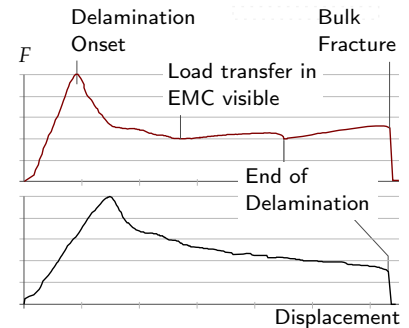


Figure 4.22: Load reactions of specimens with backside notch (lower graph) and without (upper graph).

	Typical Interface length and area	mm	mm ²
4PB sample		60	600
ENF sample		60	600
MMB sample		33	33
MMC sample		7	14

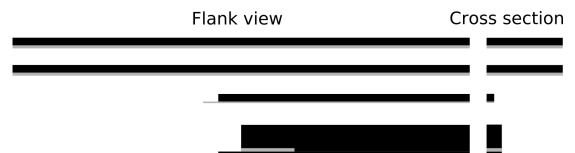


Figure 4.23: The MMC specimen dimensions in comparison with typical dimensions of the MMB, 4PB and ENF specimens.

Suggested re-design of the 4PB

To enable a benchmark test on a different setup and to enable a rapid evaluation for one mode mix setting, it was desirable to try a four point bending design for the Si-EMC interface. To prevent

pre-test fracture of the specimens due to asymmetry, the intended bi-layer specimen was also equipped with a third layer. The fabrication followed the MMC specimen in transfer molding until singulation, except for the pre-crack layer that was applied centrally on the Si strip. The specimens were notched to separate the zones of load application and to ease the pre-crack opening. The design is shown in Figure 4.24.

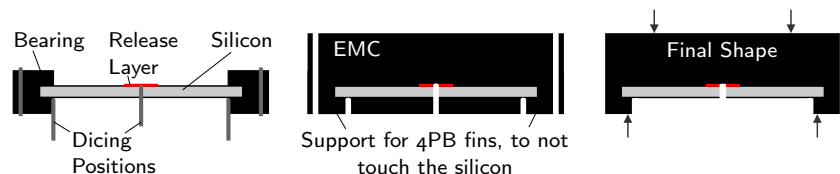


Figure 4.24: Steps to a 4PB specimen using the same transfer molding bearings as in the MMC specimens.

An appropriate 4PB apparatus for the miniature specimens was designed after the first delamination success in Si-EMC specimens by Ritter.¹⁰ The following photos in Figure 4.25 show a successfully initiated delamination by four-point bending a Si-EMC specimen.

¹⁰ Ritter 2011

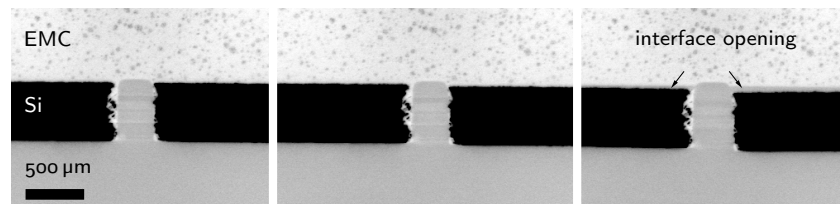


Figure 4.25: Image series of the first successful delamination of the Si-EMC interface using 4PB. The photos are taken from a sequence in time (left to right), and are inverted for clarity. In the very right photo the asymmetric opening of the interface indicates delamination.

Specimen generations

The following table lists specimen combinations that were tried. In the result column fail names specimens that did not delaminate at all, or whose data analysis was too complicated; partial success refers to experiments that were not fully analyzed throughout this work.

pre-crack type	loading type	lip thickness	notches	molding process	intended setup	result
PTFE	EMC lip chisel	<0.5 mm	-	compression	MMC	fail
spray	Si lip pendulum	=Si	-	compression	MMC	fail
spray	EMC lip pendulum	>0.5 mm	-	compression	MMC	fail
release agent	EMC lip pendulum	>0.5	-	compression	MMC	partial success
release agent	leaf spring	>0.5	front	compression	MMC	partial success
release agent	leaf spring	>0.5	both	compression	MMC	success
release agent	leaf spring, Si flanks	>0.5	both	compression	MMC	fail
release agent	leaf spring	>0.5	both	transfer	MMC	partial success
release agent	4PB	n.a.	three	transfer	4PB	partial success
gold	leaf spring	>0.5	both	transfer	MMC	fail
gold	4PB	n.a.	three	transfer	4PB	fail

Table 4.3: Different specimen generations for testing release layer methods and loading principles.

The following section describes the way from the specimen to fracture mechanical data by experiment and simulation (page 65 ff.), the results (p. 80 ff.), and section 6 discusses the results (page 89 ff.).

5

From Specimens to Interface Properties

5.1 The Delamination Experiment

This section describes the steps that are necessary to run a delamination experiment in the MMC setup. Some of the following steps need the understanding of the EMC material properties and the crack tip recognition. To obtain the interface properties each experiment is followed by simulation of a finite element model (*page 67*). Besides the experimental load data, the model needs information about two more aspects: the crack position at a certain load value (*page 70*), and the material behavior under a certain load situation (*page 75*).

The steps of the delamination experiment are:

- Dryback of the specimen
- Re-juvenation of the specimen
- Machine preparation (change load cell, calibrate, adjust clamp, adjust camera and lighting)
- Clamp the specimen
- Adjust the load angle
- Apply the leaf spring, bring load axis to contact
- Adjust light and camera
- Choose software control settings, ramp up temperature if desired
- Start loading and monitoring
- De-load the specimen
- Stain the delaminated interface if desired
- Analyze the specimen
- Analyze the recorded data

Preconditioning: Dryback and Re-juvenation To remove any moisture from previous processing or storage, the specimens were dried back as per JEDEC¹ standard *bake out* at a temperature of 125 ± 5 °C for 24 h. Due to the difference in thermal expansion and contraction during the temperature changes of fabrication molding, any fracture specimen is already in a residually stressed state before other additional loads are applied. This has to be considered in the preparation as well as the modeling. To obtain a well defined residual stress situation and to remove possible physical aging², and to define a comparable cool-down ramp the specimens were re-juvenated directly before the experiments. A storage for 0.5 h at a temperature above T_g ($\tan \delta$) not exceeding post mold cure temperature, followed by a controlled cool down ramp re-establishes production like built-in stresses. The cool down ramp used was a production relevant $2 \frac{^{\circ}\text{C}}{\text{min}}$, which enables a reference state for comparisons and the simulation of the cool down procedure.³

¹ JEDEC Solid State Technology Association 2006

² *physical aging*, for time dependent material behavior see page 75

³ a storage of 20 minutes above glass transition region temperature is sufficient to establish thermodynamic equilibrium, see Vreugd 2011.

Clamping and Loading For the machine preparation, clamping and load angle setting attention was given to the tolerances described on page 44, and the clamping steps described in figure 3.10 on page 43 were followed.

After applying the leaf spring to the specimen and adjusting light and camera focus, the specimens were loaded strain controlled at a rate of $50 \frac{\mu\text{m}}{\text{sec}}$. During testing the experiment was monitored by taking $3 \frac{\text{frames}}{\text{sec}}$ with digital camera equipment. Experiment outputs were reaction force and photographs—both dependent on displacement and time. The specimen was deloaded before the end of delamination for staining the crack position (see page 74). A typical load reaction of a MMC specimen is shown in Figure 5.1 below.

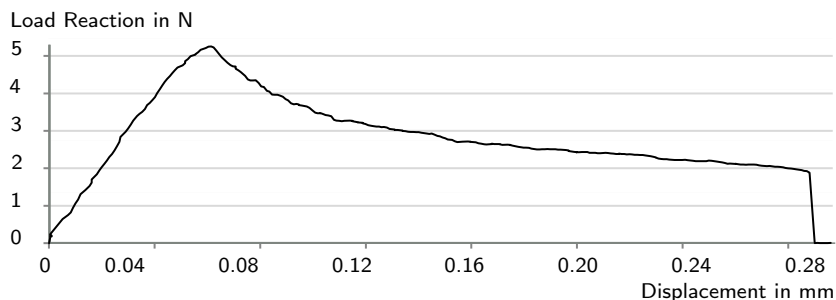


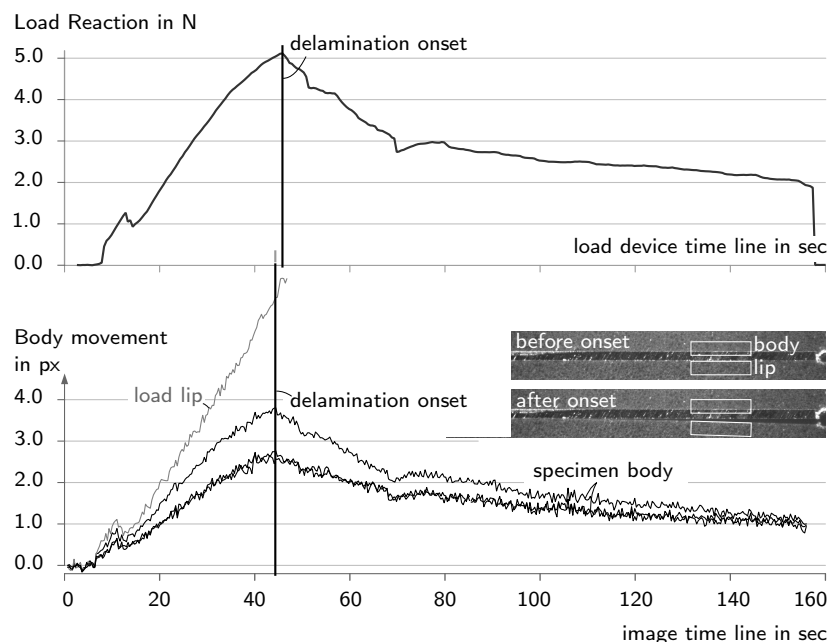
Figure 5.1: Typical load reaction for a MMC delamination.

The force increases linearly with displacement, the slope depending on the pre-crack length and load lip length. After a force peak, which depends on the pre-crack quality, the reaction force decreases continuously until the loading stops or the specimen fails. If a part of the interface is still intact the specimen can be re-loaded and the exper-

iment continued. The specimens made by compression molding had interface lengths shorter than the specimen. After the interface has delaminated the EMC fractures and therefore the force value drops suddenly.⁴

Specimen and Data Analysis After the delamination the geometry of the specimen was measured using a micrometer screw gauge ($\pm 3 \mu\text{m}$). The silicon die width and length were measured using a digital camera and microscope lens, and patching the microscopy images ($\pm 1 \mu\text{m}$). This ensured using accurate measures in the model, measures that changed during the polishing procedure. Images were also taken of the delaminated surface, to observe the pre-crack shape, to measure the delamination front shape in stained specimens⁵ and to exclude specimens with substantial silicon fracture.

For accurate use of the recorded data, the time lines of the displacement values and of the images had to be aligned. This correlation allows to use load displacements that belong to the according crack length. Figure 5.2 shows the procedure.



⁴ for the load reactions of a specimen without back notch see page 61

⁵ The staining procedure is described on page 74

Figure 5.2: Correlating the time lines of the load device and the image acquisition: The upper graph shows the load reaction of the specimen against time. The lower graph shows the displacement of surface regions above (specimen body) and below (load lip) the interface in load direction. The displacements were obtained from gray value correlation, and thus expressed in pixel shift values. Because load displacement is prescribed, and the load lip is displaced, its movement continuously increases with time. The movement of the specimen body above the interface however changes with the onset of delamination. The two small photos show the corresponding monitored gray value areas. The white frames show the zones used for the plot, both before and after the onset of delamination, and both above and below the interface, the specimen body and the load lip.

5.2 Model and Simulation

In order to establish the fracture mechanical properties of the interface, the stress state around the crack tip was simulated numerically using ANSYS[®] version 11. Simulation inputs in this case are geometry including the crack length, the loading conditions including the

cool down procedure, the load angle and the prescribed displacement, and the material properties.

The load reaction in the model was verified by comparing it to the measured force values. Figure 5.3 shows a comparison of measured and calculated load reactions at given displacements. Factors that impact a potential difference are the material model and its implementation, the load model, the consideration of frame stiffness and geometry including the leaf spring rotation, a correct data time correlation as described on the previous page, and errors from the load measurement and the load angle change. The material model is described on *page 75*. The frame stiffness has as significant impact at crack initiation, because if there is no well-defined pre-crack the elastic energy stored in frame *and* specimen suddenly release into a crack. A comparison of simulations including the frame and leafspring materials and geometry showed that their impact can be neglected during crack propagation.

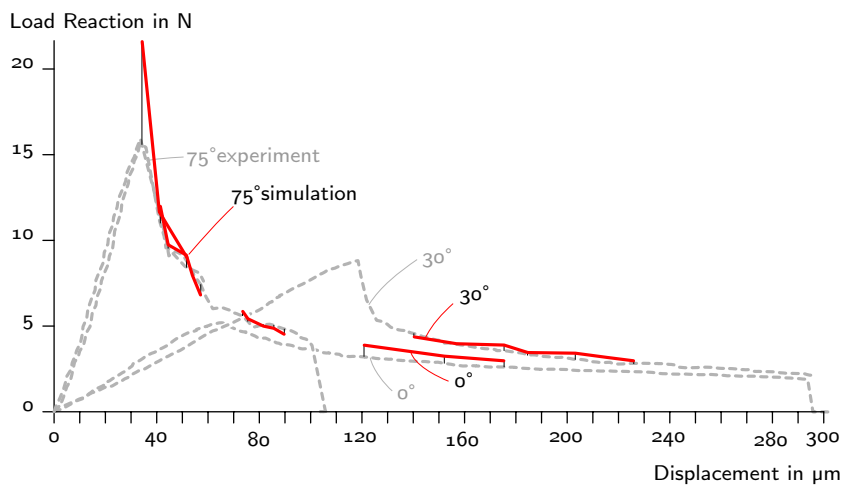


Figure 5.3: Comparison of load reactions in experiment and simulation. Both the linear force increase before crack propagation and the force levels during delamination are different for different load angles. The force deviations are biggest at crack initiation and at load angles with larger load lip bending. The values at crack initiation have not been used for energy release rate comparisons.

During the bending of the specimen load lip it displaces horizontally, and therefore the loading leaf spring rotates as explained on *page 42*. This has two consequences: The load cell used, which does not sense horizontal load components, changes its vertical measured component value about max. 8% for the maximum values achieved during the experiments described here. Secondly the external load angle is affected and changes during the experiment. The impact of load angle deviations is described on *page 87*. The comparison of measured and calculated values shows a difference of up to 19%, biggest for a load angle of $\alpha = 0^\circ$, for which the horizontal lip movement and thus the load cell error is biggest. The load force was not used as simulation input value.

Beside the specimen geometry measured as described in the previous section, the crack length was recorded as described on *page 70ff*.

The crack length determined the open part of the interface, modeled also in the opened state because the VCCT demands only one simulation run to determine the fracture mechanical parameters. The specimen was modeled in two dimensions using plane stress assumptions. The stress assumption affects mainly the residual stresses across the interface. During cool down the EMC contracts more than the silicon. This mismatch builds up stresses and warps the specimen as described on *page 31*. The specimen flanks tilt inwards because the material interface at the flank bottom restricts the EMC contraction. A plane strain assumption for a 2D model would constrain the strains normal to the specimen flank to zero thereby neglecting the initial strains. In the comparably narrow specimens used in the MMC setup the fraction of EMC volume tilting compared to the whole EMC volume is greater than in wide specimens. The narrower the specimen the better a plane stress assumption can model the stress state caused by the loading conditions.⁶

6 Zehnder 2009

The clamped specimen section was fixed in its movement in the model according to the setup. The contacting features such as the bracket, pendulum and leaf spring were included in several preliminary simulations to observe the influence of additional displacements caused by the setup bending on the energy release rate and mode mix. After replacing the 15 mm long pendulum with the 25 mm long leaf spring, the length increase lowered the difference to $\Delta G_c < 4\%$. Therefore the prescribed displacement load was directly applied at the load lip of the specimen. The load was applied at the experiment temperature, but after the cool down of the specimen.

To answer the question whether residual stresses have a significant influence on the G_c results, two different scenarios were simulated. One considered the cool down of the specimen in a two-step simulation, with the parameters taken from the re-juvenation procedure. The other scenario did not consider the cool down procedure and thus no thermal residual stresses in the specimen. The behavior of the silicon layer was considered linear elastic, and taken from Brantley and Taylor et al.⁷ The material properties of the EMC were measured as described from *page 75* onwards. Two scenarios were considered also here, one assuming the EMC to behave linear elastic but temperature dependent, the other assuming the material to behave viscoelastic and temperature dependent, and thus being able to relax some of the residual stresses already during cool down.

7 Brantley 1973, Taylor et al. 1998

Figure 5.4 shows the meshed model including the refined mesh around the crack tip. The elements were 8-node elements.

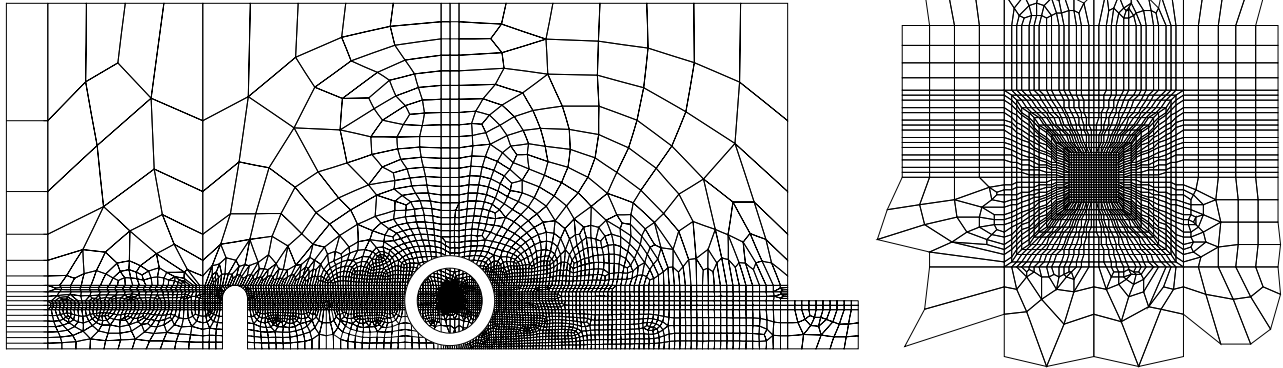


Figure 5.4: The meshed model of the delamination specimen (left), and the refined mesh around the crack tip (right).

5.3 Finding the Crack Tip

To measure the crack length at a given time point different methods are available. For a monitoring during crack propagation there are for instance different crack opening interferometry methods⁸, and optical crack tracing (OCT)⁹. The latter was shown to work well even in the nanometer range by Keller.¹⁰ Destructive methods include scanning acoustic microscopy (SAM)¹¹, and crack tip staining done with the fluorescent ink or the ink of a marker pen. Staining is also known as *Dye and Pry* technique to indicate that the analysis demands destroying the samples. Due to the small opening displacements at the crack tip and the characteristics of the acquired images the methods used within this work are deformation analysis by correlating the taken experiment images (DAC)¹², image difference calculation, and post-experimental crack tip staining in CT specimens with fluorescent ink for pre-crack analysis, and marker pen ink in the MMC specimens. These approaches are described below.

Image Correlation

For the image correlation several patterns of gray values in an image B are compared to a reference image A. Image B was taken at a certain point of the experiment of which the crack length is needed. The comparison yields displacements of the patterns. Displacement data out of both regions below *and* above the interface are then fitted with respect to beam theory and sample geometry. The intersection of the data fits gives the crack tip. Figure 5.5 demonstrates how the crack tip is found for geometry input.

Considering the correlated pixel lines' z-distances from the interface did not show a significant difference in the crack tip position. Note that scatter increases in the crack tip region, because gray value

8 Liechti 1993

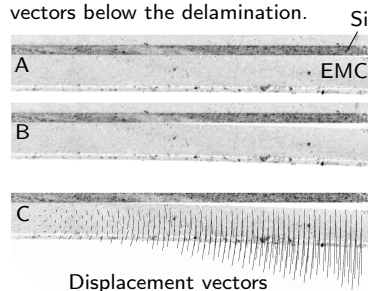
9 Uhlig et al. 2000

10 Keller 2005

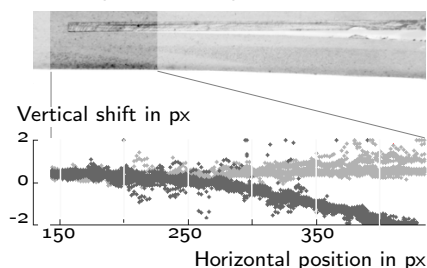
11 Durix 2010

12 Vogel et al. 2002

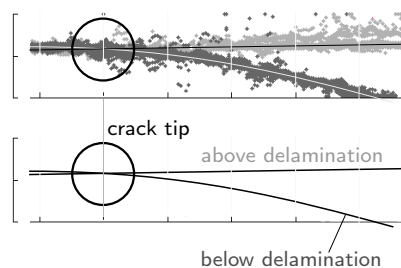
Images A,B are correlated to track displacements above and below the interface. C shows the displacement vectors below the delamination.



To show how the crack tip can be found, a correlated area is shaded darker in this specimen flank image. Below the pixel shift is plotted vs. x -position.



Polynomial fit of the px shift data on each side of the interface.



patterns in the images change substantially. Also the two polynomial fit curves intersect and suggest that the areas penetrate, which they of course do not.

After the first results the method was modified and improved by Keller et al. comparing not only two experimental images, but comparing displacement field results from a finite element simulation to DAC results of several image comparisons¹³. There the crack tip position is given by the global maximum of the correlation coefficient.

Figure 5.5: Plot of DAC results, different images of the experiment under each other allow comparison of different experimental stages. This plot shows the end of the delamination (see px range). The ordinate shows vertical shift in pixels, the horizontal shows pixel position along the chip orientation. The chip ends at x -pixel 191.

¹³ Keller et al. 2010

Image Difference

In an animated sequence of delamination images, an out-of-plane effect is visible as a gray value change just ahead of the "visible-to-the-eye" crack tip, a change that runs with the crack tip position. Image 5.6 shows two examples of such gray value changes.

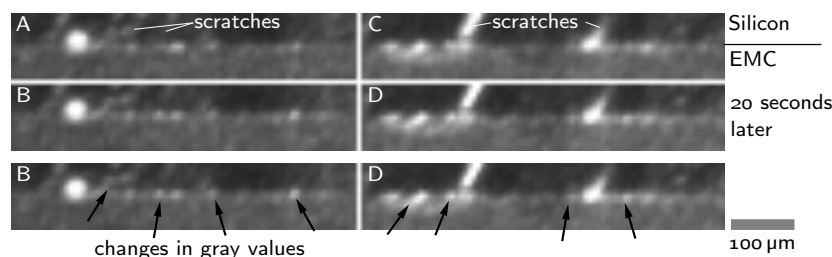


Figure 5.6: Ahead of the "visible-to-the-eye" crack tip position the gray values change to a lighter tone at the very interface. The black arrows point to the tone changes, when comparing images A to B, and C to D.

The gray value change coincides well with the actual delamination front position at the specimens flank. Figure 5.7 shows a comparison of a crack front staining¹⁴ and the related flank image. The position of the crack tip in the flank image was determined manually by comparing the gray values of the last recorded image (the one before staining) to a 20 seconds earlier recorded image.

¹⁴ see method description page 74

Among the possible means to automate the extraction of this pattern's position there are DAC as described above, as well as cal-

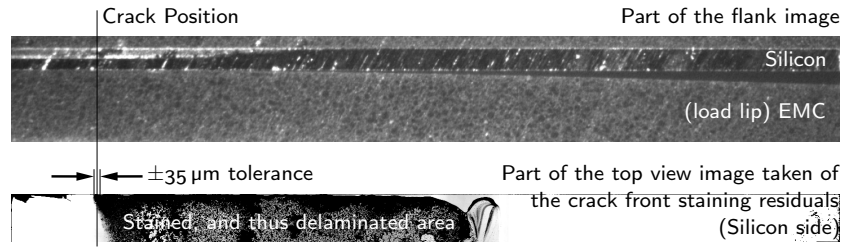


Figure 5.7: Example of how far the crack tip is found ahead of the "visible-to-the-eye" position. The $\pm 35 \mu\text{m}$ correspond to ± 5 pixels in the flank image. Both the flank and the staining image show the full length of the 7 mm long interface. For a description of the staining method see page 74.

culating the difference between two images. To keep the effort small the difference calculation was applied. This procedure automates the manual recording of each moving gray value change ahead of the crack tips.

The procedure is as follows. Two images are chosen with a sufficient time distance in the experiment, and thus with a different crack length. For each pixel position the difference of gray values is calculated—a standard procedure for each image manipulation software.¹⁵ A gray value difference of zero turns the pixel to black, a difference of 100% is written as white value to the position. In the ideal case the image remains for most parts black and dark gray, and is close to white at the interface region for the crack length difference of the images. That means the longer of both crack lengths becomes visible. The image can then be increased in contrast with care to not distort the position. The number of pixels between one silicon side and the crack tip position gives the crack length, and can easily be translated using the image resolution. Figure 5.8 shows several examples.

¹⁵ such as GIMP, or Adobe® Photoshop®.

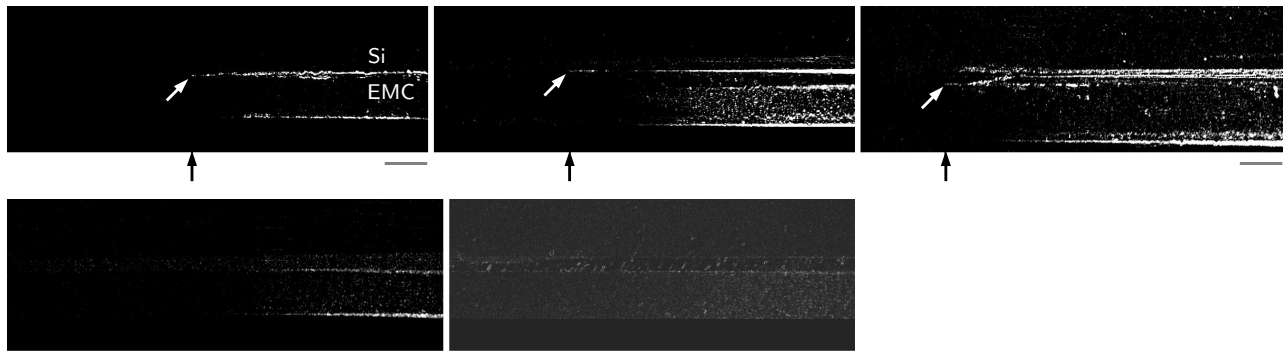


Figure 5.8: Examples of crack tip positions (arrows) found by subtracting images of different crack lengths. The scale bars are 0.5 mm long.

In the first three images in the Figure 5.8 the crack tip position is very well visible. Even a kinking crack can be seen in the third image. The image quality is crucial for subtracting images from each other. The fourth and fifth images were created by subtracting images with substantial noise due to poor lighting and high CCD sensor amplification. The noise increases the image difference to a state where it becomes impossible to recognize the crack tip position. It is

thus important to pay attention to the lighting conditions, especially if additional objects are necessary between camera and specimen flank, such as a climate chamber window or optical filters.

Constructive Changes to the Available Climate Chambers.

To ensure appropriate lighting conditions also under elevated climates, the door of the Eplexor climate chamber was adapted.¹⁶ The door was equipped with an observation window consisting of a metal cylinder and two glass panes. The double glass concept prevents water condensation at the inner window. For image acquisition a camera system was mounted to the structural columns of the Eplexor device, to reduce vibrations in the images when using a tripod, and to reposition the camera to the specimen. The cameras¹⁷ used have a 1624×1234 and a 1300×1026 pixel matrix respectively. Telecentric fixed distance lenses allowed a resolution of the final images between 5 and $7 \mu\text{m}/\text{pixel}$ and a recording of the full interface length of 7 mm. The camera mount shown in Figure 5.9 can be opened easily between experiments to access the chamber space.



¹⁶ Neinaß 2008, Larisch 2010

¹⁷ Cameras of AVT, and lenses of Sill Optics.

Figure 5.9: The camera equipment mounted to the GABO Eplexor device.

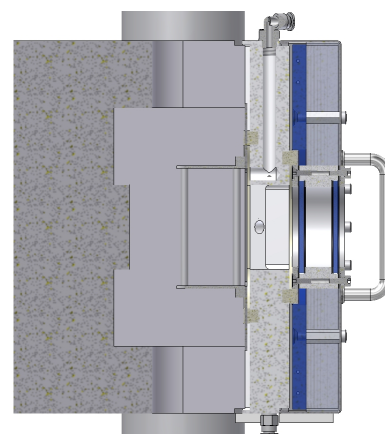


Figure 5.10: A cross section schematic of the door and window in front of the climate chamber.

During the development stage of the climate chamber door for the Eplexor device, the image quality under different light conditions was analyzed. As the image quality increases with a wide spectrum of gray values that resemble object detail, the histograms of gray value distributions were observed accordingly as shown in Figure 5.11. The specimen chosen for this comparison consisted of different materials to simulate differently reflecting parts, such as molding compound, copper and silicon. Also the gray value correlation coefficient was compared when correlating patterns in the image of the same object but different lighting conditions. The comparison led to installing a fix focal distance lens. This choice avoids undesired amplification of the CCD signals. Since the interface objects including molding compound are usually dominated by a gray value range, the log plot of histograms is more useful.

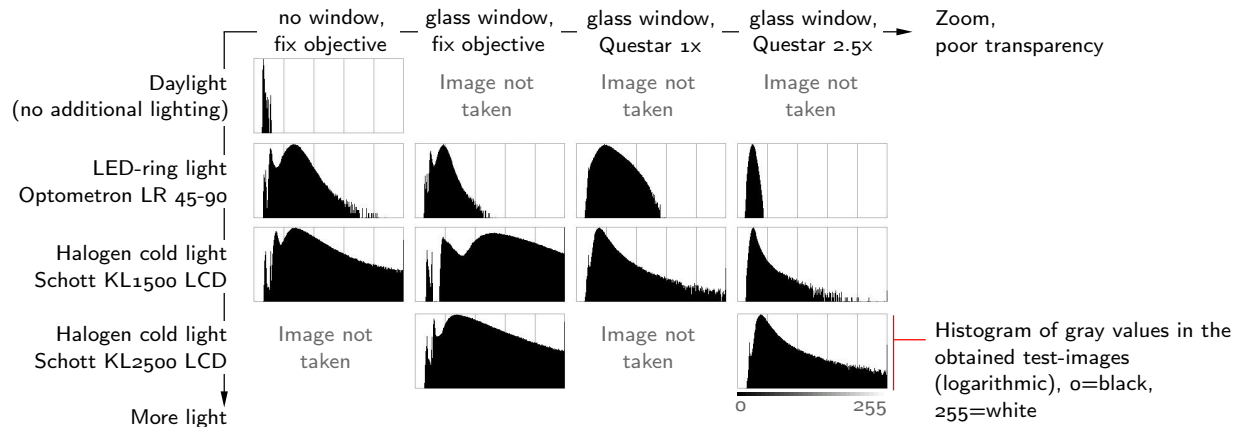


Figure 5.11: The histograms show the gray value distribution in images of an EMC test specimen under different light conditions. As a result all zoom lens options were excluded for the delamination experiments. The telecentric lens is described on page 73

Staining of the Crack Tip and Delamination Front

To analyze the shape of the delamination front and establish the crack tip positions, several specimens were de-loaded before the end of the delamination. Using a permanent marker pen, both specimen flanks were covered with the marker ink. After letting the ink settle for at least 30 minutes, the specimen delaminated by hand. The ink penetrated the delaminated part of the interface and by settling left the trace of the delamination front behind. Figure 5.12 shows two results of such stainings.

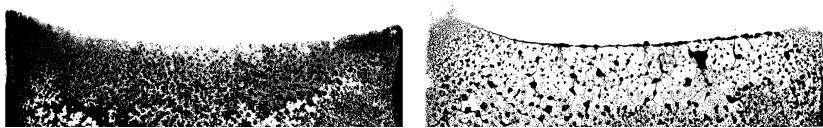


Figure 5.12: Two examples of a crack staining. The ink (black) shows the top view of the delaminated Si surface. Delamination ran from bottom to top, both silicon dies are 2 mm wide.

As the delamination ran from bottom to top, the flanks appear to delaminate first in terms of position. The center of the specimen ran behind. Similar investigations for specimens with low aspect ratios, that is wider than high, showed a reverse behavior. In 10 mm wide but 1 mm thick 4PB specimens the delamination ran ahead in the center of the specimen.¹⁸ Different reasons may contribute to the shape of the delamination front. Across the interface in lateral direction the stress state varies due to the bending load itself, due to the different poisson ratios of the two materials that induce lateral stress components, and due to the thermal contraction mismatch that also creates lateral stress components. A pre-damage of the interface near the flank could be excluded by the color dye penetration. Further aspects of the crack shape and width dependency were not investigated.

5.4 Material Properties of the EMCs

As described on page 21 two out of four elasticity properties for each material are required for an accurate description of its behavior. The four properties to choose from are the Poisson's ratio ν , the shear modulus μ , the compression modulus C and the Young's modulus E , which are time dependent functions for viscoelastic materials such as the EMC. Only in the glassy and the rubbery state the time dependence can be abandoned. Additionally a measure of thermal expansion is necessary to capture the contraction and expansion driving forces during temperature changes, the coefficient of thermal expansion (CTE). Of these parameters the measurements have been done to capture E, ν and the CTE. The following paragraphs describe the procedures and results.

The Material Behaves Visco-Elastically: DMA results

The most common measure to take, and measured first here is the Young's modulus $E = E(t, T)$. If the material behaves viscoelastic, and molding compounds do, the stress reaction of the material lags in time compared to a strain load. For sinusoidal excitation of specimens the stress reaction can be expressed as a complex term, which gives also a complex description \mathfrak{E} of the modulus of elasticity. The phase angle of this complex number is the lag δ behind the frequent excitation. The modulus components are called *storage modulus* E' and *loss modulus* E'' , because they are proportional to the elastic energy stored in the material and the dissipated energy respectively. Their relation is thus:

$$\mathfrak{E} = E' + iE'', \quad (5.1)$$

$$\frac{E''}{E'} = \tan \delta = \frac{\frac{\sigma_0}{\epsilon_0} \sin \delta}{\frac{\sigma_0}{\epsilon_0} \cos \delta}. \quad (5.2)$$

Due to the time and temperature dependent behavior of the EMCs the experiments carried out were run on a DMA device.¹⁹ Therefore T69 specimens of $4.8 \times 40 \times 0.4 \text{ mm}^3$ were clamped in tensile mode and strain loaded with different frequencies from 0.5 to 10 Hz at temperatures from -40 to 260°C. The specimens were dried first for 24 hours at 125°C and then clamped with a clamp distance of approximately 20 mm and the strain settings 0.06 % for the static and 0.02 % strain for the dynamic load. The results for the T69 material scanned at 1 Hz are shown in Figure 5.13 below. The DMA data for the CEL material was analyzed in detail by Patel et al.²⁰ and thus taken from their report.

¹⁹ TA Q800

²⁰ Patel et al. 2008

To use the acquired viscoelasticity data in the finite element simulations, the concept of time-temperature superposition was applied.

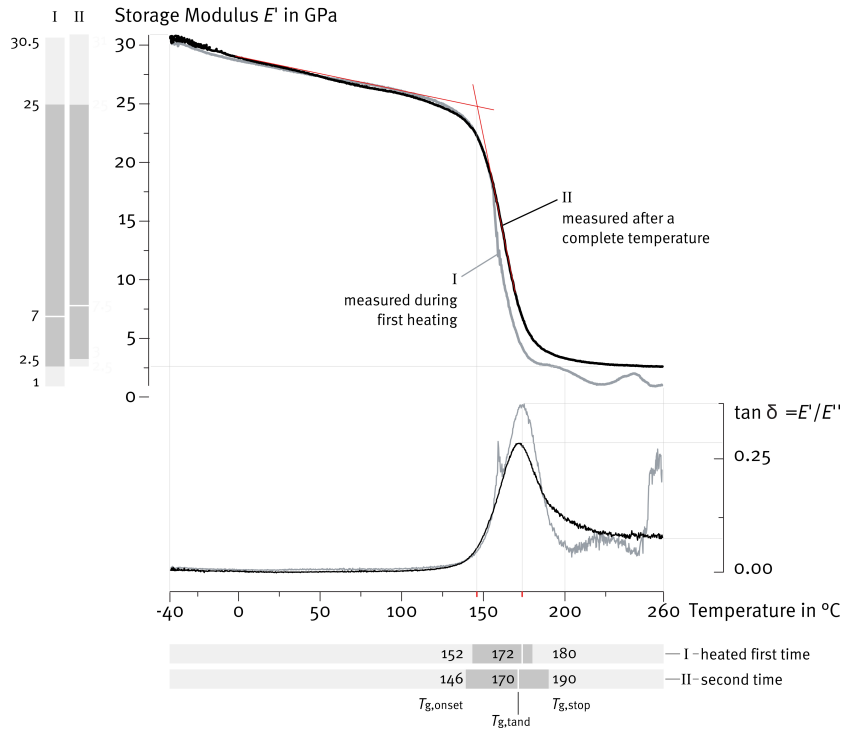


Figure 5.13: The graph shows the viscoelastic reactions of two T69x samples loaded in tensile mode with a frequency of 1 Hz. After a full temperature cycle of up to 260°C the glass transition region has expanded. Before a first solder reflow process the EMC has a lower rubbery modulus (gray) than after reflow (black). Then the rubbery modulus shows a stable plateau. This indicates that additional curing took place. Note that the temperature with the biggest energy dissipation in the viscoelastic part is different from the TMA determined glass transition temperature, and about 20 to 30°C higher. The T_g (TMA) corresponds approximately to the onset of the glass transition region in the 1 Hz DMA response.

The procedure to fit a mastercurve, calculate shift factors and Prony coefficients was described for EMCs already in detail by others.²¹

There is discourse on the use of time temperature superposition and multiple frequency loading instead of relaxation loading experiments. This is based on the problem, that when concluding for long time relaxation, that is several decades of magnitude longer than the experiment takes, the relaxation experiments may be much more suited to create appropriate data for the models. This question was not pursued in this work, and the kind reader may study with other authors.²²

Poisson's ratio

The Young's modulus E and the Poisson's ratio ν can be both measured using a one-axis tensile experiment, and the same specimen. Therefore the measurements of ν were carried out using the same specimens as for the DMA runs. The Poisson's ratio is defined by the ratio of strains as

$$\nu = -\frac{\epsilon_{\text{transverse}}}{\epsilon_{\text{axial}}} \quad (5.3)$$

To obtain the strains of the ratio different methods are suitable. At higher temperatures, at which the EMC material behaves rubbery and mechanically contacting methods are at their limits, a contact-

²¹ Wittler 2004, Jansen 2007, Vreugd 2011

²² Walter 2003, Wittler 2004, Jansen 2007

less method should be used. Such methods are laser scanning,²³ laser speckle²⁴ or digital image correlation²⁵. Since the equipment of correlating images was used for the crack tip recognition (*page 70*) the image correlation was also used for determining ν , as previously described by Wittler et al.²⁶. The specimens were thus clamped in tensile mode, loaded and deloaded at room temperature and at 200°C at a rate of 200 $\mu\text{m}/\text{second}$. The results for room temperature varied between 0.25 and 0.37 with a mean value of 0.29. For 200°C it was not possible to determine a Poisson's value within less than 50 % deviation.

The Poisson's values were then implemented in the finite element model using three different assumptions for their temperature dependency, as shown in Figure 5.14. This allowed a comparison of the different impact of a constant $\nu = 0.29$ and a plateau of 0.29 at room temperature until 130°C below T_g changing into a continuous slope of up to 0.48 at 200°C. The difference in energy release rates and mode mix remained small: for G_c a change of less than 0.01 % and for the mode mix ψ a change of less than 4%. As a consequence the Poisson's value was kept at a temperature independent value of 0.29 in all simulations.²⁷

The experiments were carried out at a single load rate, which might hide a potential time dependency of ν . Wittler argued that if the bulk modulus can be assumed constant $C(t) = \text{const.}$, the Poisson's value measurements against temperature suffice for a numeric representation of the material behavior.²⁸ The assumption of the Poisson's value was sustained, because for both materials involved in this work the PVT experiments described in the following section show no time dependency of C .²⁹ For instance Figure 5.15 shows the volumetric changes in T69 after a sudden pressure change. The first approximately 500 seconds cannot be used for a time dependency interpretation because of the temperature change inherently coupled to the pressure change.

23 Kugler et al. 1990

24 Schubach and Ettemeyer 1997

25 Zhao and Jin 1996, Vogel et al. 2000

26 Wittler et al. 2000

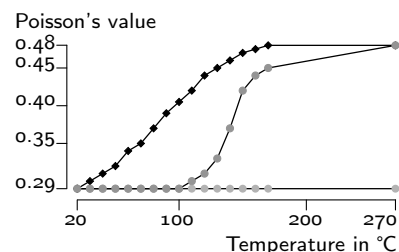


Figure 5.14: Assumptions of a constant Poisson's value, and two different slopes of increase, one more abrupt, the other a continuous change.

27 The ν -influence on the fracture properties described on *page 23* is related to fracture at higher temperatures, the discourse here relates to all experiments at room temperature.

28 Wittler 2004

29 Saraswat et al. 2008

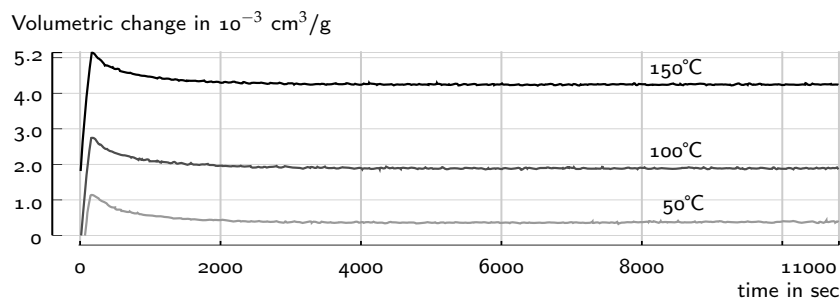


Figure 5.15: The time variation of volumetric changes after a sudden pressure change.

PVT and TMA results

To determine the EMC's coefficient of thermal expansion two devices were used: a high pressure dilatometer and a thermo mechanical analyzer. In the dilatometer the expansion of a mercury filled cavity containing a material sample is measured, while exposing the cavity to temperature and pressure. This assumes isotropic behavior and demands to divide the expansion measure by three to obtain the expansion for one dimension. By measuring the sample reaction to pressure changes, the dilatometer allows also to determine the temperature dependent bulk modulus.

The TMA measures the length change of the specimen by directly touching it with a glass plate and hook setup, while changing the temperature of the chamber that contains this setup. The sample can be oriented to different axes if desired, and thus the expansion can be measured for each orientation separately. It however does not catch the out-of-axis expansion or contraction of the sample. Although both devices can be charged with a cube type of specimen, the TMA can also run a film elongation measurement. Since the compression molding usually creates layers thinner than 1 mm, the T6g material was measured in both a cube and a film sample. The cube EMC samples had an approximate cross section of 5×5 mm, the PVT cavity was filled with about 1 cm^2 of the material, and the DMA type specimen was used as well for the film TMA measurement. Table 5.1 shows the obtained mean values for the different EMCs.

EMC Material	Measurement Method	Sample Geometry	CTE ($T < T_g$) in ppm/K	T_g (TMA) in °C	CTE ($T > T_g$) in ppm/K
CEL	TMA	cube	8.0	103.6	25.0
CEL	PVT	cube	11.0	91.7	31.3
T6g	TMA	film	5.0	137.5	30.0
T6g	TMA	cube	7.5	150.6	25.7
T6g	PVT	cube	10.0	145.0	32.0

The table shows that expansion values, depending on the method chosen, differ by more than 20% or even double, and the transition temperatures change as much as 11%. The impact of CTE differences is described on *pages 86 ff.* If not stated differently, all simulations used CTE values of the TMA cube measurements, and the T6g material above T_g specifically values of 24, 26 and 28 ppm/K for temperatures of 160, 170 and 270°C. TMA cube based values allow to compare the simulation data to other package models based on similarly measured values. The CTE properties can however change depending on the further temperature treatment of the material, such as takes place

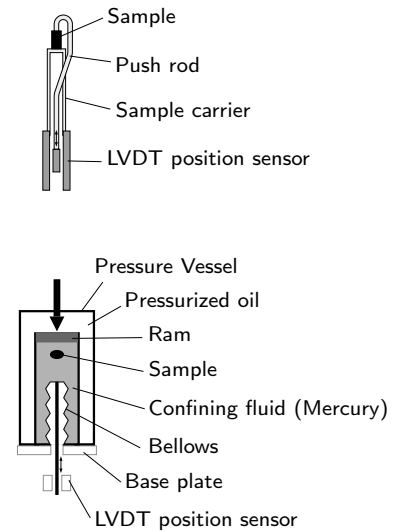
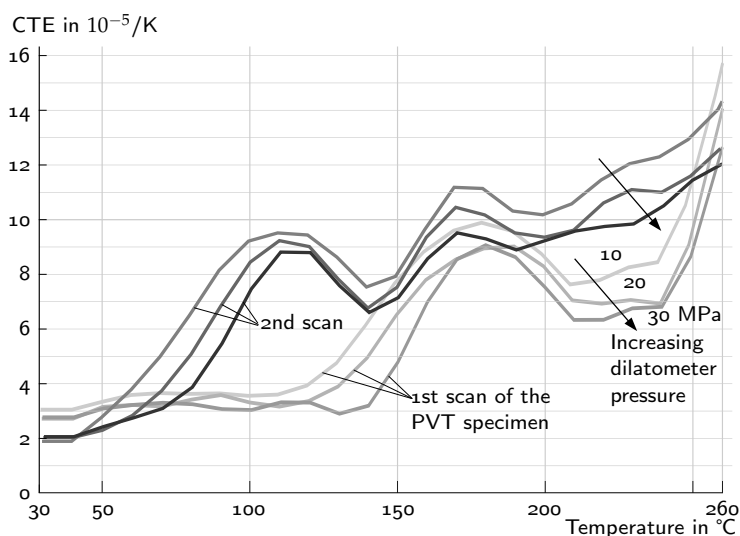


Figure 5.16: Schematics of the Netzsch TMA 202(above) and the Gnomix high pressure dilatometer (below) principles to measure thermal expansion.

Table 5.1: Mean values of thermal expansion coefficient of the molding compounds. Film specimens for the CEL material could not be produced with the molding equipment.

during further packaging steps at higher temperatures. Figure 5.17 shows an example of such temperature changes.

To compare the properties in processing *one* isotropic material, it may be helpful to use PVT measurements. The PVT measurements carried out with the T69 material were however discontinued due to a proceeding cure behavior above 150°C. Although the degree of cure of EMCs has been extensively studied and implemented for numerical simulations, the experimental effort to consider the different stages of eWLB processing had been enormous. Figure 5.18 shows the three-dimensional expansion behavior of the T69 material in the temperature range of the processing shown in the margin figure.



Examples of the detailed cure behavior of EMCs and its implementation in numerical software are given by Fařat and Vreugd.³⁰

5.5 Residual Stresses

To include the before mentioned residual stresses in the numeric model and to ensure that the material model can represent the stress state sufficiently, the following comparison was carried out. Since the different amount of contraction of the EMC as compared to the silicon can be expressed both in stresses and strains, such strains were measured. They are caused by the different amount of contraction of the EMC as compared to the silicon. The materials contract during both the chemical cure of the EMC, as well as during the cool down of the specimen. The contraction strains can be measured indirectly by observing the warpage of a two-layer or sandwich specimen, or directly by measuring the microstrains in interface vicinity or calculating

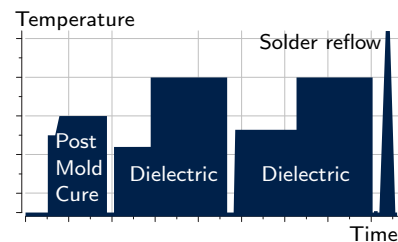


Figure 5.17: The eWLB needs several temperature blocks after molding, blocks that influence the EMC's properties. After molding the redistribution layers are formed and solder balls undergo reflow. Adapted from Brunnbauer et al.2008.

Figure 5.18: Volumetric expansion values plotted over temperature for three different dilatometer pressures and two measurement scans.

stresses from the changes in the crystalline properties of the silicon die. Both direct means were tried by electron backscatter diffractometry EBSD and x-ray diffractometry³¹. These methods were not further pursued because the values relate to the atomic length scale of the material. In the bond region of several atom length scales, it is not Silicon bonding to EMC, especially the interface vicinity of the EMC is an inhomogeneous composite of several components such as epoxy matrix, silica fillers and additives. Looking at the residual stresses at the atomic scale must include these inhomogeneities in the models and thus abandons the continuum approach.

The warpage of a Si-EMC bimaterial sample was measured using the shadow moiré method in combination with ramping up to molding temperature and back to room temperature twice. Figure 5.19 compares the warpage measured after the second temperature load cycle with the simulated warpage using the viscoelastic material model. The first cycle puts the sample in a state of reference, representing the state after molding. The second cycle is intended to repeat the first cool down ramp. The simulation should reconstruct the cool down behavior.

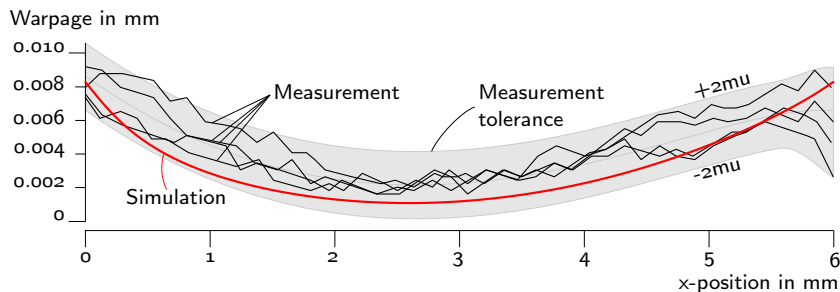


Figure 5.19: Comparison of the measured warpage of a Si-to-EMC bimaterial sample and the simulated warpage using the viscoelastic material model. The curves show the warpage at room temperature after cooling down from molding temperature.

5.6 Fracture Mechanics Results

In summary the steps to determine $G_c(\psi(l_{ref}, \epsilon))$ after acquiring all data are as follows.³² The FE model is built and simulated with an input of crack length, load displacement, and material model. The material model is varied twice, a simulation run for each the linear elastic model, and the viscoelastic model. The preconditioning assumptions in the model are also varied twice, one simulation without a cool down simulation, and two simulations for considering the build up of residual stresses throughout cool down after molding. The output of the FE simulations are nodal displacements and forces in the crack tip vicinity. These measures serve to calculate both the critical energy release rate and the mode mix subsequently. The necessary initial reference length used is half of the chip height in the unit mm,

³¹ Auerswald 2008, 2009

Experiment	page 65
Determining experimntl. time	page 67
Finite Element Model	page 67
Finding the Crack Tip	page 71
³² Material Model	page 75
Equations 2.26,2.27 for $G_{cI,II}$	page 28
Equation 2.32 for $G'_{cI,II}$	page 29
Equation 2.33 for $\psi_{G,VCC}$	page 29

$l_{\text{ref}} = l_{\text{norm}} = 0.092\text{mm}$. The crack extension size is bound to the crack tip element size, which is $\Delta a = 0.002\text{mm}$. The used equations are repeated here for convenience,

$$G_{\text{I}} = -\frac{1}{2\Delta a} [f_{y,5}(\Delta u_{y,1-3}) + f_{y,6}(\Delta u_{y,2-4})], \quad (5.4)$$

$$G_{\text{II}} = -\frac{1}{2\Delta a} [f_{x,5}(\Delta u_{x,1-3}) + f_{x,6}(\Delta u_{x,2-4})], \quad (5.5)$$

$$G = G_{\text{I}} + G_{\text{II}}, \quad (5.6)$$

$$\psi'_{\text{G,VCC}} = \arctan \sqrt{\frac{G'_{\text{II}}}{G'_{\text{I}}}}, \quad (5.7)$$

where each G is critical $G = G_{\text{c}}$ if the input data comes from the simulation of a propagating crack, and with the modified components $G'_{\text{I,II}}$ of equation 2.32 on *page 29*.

To investigate the influence of errors on the results, all the above procedure is repeated for the elastic case including the cool down step from molding temperature to room temperature *and* it is repeated with two-directed deviation assumptions for the parameters specimen width, height, lip length, crack length, load angle, load displacement and CTE.

The following pages list these values $G_{\text{c}}(\psi(l_{\text{ref}}, \epsilon))$ and the findings related to them. They include the qualitative and quantitative relation of G_{c} and ψ , how they alter depending on residual stresses, depending on which part of the data is analyzed, how the mode mix range can be extended and extrapolated, and which errors have the biggest impact. The discussion starting on *page 89* shows implications and new questions of the methods of shifting, fitting and obtaining the data.

From Load Angle to Mode Angle The values of $G_{\text{c}}(\psi)$ are plotted in Figure 5.20. The external load angle range of $\Delta\alpha=75^\circ$ changes into a mode mix range of $\Delta\psi=10^\circ$ at the crack tip. This ψ range is close to pure tensile mode opening, which at the first view needs the lowest energy to fracture. Within the ψ range G_{c} increases with ψ , that is higher local shear components demand more energy per area to release the same interface area. The translation of α to the mode mix at the crack tip deserves more attention.

The angle relation of α to ψ is nonlinear. An external load of $\alpha=0^\circ$ induces a higher shear load at the crack tip than a 75° angle. The shear loads at low external angles are not caused by intrinsic interface properties but by the bending at the top zone of the load lip. This causes an opening load plus, in the crack tip, a shear load component. When an external shear component adds to this situation, such as happens when moving towards $\alpha=75^\circ$, it might counteract the former

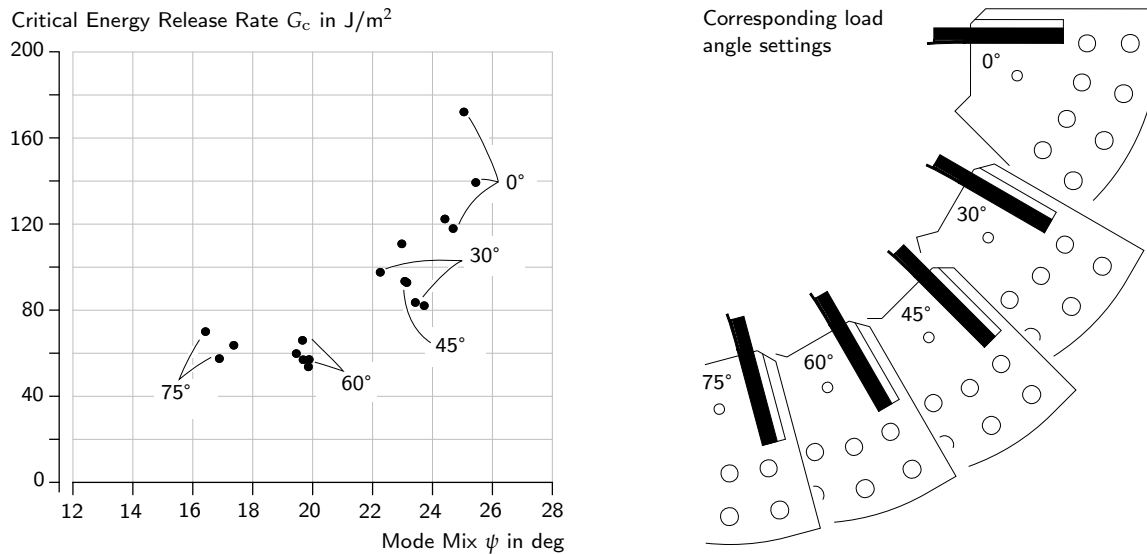


Figure 5.20: Energy release rate plotted against mode mix.

shear component and thus favors the local tensile load. The Figure below demonstrates the impact of gradually increasing the shear load and thereby increasing the local tensile load component using the von-Mises stress field. In the case of a homogeneously distributed tensile load at a bulk material crack tip, the stress field orients in a perpendicular butterfly shape, such as shown on *page 23*. At the interface the butterfly is asymmetric and tilted even for a purely tensile mode. The orientation change with the load angle strongly depends on the load displacement. It opens way to predict load angle extensions as shall be seen later on, and it helps to estimate the residual stress impact in the model.

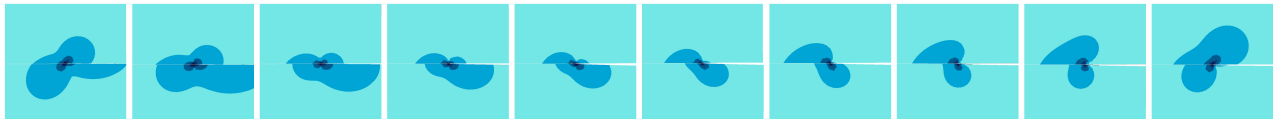


Figure 5.21: A von-Mises equivalent stress field at an interface crack tip shows the gradual change of external load directions. The directions range from pulling the load lip below the interface out of the crack tip towards the right (image very left), pushing the load lip straight downwards (mid image), and pushing the load lip into the crack tip towards the left (outer right image). (Hypothetic load cases)

Including Thermal Residual Stresses Section 5.2 on *page 69* posed the question of residual stress influence on G_c and explained that two different temperature histories were assumed in simulating the experiment. Figure 5.22 shows the calculated energy release rates for the cases with and without residual stresses present when the crack propagates along the interface.

The G_c values are quantitatively different, and their qualitative relation to ψ changes as well. When excluding the cool down procedure in the simulation, the before described increase of G_c with mode

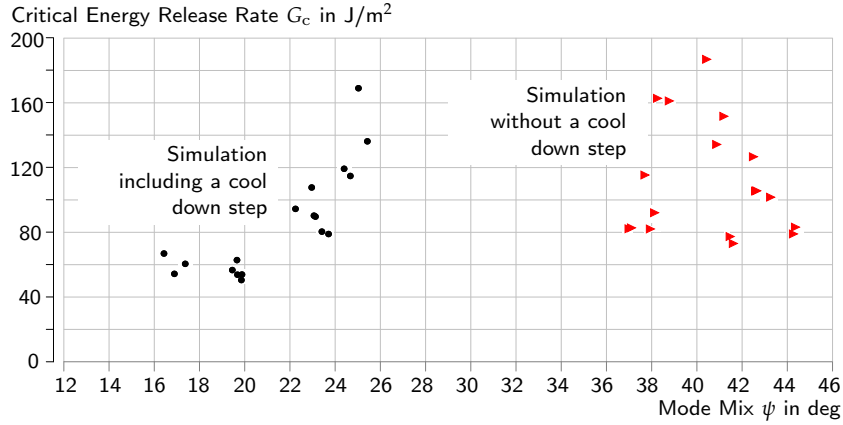


Figure 5.22: The critical energy release rates calculated in- and excluding a cool down step.

mix cannot be clearly seen in the data. When maintaining the relation of $G_c = f(\psi)$ however, the graph suggests a weaker interface when excluding the cool down step, because the critical data points are lower than the trend of the former ones towards higher ψ values. The residual stresses can thus be described as a form of pre-loading the interface. Once taken into account in the modeling, the interface toughness relates to a different mode mix range, because both loads participate to the critical state, the load displacement and the thermal contraction. To obtain the interface property accurately, it is crucial to include the cool down procedure the specimen experiences before the delamination experiment in the numeric model.

For lead frame-to-mold compound interfaces Xiao et al. also found that residual stresses are crucial to take into account.³³ The results for the Si-EMC interface have been published already.³⁴

The different impression of $G_c(\psi)$ depending on a preceding cool down step can also be seen in the stress plot shown in Figure 5.23.

The horizontal load component switches direction when adding

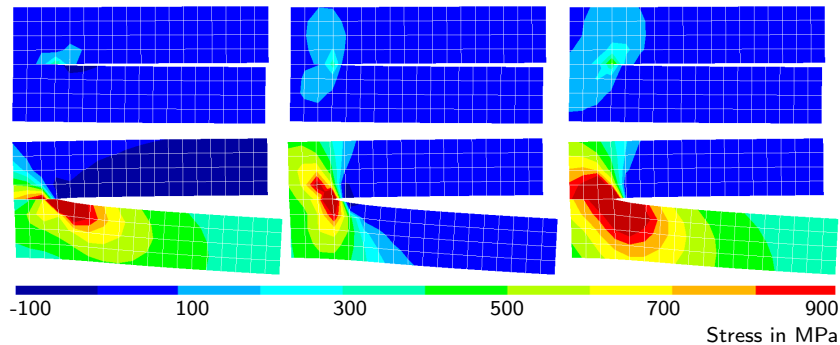


Figure 5.23: Stress plots for σ_{xx} , σ_{yy} and 1st principal stress (left to right) in crack tip vicinity. The upper row plots the stresses after the cool down procedure, the lower row the stresses after adding the critical displacement loading – in this case $\alpha=0^\circ$.

the critical displacement load after cool down. Also the 1st principal stress field orientation changes. The pre-load of the residual stresses is

³³ Xiao et al. 2008a

³⁴ Schlottig et al. 2009a,b, 2010a,b, 2011

in opposite direction to the additionally applied load during delamination.

Excluding Short Crack Lengths—Development of a Delamination Profile Figure 5.24 emphasizes the G_c data from crack lengths shorter than 1.6 mm. These are somewhat distant from the other data

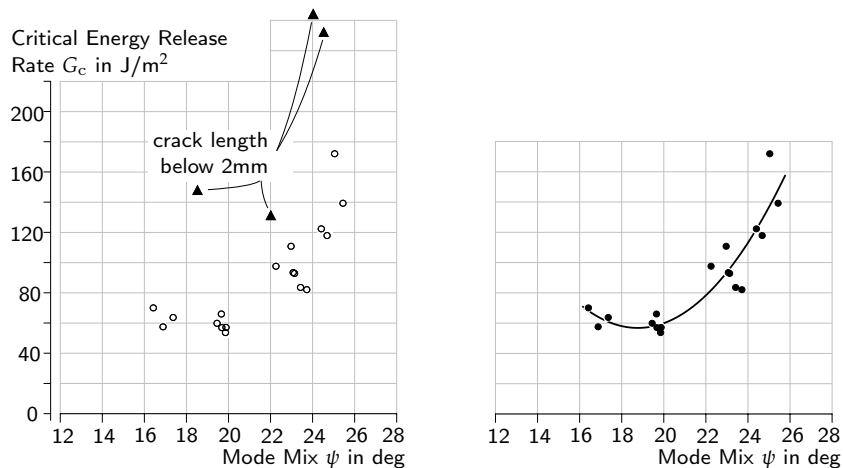


Figure 5.24: Energy release rates as shown in Figure 5.20, and such values with crack lengths shorter than 1.6 mm.

points, and deviations in measuring the crack lengths do not compensate the differences in G_c or ψ as shall be seen later on. But two more factors influence these values. The first one is the force drop after the onset of delamination. As described in Figure 3.2 on page 35 the data should be obtained from a steady propagating crack. For the crack length this implies that data from short crack lengths should be skipped, and more specifically such data points, for which the load device control loop is too slow. The second one impacts both the short and long crack lengths. Crack lengths are observed at the specimen flank only and the delamination profile across the interface can deviate from the impression at the flank, as shown in Figure 5.12 on page 74.

Since the pre-crack does not show the same shape, the delamination front needs an initial cracking area to fully develop. This area must fall to short crack lengths. This contributes to explaining the difference seen in the results. Likewise a delamination front shape change must happen at the end of the delamination, as will be discussed in Figure 6.6 on page 94. The developing shape was not studied further within this work. Instead the following considerations were taken. Crack lengths of the data presented further on were chosen neither at the onset nor close to the end of the delamination, in this case between 2 and 5 mm of a total of 7 mm interface length. A plausible delamination profile is discussed on page 94 with its impact on short and long crack lengths.



Figure 5.25: One of the delamination front stainings shown on page 74: the shape is not a straight line. Delamination ran from bottom upwards, the ink reflects the delaminated area, that is the area where the color penetrated the crack.

Extending the Load Angle Range After having seen that an external load angle of 0° in the MMC setup does not necessarily load the crack tip in opening mode, and after having seen that data from short crack lengths should be excluded, the question opens how the data trend continues in both directions along ψ .

The load extension by flipping the specimen, described in Figure 3.11 on page 44, was applied for $\alpha=-15^\circ$. The 90° setting was avoided because the leaf spring design does not include this setting. However to extend towards a higher load angle the specimen was aligned with its topside instead of bottom to the bracket, using the 75° position. This extended the setting to $\alpha=78.5^\circ$. The additional data points are plotted in Figure 5.26.

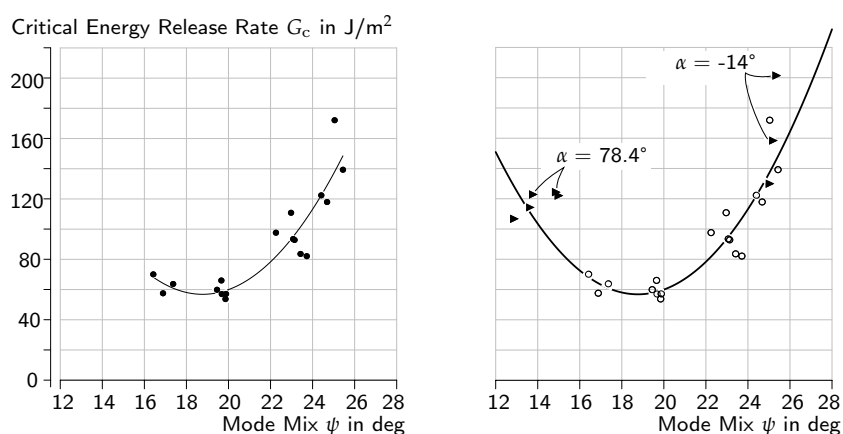


Figure 5.26: Energy release rates for load angle extensions in both directions along the ψ range.

An extension towards $\alpha=-15^\circ$ gives larger energy release rates, indicating a higher shear load at the crack tip. The trend of lower G_c at lower ψ values reverses for the mode mix of the $\alpha=78.5^\circ$ case. This supports the interpretation of stress components at the crack tip given on page 82 and in Figure 5.21. The data now shows a minimum along ψ , which allows to shift to $\psi=0$ for better interpretation. This is done using the reference length.

Reference length impact on G_c To demonstrate the impact of reference length the following graph shows three examples of G_c , for reference lengths of 0.001 mm, 0.092 mm and 7.66 mm. The 0.001 mm is chosen to consider an interface specific length scale³⁵, half the silicon height 0.092 mm to represent a geometric length scale of the specimen, and finally 7.66 mm obtained from the fitting the polynomial in equation 5.8 that finds its minimum at $\psi=0$. Note, that it is important to stick to one unit when calculating the $G_c(\psi)$ data, since ψ changes substantially when switching from mm to m or similar.³⁶ The unit mm was used for all length input in this work.

35 Rice 1988

36 Rice 1988

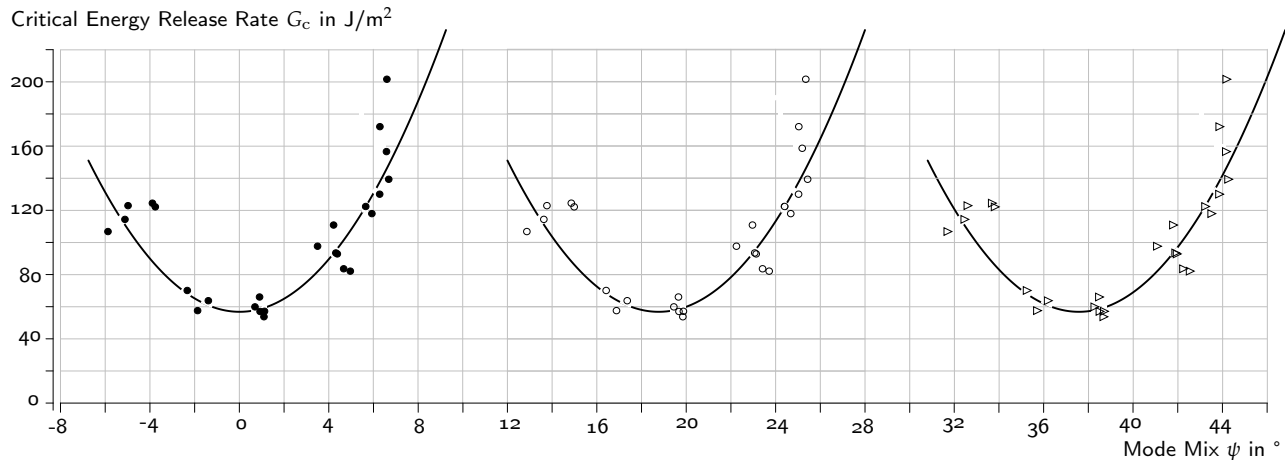


Figure 5.27: Energy release rate behavior depending on a choice of l_{ref} . The plot shows the data calculated for reference lengths of 7.66 mm, 0.092 mm, and 0.001 mm (left to right).

Extrapolation of G_c data The data range becomes interesting for application when at least one assumption can be made for mode I or mode II G_c . Since the modes are inherently coupled such a value may be called *virtual* mode I or II. Information about a *virtual* G_{Ic} , that is the critical mode I energy release rate component, can be obtained when the $G_c(\psi)$ data shows a minimum, which can be shifted along the ψ -axis by changing the reference length as explained before.³⁷ Once the zero-position is defined, a second assumption can be made for the *virtual* G_{IIc} by extrapolating the given G_c data. The before given data can be fitted based on a polynomial of 2nd order, leading to

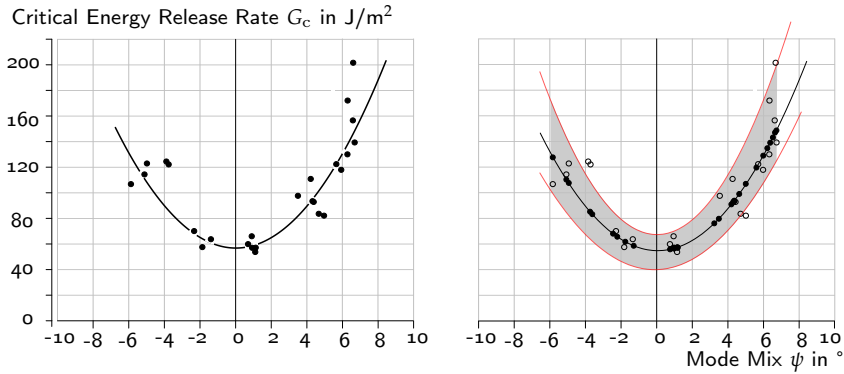
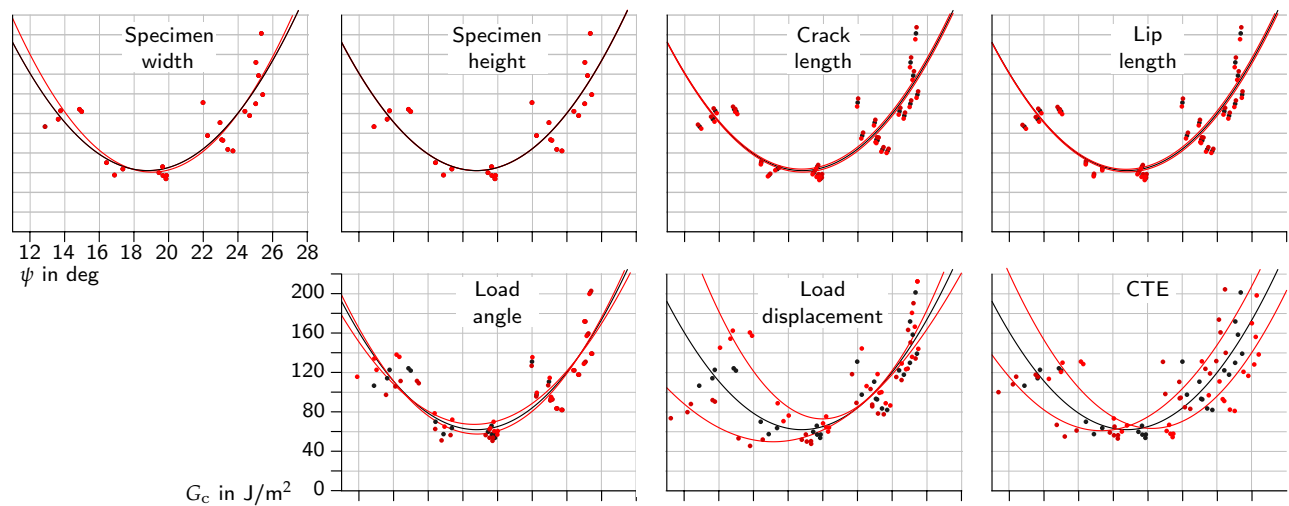
$$G_c = G_{Ic} \left(\frac{1}{31} \psi^2 + \frac{1}{76} \psi + 1 \right). \quad (5.8)$$

Although this may be a rough approximation³⁸ for G_{IIc} , it provides a means for studies within the given ψ range with an experimental basis. The projection of the measured mode mix values on the fit curve gives the following result graph. The experimental energy release rate data above and below the polynomial fit were separately fitted using the same approach accordingly, and plotted as a deviation area. They can be used to estimate limiting cases in failure modeling based on the deviations without error estimates. The deviations of the G_c values from the fit reach $\pm 16\%$, the maximum deviation of a single G_c data point reaches $+20\%$. This finding excludes deviations from error sources that are described in the next paragraph.

Deviations Figure 5.29 shows the measures that impact $G_c(\psi)$ the most: four geometry measures, one setting, one read out, and one material property.

³⁷ Hutchinson and Suo 1992, Liechti and Chai 1991

³⁸ For other fitting approaches see Pape et al. 2012.

Figure 5.28: Fitting the $G_c(\psi)$ values.Figure 5.29: Deviation of G_c results in case of errors in the different simulation model inputs. $l_{ref}=0.092$ mm.

The errors were assumed as follows. The specimen width and height taken directly from the sample with $\pm 10 \mu\text{m}$, the lip and crack lengths with $\pm 35 \mu\text{m}$, the load angle with $\pm 1^\circ$, the load displacement with $\pm 5 \mu\text{m}$, and the CTE with $\pm 2 \text{ ppm/K}$.

Considering the application of critical data, too large deviations might be misleading in decision making based on fracture mechanics simulations. One would calculate a certain condition using a failure model, and then look at the comparison: Is the situation critical for the interface or not. That means, is G for the given case higher than G_c or is it lower? Lower is fine and safe, higher means fracture. The *crucial* deviation in a decision supporting simulation is thus to obtain lower G_c values than they really are. Likewise the crucial deviation when establishing the interface properties is to obtain higher G_c values than they really are. As Figure 5.29 demonstrates, the impact of the load displacement measurement and the thermal expansion are the

biggest. The deviations clarify that the fracture criterion is not merely a matter of higher or lower G_c values:

$$G(\psi(l_{\text{ref}}, \epsilon)) \geq G_c(\psi(l_{\text{ref}}, \epsilon)). \quad (5.9)$$

To setup this criterion a simulation needs to accompany any decision making, and the error influences need care.

State of the Delaminated Surface

All delaminated silicon surfaces were free of EMC residuals. In some specimens parts of the silicon die fractured instead of delaminating. But none of the specimens showed cracks partly running through the EMC or its epoxy rich layer, such as observed at the EMC-Leadframe interface delamination by Xiao et al. 2010, and as shown in Figure 5.30.

The obtained mode mix angles are however restricted to low shear components at the crack tip, so that it is still to be answered, whether similar residuals occur at higher shear loads also on a silicon die surface with a substantially lower roughness than the leadframes. Such EMC cracking would enlarge the effective cracked area. The only kinking cracks found affected the silicon material, probably caused by flaws in the silicon strip flanks. This part of the specimen should be handled with care during the preparation steps in order to avoid pre-test fracture. Most flaws occurred at the flanks of the first prototype specimens, and vanished after adding a polishing step to the preparation sequence. Figure 5.31 shows an example of a roughly exposed interface flank without polishing. Examples of such bulk cracks through silicon can be seen in Figure 5.32. The results of delaminations with such massive silicon cracks were excluded from the G_c calculations.

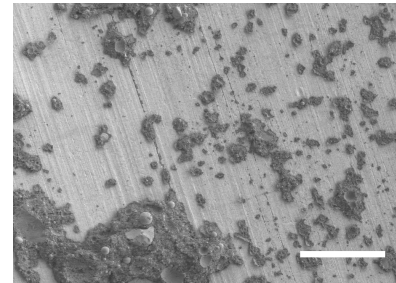
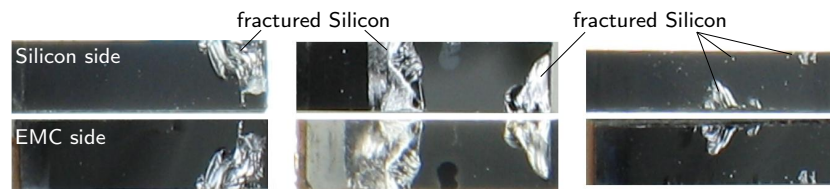


Figure 5.30: Some EMC-Leadframe specimens showed cracks running through parts of the EMC layer, as observed by Xiao et al. 2010. SEM image of secondary electron detector, at 1 kV. The bar is 100 μm .

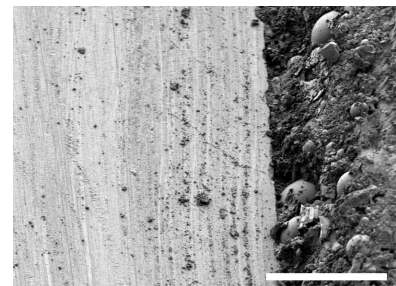


Figure 5.31: Interface flank of an early Si-EMC specimen without polishing, showing micro cracks at the edge. Such led to bulk fracture during the experiments. SEM image of secondary electron detector, at 1 kV. The bar is 50 μm .

Figure 5.32: Fracture residuals of silicon on the delaminated specimens. Three pairs of silicon bulk fracture photographed after delamination, showing both the EMC load lip and the silicon die. Interfaces are 7 mm long (horizontally), delamination running from left to right.

6

Discussion — Relevant Detail to Interpret the Results

6.1 Crucial Aspects of the Fracture Mechanics Details

Shifting G_c by a Reference Length Choosing a reference length based on geometry considerations or lattice characteristics deprives the user of an extrapolated *virtual* mode I or II. The extrapolation is always possible by changing the choice of l_{ref} , but a useful choice based on a global minimum of $G_c(\psi)$ makes the original choice obsolete. This opens questions and allows some conclusions for further studies and applications.

- 1 If adjusting a reference length later massively for a *virtual* mode I, do I have to assume a length in the first place? Past research suggested to arbitrarily choose a length, although basing it on either the geometry or an interface specific value.
- 2 If the interfacial toughness obtained by the fracture mechanics approach is a valid interface property, any setups or specimens capable to provide $G_c(\psi)$ should yield the same toughness result against a local stress state including the minimum. That means, the choices of l_{ref} by others so far are contradictory. If $G_c(\psi)$ is a geometry and thus sample-independent interface property, the minimum should always be the same. $G_c(\psi)$ should be minimal at a comparable stress state. And to describe the stress state, mode mix and reference length must be used *together*. Previously, an $l_{\text{ref}}=500\ \mu\text{m}$ was prohibitive for a case involving smaller characteristic length scales such as layer thickness. This contradicts the minimum related choice of l_{ref} . Following the shifting concept and minimum approach the size constraint of l_{ref} becomes obsolete. The question is, can two tests of the same *one* interface using different specimens in parallel experiments show consistently the same data set of interfacial toughness? Future work must answer this question.

On the other hand, if a data set is applied to estimate the risk of fracture, a reference length has to be chosen correctly as well,

except for energy release rates G_{app} that are orders of magnitude from critical. This reference length cannot be arbitrarily chosen. It might be set the same as the one of the available data set $l_{\text{ref,app}} = l_{\text{ref,data}}$. But without verification from multi-specimen experiments the representation of a *virtual* mode I is not available for both the application and the data acquisition.

- 3 Despite questions 1 and 2, the parameter l_{ref} is crucial to make use of published data sets.
- 4 If l_{ref} expresses the crack tip stress orientation *together* with ψ uniquely (and ψ cannot do this alone), and if every interface exhibits a global minimum associated with a *virtual* mode I, can then two low-error experiments show actually a different curve? And must not a shift to $\psi=0$ using l_{ref} lead to an inherent interfacial $l_{\text{ref,IF}}$, instead of being unique to the experiment? And how can such an $l_{\text{ref,IF}}$ possibly be determined before a first arbitrary choice?
- 5 To better understand the choice of $l_{\text{ref,IF}}$, how can the relation of tensile to shear load field at the crack tip be efficiently visualized?

Fitting G_c to Provide Look-Up Properties Figure 6.1 compares the Si-EMC data with two examples of a wide range of $G_c(\psi)$ values. The used polynomial fits follow equation 5.8, and read for Liechti, Durix and Schlottig:

$$G_c = G_{\text{Ic}} \left(\frac{1}{142} \psi^2 - \frac{1}{10} \psi + 1 \right), \quad (6.1)$$

$$G_c = G_{\text{Ic}} \left(\frac{1}{140} \psi^2 + \frac{1}{34} \psi + 1 \right), \quad (6.2)$$

$$G_c = G_{\text{Ic}} \left(\frac{1}{31} \psi^2 + \frac{1}{76} \psi + 1 \right). \quad (6.3)$$

Whether the plot for different interfaces in one graph is fruitful remains to be seen.¹ Shifting all these data to its global minimum of $\psi=0$ as suggested by the according authors, reveals two crucial questions for the application of such critical interface toughness. Both of these questions have not been answered yet to the knowledge of the author.

¹ see page 99.

- 1 Do *any* two curves of two different interfaces cross at all; and if yes, can it be verified that when the load state reaches the cross point their toughness relation does change accordingly in reality?
- 2 Can for one interface a second, identical curve be found from a second, yet different delamination setup?

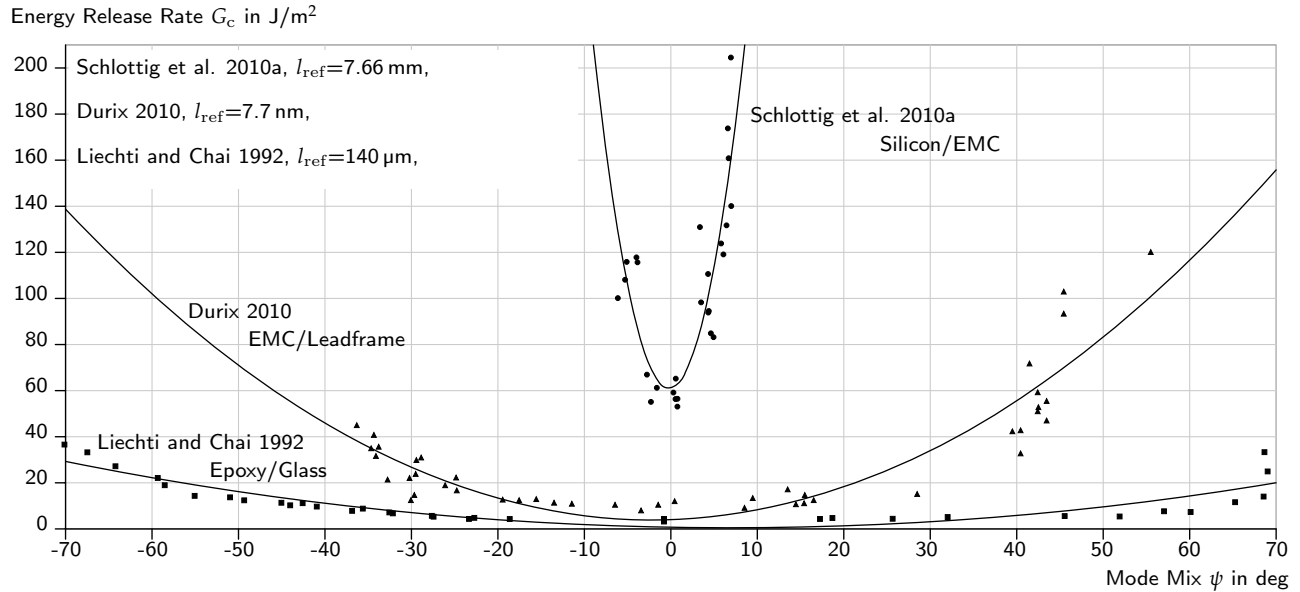


Figure 6.1: Comparison of three different interfaces for a range of ψ values. The reference lengths used are different. All polynomial fitting shown is authored in this work.

The first question might sound hasty on the first read. And indeed when using the same reference length for two different interfaces, their G_c curves most likely *do* cross. And the curves do also likely cross if one data set is asymmetric to $\psi=0$, an aspect of interface properties discussed by several researchers. Although observed, asymmetry could up to today not be identified to be an interface property.² Except for a plastic zone³ it might be rather due to aspects such as micro-cracks that shield a macroscopic crack or friction of the crack faces.⁴ If present, such effects must obviously be considered in the analysis to obtain inherent interfacial fracture toughness. Based on the lack of significant evidence for a G_c asymmetry as an interface property it is neglected here. Despite possibly different interface behavior the question of cross points remains, considering the reference lengths chosen for the sake of a *virtual* mode I such as in Figure 6.1.

The second question demands a double testing to benchmark a delamination test. This procedure is easily done in material property modeling, when the properties can be extracted without numerical simulation. In such cases the experiment can be simulated itself to compare a sample behavior in the model to its reality. But if numeric modeling is necessary for the interpretation of the testing itself, a different comparison is necessary.

Multi-specimen approaches have not been published except for experiments with different intentions⁵ and except for *double-interface* experiments, that is specimens whose materials are bonded by an adhesive. Cao and Evans for instance compare $G_c(\psi)$ of such interfaces

² Liechti and Chai 1992, Mantić 2008, Karlsson 2008

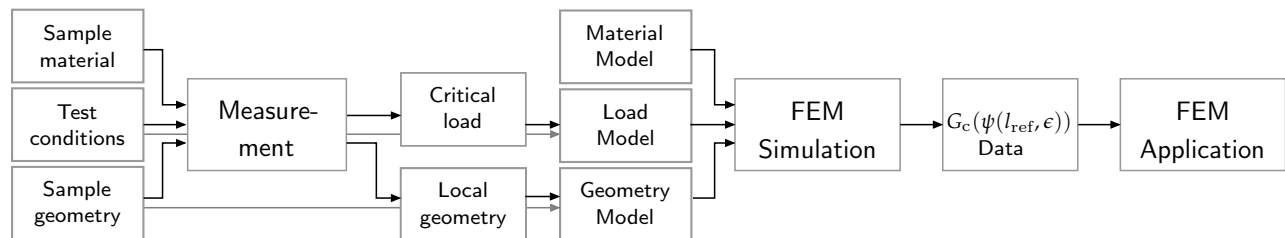
³ Dollhofer et al. 2001

⁴ Hutchinson 1987, Liechti and Chai 1992

⁵ Rosenfeld et al. 1990

using two different specimens and setups.⁶ However double-interface specimens are limited in their material selection⁷, and experience different stress states, especially if elastically similar materials such as glass and aluminum are bonded together. Figure 6.11 on *page 101* shows the impact of differently mismatching material combinations. Depending on the adhesive thickness the crack tip stress field is largely dominated by elastically similar materials. A multi-specimen benchmark is especially interesting for interfaces with a larger mismatch, that is with a stronger need for interfacial fracture mechanics.

The 4PB specimen demonstrated on *page 61* could serve such purpose, although it is limited to a small ψ range. Future work might provide such benchmarks. Without, the procedure to obtain interfacial fracture properties is as shown in Figure 6.2 below.



6 Cao and Evans 1989

7 although with easier specimen preparation

Figure 6.2: The procedure to obtain interfacial fracture properties without a benchmark.

Limits of the mode mix The mode mix ψ considers only one interfacial bond at a time, plus in some cases the neighbor interfacial bond. For this assumption, and *only* based on this assumption, the empiric values were found for different mode components. This model is simple and serves the engineering needs very well. It is questionable whether the model should be kept up when looking into the future of multi-scale modeling. In reality different aspects are involved in adhesion, and even when using a macro-scale continuum mechanical approach, the *one bond at a time* approach is not a fully bijective description. If one interfacial bond opens in the model, the neighboring bonds dominate the stress field around that opening bond. These neighbors are not necessarily interfacial ones only, but should be considered in the stress state description. This is not to confuse with the force implementation of the neighbor nodes in the VCC method in numeric modeling. The CSDE approach only considers a number of interfacial bond displacement ratios. The CSDE-based mode mix as part of the stress field description draws from this ratio alone. Figure 6.3 shows an example of such ratios for the Si-EMC interface.

This description does not show the difference for negative u_x or u_y . CSDE does distinguish between positive and negative u_x direction, that is whether an interfacial bond is compressed or pulled in the

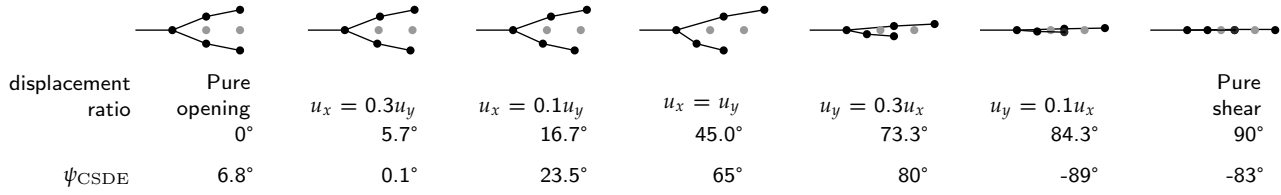


Figure 6.3: The different ratios of nodal displacements in the CSDE approach for positive values of both u_x and u_y at the Si-EMC interface.

x -coordinate sense. CSDE does not distinguish between positive and negative u_y , because negative u_y express penetration of the crack flanks. From Figure 6.3 it is however clear that ψ crosses its quadrant limits two times for the positive displacement differences only, and accordingly for a negative u_x . This gives four crossings, or ψ values in five quadrants for all possible cases that the CSDE method handles. Unfortunately publications of such a wide load range are hard to find. Moreover, the following hypothetical nodal displacements are regarded the *same* load cases using the CSDE.

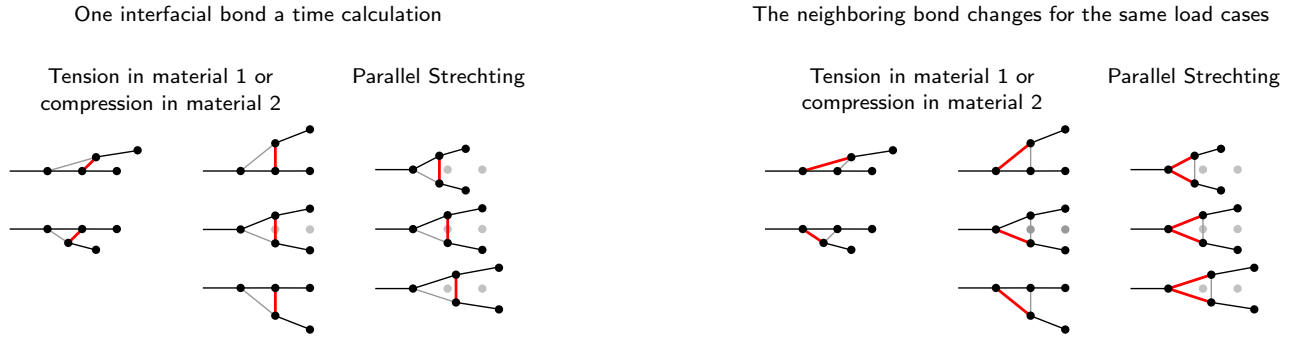


Figure 6.4: Three groups of hypothetical load cases that CSDE cannot distinguish.

Although beside ψ there are two more parameters l_{ref} and ϵ to describe a stress state uniquely, they do not add information to distinguish these hypothetical cases when modeling a one interfacial bond a time description. The recent advances in MD simulations might soon contribute to the potential of neighboring bulk bonds for a stress state description.

6.2 The Largest Impacts and the Uncertainties

If assuming the errors described on page 87 for the specimen geometry measurements, for the crack length estimates, and the load angle, their impact on G_c can be neglected. The tolerances in the contact points as described in section 3.3 were not analyzed further, because the symmetry of all stainings to the specimen's center line did not indicate any substantial angular errors, except for specimens with substantial silicon fracture. The crack front shape however has another implication.



Figure 6.5: Example of a stained crack front (topview), delamination ran from bottom upwards, the image covers the entire specimen thickness which is 2mm, the ink reflects the delaminated area, that is the area where the color penetrated the crack.

The crack front is usually not straight across the interface, depending on the sample geometry as described on *page 74*. Thus also the differences between center and outer crack position vary with interface and geometry. For a curved delamination front a 2D model must introduce some error, be it plane stress or plane strain, because the delamination front is assumed straight, and because any delamination front curve is reduced to one projected point. But errors can also be made in other assumptions. During the delamination experiment the shape of the delamination front can change. Figure 6.6 shows such a possible change.

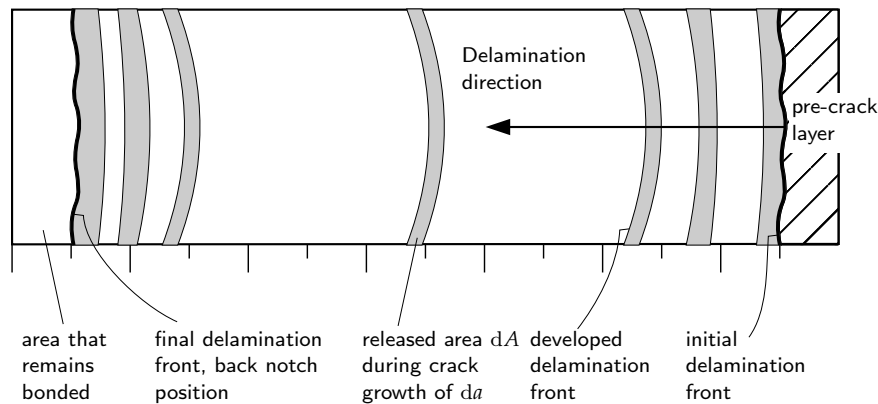


Figure 6.6: Developing delamination profile, topview.

Calculating G_c always demands an assumption for the crack length, and for each such calculation a infinitesimal crack extension of da is assumed. This extension refers to the release of an area dA during crack growth along the length da . When now comparing the results G_c of a very short, initial crack length to the ones at the mid of the specimen, two different shapes of delamination front represent also different areas released. At the initial state the profile is approximately straight as defined by the pre-crack layer edge, and during delamination the crack grows faster at the specimen flanks. The energy released into new surface is related to this new surface as unit area, and is considered as one unit area only in the calculation. At short crack lengths the delamination front changes from straight to a curved profile. The released surface has a curved line at its front, just as in the middle of the specimen. But at short crack lengths, the delamination front curves less. Thus initially, the released area is bigger at equal crack length advances observed at the flank. If the released energy relates now to the same unit area, which is smaller in the middle than the real area at short crack lengths, then the obtained values G_c are bigger than they would be with the correct area related. Thus for ahead run-

ning flank delamination I might over-predict G_c at short crack lengths. And for reversely shaped crack lengths the opposite could be the case.

The profile change between compared cases should be as small as possible. If the profile changes too much a correct infinitesimal unit area cannot be established. This opens the question for future work, how much the deviation is due to profile change during one delamination, along one specimen interface. Other reasons for the different crack position at the edge may include material flaws, locally changed properties due to processing such as dicing, the residual stress state and the loading stress state.

In addition to the crack length findings presented in Figure 5.24 on page 84, the plot below shows results from short and long crack lengths. Short and long crack lengths are here defined as less than 3 mm and more than 5 mm long. Considering the areas as drawn in Figure 6.6 these limits correspond to three zones to compare. These are of approximately 2 mm length and take the potential delamination front change into account. The data points of delamination fronts closer to the pre-crack and closer to the backnotch would give an impression of insignificant $G_c(l_{ref})$ dependency.

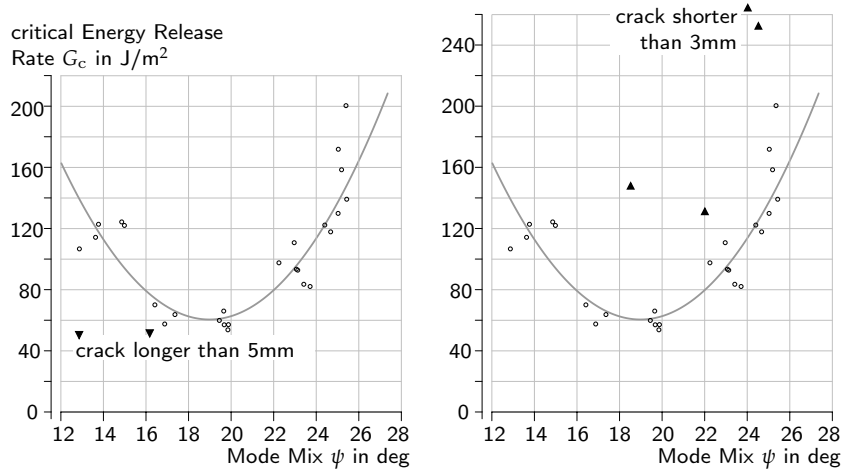


Figure 6.7: The effect of calculating G_c from too short or long crack lengths.

To exclude any artefacts of the setup or specimens within the mid range of crack lengths from 3 to 5 mm, Figure 6.8 shows the mode mix plotted against the crack length for different load angle settings. Within no load angle setting any outlying data point can be seen. The maximum angle difference for a load angle setting is approximately $\Delta\alpha = 2^\circ$ and thus the change of mode mix with crack length for most settings low. The steepest load angle of 75.8° with a most rapid change in external tensile load component shows the biggest variation of mode mix for a crack length span of 0.4 mm. Potential further investigations on delamination front changes with crack length could benefit from a load angle setting with a low change

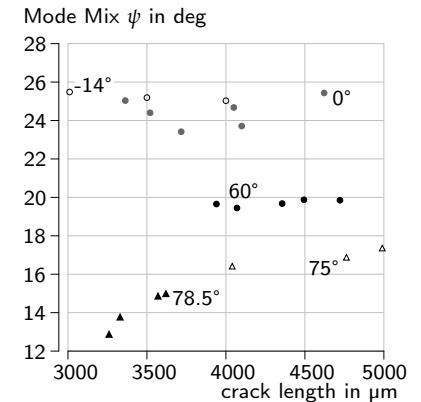


Figure 6.8: The effect of calculating G_c from too short or long crack lengths (left), and the control against a direct dependence of mode mix on crack length.

of mode mix to expect. Mode mix changes in short and long crack lengths may be detected easier.

Attention should also be given to the displacement measurement and the material data. Although the displacement measurement profits from the load device accuracy, in this case about $\pm 0.1 \mu\text{m}$, the correlation of two data set time lines influences this accuracy. The procedure was described on *page 67*, and its accuracy can be improved by a high data acquisition rate for both the images and the displacement records. The deviation graph in Figure 5.29 is asymmetric in respect to the mode mix ψ . Both G_c and ψ increasingly deviate at higher external shear loads, that is experiments with higher force ranges and smaller absolute displacements. While for tensile loads a displacement difference of $1 \mu\text{m}$ between a pair of neighboring data points is sufficient, this difference should be an order of magnitude smaller at high external shear loads.

The CTE impacts the $G_c(\psi)$ curve in a different way. While the G_c values deviate by a maximum of 7% but not significantly between the polynomial fits, the mode mix is significantly shifted by 1.7° or 14% of the given ψ range for a difference of 2 ppm/K in expansion only. This suggests two future activities.

First the discrepancy between the PVT and the TMA measurements should be explained to use most accurate data in the simulations. Second, the cure shrink should be included in future EMC delamination studies, because the deviations shown in Figure 5.29 on *page 87* indicate a strong dependence on the expansion and contraction behavior of the materials. Including the cure shrink in the modeling would account for an additional contraction load in the initial state of the specimen, a contraction contributing to thermal contraction caused loads. Consequently the model would exhibit a higher residually stressed state. Since the experimental results do not change and can be readily used, the energy release rate calculation will presumably yield an even higher value. The opposite is to be expected for the viscoelastic model, allowing the specimen to relax some of the stresses during cool down. Figure 6.9 shows $G_c(\psi)$ determined from both the viscoelastic and linear elastic model using the same CTE.

The approximate maximum difference of $G_{c,ve}/G_{c,el}$ is about 8.7% when neglecting the mode mix differences, which vary along the mode mix from 0.1% to 16%. The polynomial fits of both appear to mainly differ in G_c , and reach approximately 8% as well. The fit curves suggest that at room temperature the CTE influence on the residual stresses and thus the values of G_c is bigger than the influence from choosing a viscoelastic or linear elastic material model. This finding is specific to the specimens and preparation procedure used in this

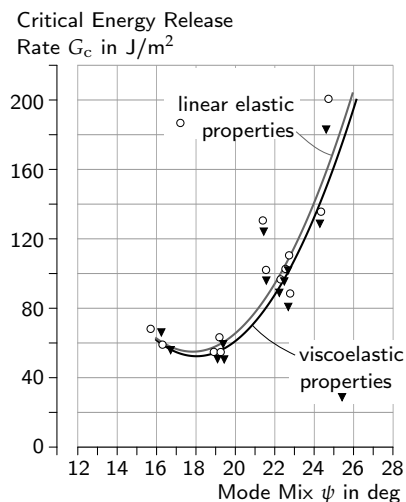


Figure 6.9: Critical energy release rates determined for viscoelastic and linear elastic EMC behavior.

work. For applied problems in electronic packages the results may be different.

For electronic packaging such stresses can change the model significantly and were recognized early by Bailey and Parvizi, Miyano et al., and Nakamura et al.⁸ and implemented into reliability modeling already⁹. Although residual stresses can be neglected for some applications, their role is often influential when composites are involved.¹⁰

6.3 Comparing Interface and Bulk Fracture

EMC Fracture The mode I energy release rate of the CEL compound was measured to be 140 to 170 J/m² using the CT specimens described on page 56.¹¹ For both materials involved in this work, the EMC bulk cracks ran around the filler particles of the material.

Silicon Fracture The mode I fracture properties of bulk silicon are well established to be 8.7 to 36.3 J/m² depending on the crystal orientation.¹² These values were given for a crack starting from a stress concentration such as around a micro-notch. Silicon fracture properties have been applied to various problems for instance in mechanical silicon structures.¹³ An important finding is that the penetration depth of flaws and micro cracks can be evaluated to determine the fracture risk¹⁴, and it is thus to keep the damage of silicon bulk involved in interface specimens low and the damage size small.

Aspects of Comparison A detailed comparison between the interfacial fracture toughness and that of Si and EMC was not carried out in this work. Yet the observations might contribute to future studies. Interestingly the values for the EMC given before are comparably high for the mode I load. Before introducing the back notch feature in the MMC specimens, the bulk crack through the load lip, after the delamination ended, was bound to a substantial load increase as shown in Figure 4.22 on page 61. This hints that for the mixed mode loading situation to be critical, additional energy had to be supplied in comparison to the mixed mode loading situation at the interface. To fully compare the fracture toughness in different load situations more experiments would be necessary for the EMC fracture. But it might also be helpful to change the modeling approach from the continuum approach working with homogenized material properties of a composite to a more detailed micro-scale model.

One related aspect encountered during the EMC-fracture experiments is the fact that EMC cracks run always around its filler particles. Figure 6.10 shows an example of such crack paths.

8 Bailey and Parvizi 1981, Miyano et al. 1982, Nakamura et al. 1988

9 Wunderle 2003, Driel et al. 2003, Vreugd et al. 2008

10 Hutchinson and Suo 1992, Chandra 2002

11 Walter and Hartmann 2010

12 Brantley 1973, Ando et al. 2004

13 Mariani et al. 2010

14 Petersen 1982

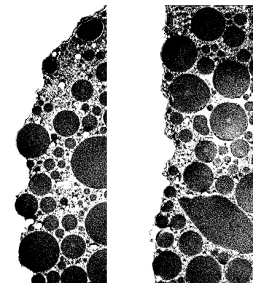


Figure 6.10: Two examples of typical cracks through EMC bulk material. Shown are microscopic photos of polished cross sections made from fractured EMC. The embedding resin is shown white and thus invisible. The straight perpendicular lines are the photo edges. The cracks run around the filler particles. The largest filler particle diameter is 75 μm .

The macroscopic crack path observed for the EMC bulk is shorter than the actual path. If considering this micro-scale geometry, the critical energy relates to a larger released area and therefore G_{Ic} becomes smaller. When assuming a delamination from filler equator to filler equator¹⁵, the created surface is dominated by semi-spheres. It is then $2\pi r$ for each filler involved – two times the flat interfacial area with zero roughness. For a 2D model of the problem the crack path would only be about 57% longer, a considerable difference.

¹⁵ This assumption is theoretical, involves a wide range of filler diameters and a dense packing of the fillers, and cannot be achieved fully in technical materials.

But other aspects would enter the model as well, such as filler size, shape and distribution, as well as their material properties and those of the epoxy matrix and other EMC components. Therefore the stress situation would be different, both for EMC bulk fracture and the interface fracture EMC to silicon. Beside the new surface area, a microscopically analyzed crack path will also show changes in mode mix, because the crack direction changes several times. Such changes can involve range up to 180° for a 2D model. In a 3D model the local crack tip must involve mode III components. If the energies needed for the different local modes are different, a microscopically zick-zack shaped crack path can be explained.

Accordingly, a comparison at the micro-scale would also need surface roughness included in the model of interfaces, an aspect that for the here used composite model is not modeled but listed in the interface properties. To summarize, a comparison needs the bulk fracture data of different load cases, and it might be helpful to use models at smaller length scales to consider a difference of real created surface to projected (macroscopically seen) surface, a continuous change of stress mode mix in the bulk crack, multiple mode mixes in parallel during a bulk crack, a dependence of real created surface in the bulk on filler distribution, shape and size, and the surface roughness of the compared interface partner.

6.4 *Limits of the MMC*

The Mixed Mode Chisel setup offers several ways for improvement. Mainly the mode mix range should be extended, the contact line should exclude one degree of freedom more, and the cage re-design could extend the maximal possible load displacement. The first two options are connected to each other. The chisel concept for instance constrains the specimen movement much less during the delamination than the leaf spring loading does, which can extend the mode mix range. Thus a major improvement would be a chisel design that rids the contact line of the friction problem.

To clamp smaller size specimens in the MMC setup, adaptations are necessary to accurately align the specimen to the load axis. A 1 mm

high EMC-to-leadframe bimaterial sample as used by Xiao et al.¹⁶ was successfully clamped and delaminated. Smaller specimens are difficult to clamp by hand and eye. A possible approach of flank clamping was shown by Renart et al.¹⁷. And an advanced clamping mechanism could improve another aspect.

¹⁶ Xiao et al. 2008a

¹⁷ Renart et al. 2010

Crack tip recognition has consumed long time periods of the data analysis. If a method can be found to clamp the specimen sufficiently for crack length independence (see *page 33 ff.*), the delamination testing could be much faster and cheaper and thus better feasible in reliability application. Furthermore, for some questions a crack tracing will remain desirable. The transparency of some materials, such as the infrared spectrum for silicon, offers the possibility to monitor the crack shape in two dimensions. The crack shape may be especially interesting when looking at delaminations *in* electronic packages.

At the base of the MMC concept lays the idea that by mechanically inducing damage to the material interface, it is possible to determine fracture mechanical interface properties. Failure usually does however occur under a thermal load, as the case may be under an additional influence of moisture, or under a fatigue or aging phenomenon. A first simulation to show a thermally induced failure by a shock cooling from molding temperature to -80°C showed that the potential energy release rates reached at a pre-crack front would not meet critical levels. A full applicability with results obtained from the MMC or similar tests that isolate the delamination phenomenon from its surrounding factors, should thus be validated in a low-complexity electronic package. This concept was successfully shown in the solder creep damage research, as recently summarized by Wiese¹⁸.

¹⁸ Wiese 2010

6.5 Data Visualization — A Display of Energy Release Rate

The interfacial fracture chapter explained the multivariate character of the fracture mechanical description: At the interface the measures for quantity and uniqueness depend on two more dimensions, thus we describe always *four* measures at a time: $G_c(\psi(l_{\text{ref}}, \epsilon))$. Yet practice today by virtually all researchers is, to show the interfacial fracture properties on a two-variable base. While this display shows an important character of the interfacial toughness data—the change of intensity with stress field orientation—it might be misleading once another data set is added to the same graph. A data set of a different interface especially. Or a data set calculated using a different reference length or likewise. Because in all such cases an altered parameter is not displayed, and yet the graph urges to compare the data. The reader might not consider a comparison necessary when looking at one

interface. Yet if he compares, the need for a numeric simulation might be underestimated.

A comparison of interfacial toughness on this graphical basis should be avoided. At present, the most valuable fracture toughness comparison involves several simulations and establishing in each the criterion for the affected interface.¹⁹ This is a significant difference to bulk fracture mechanics, where a stress intensity factor is used for comparison without further simulations.

It might be argued, that even single valued comparisons of G_c for different interfaces are problematic. Such comparisons are apparently common practice to some extent²⁰, indicating that tendencies might be predicted correctly. Whether predictions can be upheld for different load cases is questionable.

The smaller the ϵ difference between eventually compared interfaces becomes, the less necessary should a set of four measures be. This is especially interesting for electronic packaging applications, because the interfacial strength is often dominated by engineered surfaces thinner than $1\ \mu\text{m}$. And therefore, regardless of surface treatments, the ϵ characterizing the interface and the crack tip stress state remains the same. If then also calculating with one, defined l_{ref} , the energy release rate $G_c(\psi)$ turns out to be 2-dimensional again. Therefore: Comparing interfaces of small differences in their elastic mismatch ϵ can be done graphically, without further simulations. This is especially important for interfaces dominated by surface treatments.

Suga et al. plotted the Dundurs parameters β against α for a variety of different material combinations, similar to the one shown here in Figure 6.11. The plot is limited by physical restrictions of Poisson's ratios between 0 and 0.5 and a positive shear modulus and thus forms a parallelogram. Every material combination with its four elastic parameters defines a certain point within the parallelogram, and likewise one point can refer to different material combinations. The origin of the plot represents no difference in the material properties, that is no elastically mismatching interface. As Suga et al.²¹ pointed out

... each pair of values α, β within the parallelogram is a measure for the elastic anisotropy of the corresponding material combination...

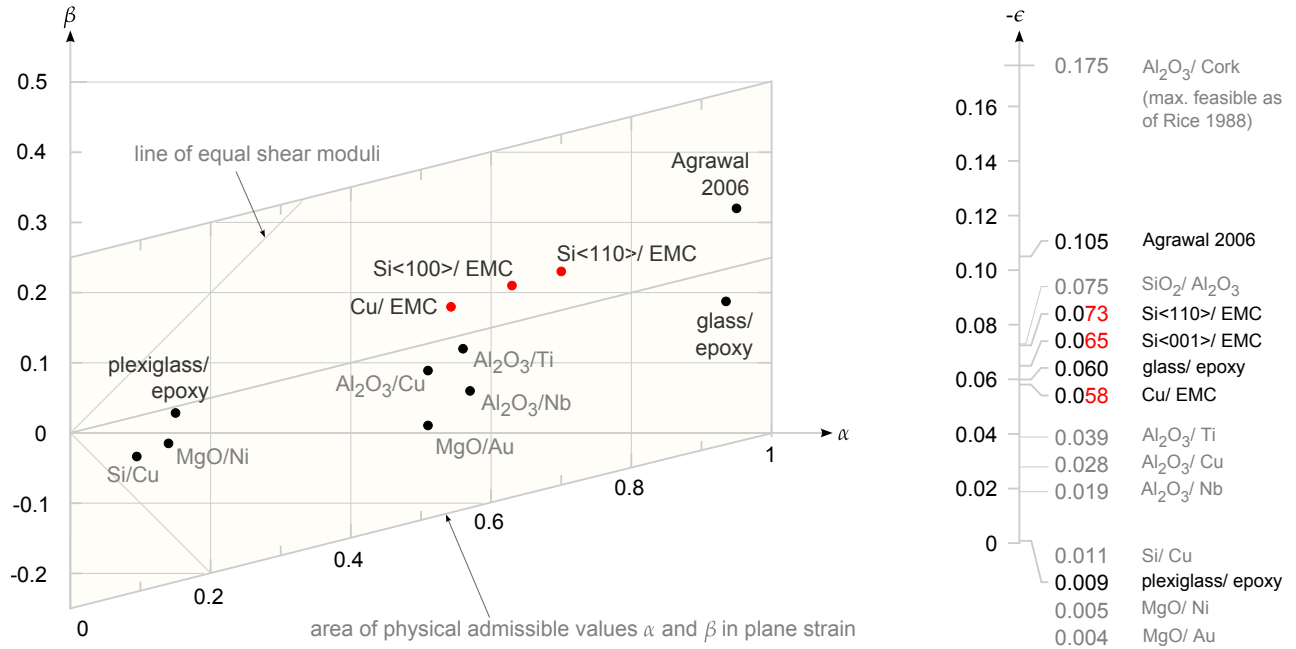
The further away the point of material combinations from the plot origin the bigger the difference of the materials, and the more important the interface specific distinction between the modes for fracture description. Accordingly, the closer to the origin, the less important it is, and when ϵ becomes very small the reference length concept can be dropped entirely.²² Therefore the plot might be helpful to estimate the effort necessary in the fracture mechanics calculations and in the interface comparisons. It may be added, that all $G_c(\psi(l_{\text{ref}}, \epsilon))$ depend on β only.

¹⁹ Rice explained in his 1988 publication on the use of \bar{K} and the reference length, that a comparison is straight forward just as in bulk fracture mechanics. Literature on this aspect is however hard to find.

²⁰ Gibbesch et al. 1992, Mukherjee et al. 1997, Chandra and Ghonem 2001

²¹ Suga et al. 1988

²² Hutchinson and Suo 1992



Furthermore, the plot can be used to deduct crack tip stress field expressions for different crack geometry scenarios. Zhang for instance explains in his 2007 work in detail the graph's features for cracks impinging upon a material interface from different angles.

Figure 6.11: The plot of β against α shows that the interfaces recently investigated do not lay in the vicinity of $\alpha/4 \geq \beta > 0$ suggested for simplifications by Rice. Note that an ϵ increase represents an increasing difference between homogeneous media fracture mode angle and interfacial fracture mode angle. Adapted from Dundurs 1969, and Suga et al. 1988.

Conclusions and Recommendations

This work started out with the aim to describe the fracture between Silicon and Epoxy Molding Compound, and therefore with finding a *first* way to successfully induce delamination in an Si-EMC interface by using any sort of specimen made at fabrication relevant conditions that does not randomly fracture before the testing. Since before no such equipment existed, it was unclear which factors influence the delamination description, and especially which role residual stresses and the viscoelastic behavior of EMC play. These questions could successfully be investigated, answered, and transformed into recommendations and more precise questions. All three aims, to describe the fracture, to induce the delamination, and to fabricate the corresponding specimens were reached. The following paragraphs give a technical summary, the conclusions, and an outlook.

Technical Summary

A Mixed Mode Chisel delamination setup (MMC) and, closely linked, the corresponding specimen were developed in systematic iterations of dimensions, structure, clamping, loading, processing and handling.

The MMC can be readily used at solder reflow temperature and at moisturized climates of 85 % relative humidity. It can be clamped to different loading devices, three of which were tested.

The MMC uses a relative angle between a displacement load axis and a sandwich specimen with a load lip feature. The bending of the load lip induces a ratio of opening and shear load at the crack tip, which together with the residual stresses, the elastic properties of the interfacing materials and a reference length defines a mode mix.

The MMC load angles can readily be set between 78° and -14° , and this angle range can be extended in both directions. The present work gives the reasoning of why and how this can be done.

The specimens were made at product fabrication relevant conditions, they were sized to package scale, including the interface area to delaminate, they were intentionally designed to not randomly fracture before the testing, and they did not.

Fabricating interfacial specimens was shown in two molding technologies, including design, assembly, pre-crack formation and flank exposure. To encourage benchmarking in fracture mechanical studies a four-point-bending specimen was shown feasible to delaminate the Si-EMC interface as well.

The set of critical interfacial fracture data $G_c(\psi(l_{\text{ref}}, \epsilon))$ was determined using the modified VCCT approach of Beuth 1996, with an initial reference length choice of half the silicon die height $l_{\text{ref}} = 0.092$ mm to calculate the mode mix based on the ratio of energy release rate components. The author suggests to shift the data using a reference length of $l_{\text{ref}} = 7.66$ mm to establish a critical value for a *virtual* mode I.

The tested external load angle range of 92° translates into a mode mix range of approximately 15° at the crack tip of dried Si-EMC specimens at room temperature. The $\Delta\psi$ establishes close to the G_c minimum, and therefore dominant tensile mode opening. No crack length dependence of ψ could be observed. Throughout the work the load angle range and therefore the mode mix range could be extended in both shear orientations through several specimen and setup iterations. Both load principles are feasible, pulling the load lip out of the sandwich and pushing it into the sandwich. These findings support the given reasons of the mode mix relation to the load angle, and they open possibilities to extend the ψ range in future work.

Within the ψ range the energy release rate increases with the mode mix. The Si-EMC G_c equals values from 50 to 200 J/m² over the range of $\Delta\psi=15^\circ$ for dried specimens that were delaminated at room temperature. A data fit of G_c with a polynomial of 2nd order shows a maximum deviation from the fit of 20%, and 90% of the data lay within a $\pm 16\%$ band.

Analyzing the error influences clarified that to evaluate a delamination criterion in a specimen or package a numeric simulation must establish the stress state at the crack tip, because a mere comparison of G to G_c values is not sufficient. The deviations are biggest for errors in the load displacement and the thermal expansion model. Since the load displacement measurement during this work always involved the correlation of two data time lines, eliminating this can be a first step in future improvements. The energy release rates change substantially both in quantity and quality when residual stresses are ignored

in the numeric simulation. To the contrary the influence of viscoelastic material behavior on the energy release rate remained below 10% for the experiments at room temperature.

Contributions to the field

With the MMC it was the first time possible to successfully induce delamination in an Si-EMC interface with specimens made at product relevant conditions and of product relevant size. Neither setup nor specimen were available before, yet both were necessary to characterize the interface. This work publishes the first quantitative data set $G_{c,\text{Si-EMC}}(\psi(l_{\text{ref}}, \epsilon))$.

This work supports previous findings that it is necessary to develop specimen and setup together when determining material properties at the package scale. To allow industry use, this work gives both design rules for the specimen and the reasoning of the design decisions of the MMC setup.

This work discusses for the first time the relevance of defining dedicated reference lengths in interfacial fracture data acquisition *and* application. This includes the question when such reference lengths have to be defined, and in which cases they cannot be chosen arbitrarily, thereby opposing previous publications. The reference length is useful and necessary to uniquely describe interfacial fracture properties. The consequence of allowing the mode mix to shift by an arbitrary choice of reference length is a loss in physical meaning.

To support their optimum use, comparison, and interpretation this work explicitly suggests ways of how to report and display interfacial fracture data, and which pitfalls to avoid in their display. Among the display suggestions are for the first time data fits of $G_{c,\text{Si-EMC}}(\psi(l_{\text{ref}}, \epsilon))$ to find and use an energy release rate minimum in the data set. The fit that was published during the thesis has sparked discussions on which basis a fit can be done, followed by recent suggestions by Pape et al. 2012.

Outlook

The MMC is limited in two major aspects. It so far allowed to cover a limited mode mix range, and it is bound to acquiring the present crack length. First approaches to improve this can be a chisel design that rids the contact line of its friction problem, a cage that allows further load displacements, the clamping of smaller specimens, and approaches that make the experiment independent from the crack tip positions.

To improve accuracy, future experiments benefit from a synchronized time line of the loading device and the image acquisition. Since the calculations are sensitive to the thermal expansion data, the corresponding measurement method should be chosen with care for accuracy. Seeing the impact of the thermal expansion difference, future studies of EMC delamination may profit from more detailed residual stress modeling for instance by implementing the cure shrink in the numeric simulation.

To successfully avoid random fracture before testing care should be taken in the specimen preparation steps for the brittle silicon easily fractures before testing due to flaws and microcracks. For the specimen design and fabrication this means avoiding bidirectional warpage that must be forced flat later on, and avoiding additional stresses on the interface such as caused by dice singulation through several material layers at once.

The four measures describing interface toughness $G_c(\psi(l_{\text{ref}}, \epsilon))$ are necessary for a fully usable description and should be given in publications of interface delamination properties. Often publications lack information about l_{ref} , mode mix and the elastic mismatch epsilon.

The reference length should be chosen such that the $G_c(\psi(l_{\text{ref}}, \epsilon))$ data has a minimum at $\psi=0$.

The comparison of interfacial fracture data should be accompanied by numerical simulations to identify the local stress state at the crack tip. Comparably high loads might accompany comparably low energy release rates, and vice versa for a different interface.

The comparison of interfaces that differ only in their interface vicinity region, such as previous surface treatments with thicknesses much smaller than the observed geometry, do not need accompanying numerical simulations.

The induced delamination of interfaces with large elastic mismatch and mismatch in thermal expansion would benefit from a multi-specimen approach, in other words determining the interfacial fracture properties twice by using two different delamination setups and the according specimens. In experiments that yield values with analytical formulae the benchmark can be done by numerical simulation, in experiments that need the simulation for the result itself, this is not possible. Identifying flaws in the models could be improved by using two different modeling approaches.

Open Questions

The development and results of the MMC have also opened the following questions for future research.

- Do I have to assume l_{ref} in the first place?
- How can l_{ref} be determined before a first arbitrary choice?
- Without verification of multi-specimen experiments a *virtual* mode I is not available for *both* application and data acquisition. Can two tests of the same interface with different specimens show the same data set $G_c(\psi(l_{\text{ref}}, \epsilon))$?
- How can the relation of tensile to shear load be visualized effectively to compare the stress states of different interfaces at the crack tip?
- Do any curves of interface properties cross if shifted to their minimum?
- Is the one bond at a time mode mix description sufficient for the entire possible mode mix range?

The work contributes the understanding of induced delamination, to a faster interface property evaluation when combining simulation and experiment, and it helps building a road towards a quantitative evaluation for future rapid prototyping.

Acknowledgements

Erich Kästner once compared the forewords in books to the little gardens one has to pass through before entering a house. To some extent the acknowledgements should give insight into the house's fundamentals, the shoulders on which the house was built. Since the basement of this house has many rooms with brick-rich thick walls, it may happen that I forget to name one or the other shoulder. Please excuse me in this case, you are in solid company.

Prof. Dr. Leo Ernst, thank you for the always open ear and open opinion of the supervisor, for your speedy yet diligent reading, and for your easy adapting to the schedules of international collaboration. I would also like to thank you for expressing your helpful opinion against all odds that have been there.

I would like to thank Prof. Dr. Bernhard Wunderle for establishing the contact between the candidate and the institutes that took part in this work and the neighboring project. Right from the beginning you kept the bureaucracy as much out of the way as possible, something that is not automatically to expect in the cost driven electronic industry or research related to it. Bernhard, I would also like to thank you a lot for your unresting capacity to encourage the candidate to build on his intrinsic motivation, or to finding back to it and the exciting possibilities. Both the technical and the balancing part I appreciate a lot.

I would like to thank Heinz Pape, for setting up the project, and for your permanent trying and succeeding to create what framework is necessary and possible for research within an industrial business environment. Thank you also especially for consistently taking the time when necessary and for building the little bridges within the company. These thanks must be accompanied by those to all Infineon Technologies AG colleagues who freed the resources and space to allow this research in an industrial business environment. I will name some of you further on.

Heinz, Leo, and Bernhard, I thank all three of you to uphold the possibility to travel to conferences all over the planet, and to thus

get to know others and their approaches, their reasons to travel and publish, and see how things are organized in other places.

I would like to acknowledge Prof. Dr. Bernd Michel, thank you for supporting the very same thought, the possibility to travel to conferences during the research. This helped a lot on finding out who of the classical fracture mechanics field and who of the classical reliability field is interested in approaching fracture mechanical topics. It also helped linking different ideas, amazing how surrounding trigger the thinking sometimes.

Special thanks go to Dr. Markus Detert, thank you for pointing towards the team at the IZM during one of many good talks at Dresden Technical University.

I acknowledge the supporting team at Gabo Qualimeter, especially Heiko Benecke for your help with the Gabo Eplexor secrets. I would like to thank the team at CWM in Chemnitz, especially Bettina Seiler, Dr. Michael Dost, and Rolf Erb for your help in using the μ DAC for analyzing large parts of the crack images. Also, many thanks to the colleagues at Disco Hi-Tec Europe for enabling the dicing of the molding compound wafers. Thanks go to Met-L-Chek for their support on the staining experiments, to Acmos Chemie for their support on de-molding process, and to Sill Optics and Stemmer Imaging for the optics support.

Since a big part of the work was carried out in the labs of Fraunhofer IZM I had to chance to get to know quite a number of unique colleagues who contributed in many ways to the success. First I would like to name Dr. Hans Walter, thank you for bringing both fundamental expertise and so much light and good mood into the labs and offices. Even in the most difficult moments you ever emphasize the positive, thank you for this great example.

The constructive atmosphere was also enabled from other sides. I want to express my gratitude to Dr. Jürgen Keller, Florian Schindler-Saefkow, Raúl Mrońko, Daniel Mai, Prof. Dr. Ralph Schacht, Dr. Ole Hölck, Dr. Hossein Shirangi, Dr. Lucas Durix, Dr. Thomas Brunschwiler, Emmanouella Dermitzaki, Ingrid Maus and Mohamad Abo Ras for your support, the fruitful discussions and the *very* good times, be it in the labs and offices to inquire even the most stupid idea until something was learnt, be it at the lunch discussion table, or be it with a beer somewhere in the vastness of Berlin. I also would like to wish all the best to the young families.

Further, I would like to thank Ilona Soremski, Margitta Uhlig, and Jürgen Hussack for keeping my back free of organisatory hazzle and promptly helping out when needed, and for the technical support from Christine Bombach, Falk Luczak and Heike Kukuk-Schmid.

Across the organizations I would like to thank Dr. Peter Alpern, Dr. Jürgen Auersperg, Dr. Ellen Auerswald, Michael Bauer, Tina Bohm, Dr. Rainer Dudek, Dr. Astrid Gollhardt, Dr. Torsten Hauck, Dr. Olaf Wittler, and Dr. Dietmar Vogel, as well as Dr. Olaf van der Sluis, Sander Noijen, Dr. Peter Timmermans, and Dr. Willem van Driel for the discussions and recommendations on fracture mechanics, residual stresses, specimen preparation and specimen analysis. When starting I almost did not know anything about fracture, and, surprisingly enough, the things I knew I did not connect to fracture. I want to thank you for bringing me closer to this subject. Not less important were the discussions with Prof. Dr. Hans Albert Richard, Prof. Dr. Anette Karlsson, Prof. Dr. Andrew Tay and Dr. Guojun Hu, thank you for sharing your opinions on the details of different approaches to bulk and interfacial mode mix. Although we may disagree on some aspects, the discussions influenced the fracture mechanical part of this work. Thank you, Prof. Dr. Xuejun Fan, for kindly sharing your thoughts on moisture sensitivity and the great discussions we had the luck to share from time to time.

Alexej Ritter, thank you for your efforts on bringing the 4pb to work, Jens Reinicke for your improvements of the crack tip tracing codes, and Steffen Hartmann for your work on the bulk cracks. You have been all quite pragmatic in your work, thanks.

Within Infineon the number of people that were affected by this work impressed me, and it was a great experience to be involved in so many aspects of the business. I would like to deeply thank Stephan Stöckl and Markus Fink for your very patient support and open sharing of long experience in numeric modeling and support in the business environment of the project. Markus and Glenn Everett, thank you for introducing me to climbing and more crucial, to securing climbers, in the breaks between the research days. May you have enough rope at disposal at all times, and Stephan, may you have best concentration in the upcoming chess challenges. Further, I would like to acknowledge the always kind and prompt support from Dirk Schweitzer, Ulrich Fröhler, and Rudi Kutscherauer, as well as from Irene Eckmüller, Birgit Zaunseder and Doris Wolf.

Very special thanks go to Eduard Knauer, Dr. Irmgard Escher-Poeppel, Peter Strobel, Thomas Schollmaier, Stefan Wein, Horst Gröninger, Teodora Ossiander, Dr. Mathias Vaupel, Gina Betz and Markus Lorenz for their continuous help in the specimen fabrication in a heavily scheduled product development and manufacturing surrounding. Similarly great thanks go to Dr. Harald Preu, Dr. Walter Mack, Bettina Seidl, Dr. Juergen Walter, Norbert Söllner, Sabine Weiß, Markus Graml, Jürgen Krumschmidt, Fred Kroninger, Paul Albert, for your help on acquiring material properties and on analyzing residual

stress and fracture problems. Also thanks go to Dr. Christian Birzer and his team such as Gerhard Schütz and Viktor Wicher for your help on the elevated climate and solder temperature runs. Further I would like to thank Dr. Joachim Mahler, Dr. Angela Kessler, Dr. Thomas Wowra, Thorsten Meyer, Dr. Markus Brunnbauer, Jens Pohl, Rainer Steiner for your ideas that changed the sample making substantially.

For relating the work to related issues it was a pleasure to have discussions with Gottfried Beer, Thomas Ort, Dr. Klaus Pressel, Edward Fürgut, Dr. Khalil Hosseini and Dr. Urs Elrod. I hope to see one or the other of you soon again for enjoying a piece of Schinken, and a good story together.

I want to thank Anton Sattelmayer, Christian Dombrowski, Michael Larisch, Gerd Bamberg, Jos van Driel, Harry Jansen and Patrick van Holst for all setup related design and manufacturing help. And especially Harry and Patrick, it was great that you found the time to enable the Q800 experiments within that window in time.

For the stays in Delft and the long distance communication I would like to thank Corinne du Burck and Marianne Stolker, thank you for always promptly supporting the needs of the remote candidates. I still feel very sorry for the failed attempt to extend my stay in Delft.

Especially I feel indebted to Dr. Kaspar Jansen. Kaspar, thank you for upkeeping the spirit of the very enterprise of science. Many of our discussions still last in my memories and I would like to thank you for always curiously contributing in the variety of scientific and non-scientific discourses.

I enjoyed the collaboration with An Xiao and Dr. Jan de Vreugd, thank you for sharing your personal experiences throughout the neighbor projects. An, thank you for bringing in a very different point of view into so many a discussion. I will ignore for once the rule of thanking you told me, so thanks for hosting me in the hours of the first delaminations, and thanks for introducing me so kindly to Chinese cuisine, this will be continued. Jan, your hospitality still echos in my memories. I hope your kids will pick up your enthusiasm about so many things, and especially music, may there always be some air in an organ tube.

Also the IBM team shall not be missing in this list, although not involved in the contents, I would like to thank you for your patience and consideration in the months of preparing manuscript parts in the free hours, specifically Dr. Bruno Michel, Thomas whom I named before, Stephan Paredes, Dr. Chin Lee Ong, Dr. Patrick Ruch, Dr. Werner Escher and Yassir Madhour. Dr. Johan Engelen, thank you for the insights into the Dutch and Zamonian languages, and for your support in the now matured link between Inkscape and L^AT_EX.

At this point all the fundamentals' walls that allowed to build this kind of house are revealed. More personal and thus more solid has been the support that had allowed any house to be built. And these shoulders are of course friends of old and those I met along the way on the one hand side. Sharing a room at work or in the sometimes really tired hours is much different. So thanks for bearing and supporting to Peter, Monika, Christine, Maximilian, Markus, Peter, Ann-Sophie, Thomas, Marita, Rachna and Sepp. Christoph thanks for hosting me in the early stages in Regensburg and for the good hours spent together. I deeply thank Fredrik for his unmatched philosophical insights and critiques.

Finally, these shoulders are my family. Thank you for the motivating words and the complimenting and pointing towards the tiny successes during the days when things did not go so well. But thank you also for leading back from ivory tower to main street, and for claiming the too short time share of some of the days.

Bibliography

- A. Agrawal and A.M. Karlsson. Obtaining mode mixity for a bimaterial interface crack using the virtual crack closure technique. *International Journal of Fracture*, 141:75–98, 2006. DOI: 10.1007/s10704-006-0069-4.
- A. Agrawal and A.M. Karlsson. On the reference length and mode mixity for a bimaterial interface. *Journal of Engineering Materials and Technology*, 129(4):580–587, 2007. DOI: 10.1115/1.2772340.
- G. Alfano. On the influence of the shape of the interface law on the application of cohesive-zone models. *Composites Science and Technology*, 66:723–730, 2006. DOI: 10.1016/j.compscitech.2004.12.024.
- G.P. Anderson, K.L. DeVries, and M.L. Williams. Mixed mode stress field effect in adhesive fracture. *International Journal of Fracture*, 10(4):565–583, 1974. ISSN 0376-9429. DOI: 10.1007/BF00155259.
- T.L. Anderson. *Fracture Mechanics*. CRC Press, Boca Raton, 1995.
- T. Ando, X. Li, S. Nakao, T. Kasai, M. Shikida, and K. Sato. Effect of crystal orientation on fracture strength and fracture toughness of single crystal silicon. In *Proceedings of the 17th IEEE International Conference on Micro Electro Mechanical Systems (MEMS)*, pages 177–180, Maastricht, The Netherlands, 2004. DOI: 10.1109/MEMS.2004.1290551.
- J.A. Arleth and R.D. Demenus. A new test for thermocompression microbonds. *Electronic Products*, 9:92–94, May 1967.
- C. Atkinson. On stress singularities and interfaces in linear elastic fracture mechanics. *International Journal of Fracture*, 13:807–820, 1977. DOI: 10.1007/BF00034324.
- C. Atkinson. The interface crack with a contact zone (an analytical treatment). *International Journal of Fracture*, 18(3):161–177, 1982. DOI: 10.1007/BF00032272.

C. Atkinson, R.E. Smelser, and J. Sanchez. Combined mode fracture via the cracked brazilian disk test. *International Journal of Fracture*, 18(4):279–291, 1982. DOI: 10.1007/BF00015688.

J. Auersperg, B. Seiler, E. Cadalen, R. Dudek, and B. Michel. Fracture mechanics based crack and delamination risk evaluation and RSM/DOE concepts for advanced microelectronics applications. In *6th. Int. Conf. on Thermal, Mechanical and Multiphysics Simulation and Experiments in Micro-Electronics and Micro-Systems, EuroSimE*, 2005. DOI: 10.1109/ESimE.2005.1502799.

J. Auersperg, R. Dudek, D. Vogel, and B. Michel. Challenges for Multi-Scale modeling of multiple failure modes in microelectronics packaging. In *Proceedings of the 10th Electronics Packaging Technology Conference, EPTC.*, pages 412–418, 2008. DOI: 10.1109/EPTC.2008.4763469.

E. Auerswald. Röntgenographische Eigenspannungsmessungen an einer Sandwichstruktur aus Siliziumchip und Moldmasse. Technical report, Fraunhofer Institut für Zuverlässigkeit und Mikrointegration, Berlin, 2008.

E. Auerswald. Voruntersuchungen zum gemoldeten Silizium. Stress- / Strain-Analyse mit EBSD. Technical report, Fraunhofer Institut für Zuverlässigkeit und Mikrointegration, Berlin, 2009.

A.O. Ayhan, A.C. Kaya, and H.F. Nied. Analysis of three-dimensional interface cracks using enriched finite elements. *International Journal of Fracture*, 142:255–276, 2006. DOI: 10.1007/s10704-006-9040-7.

J.E. Bailey and A. Parvizi. On fibre debonding effects and the mechanism of transverse-ply failure in cross-ply laminates of glass fibre/thermoset composites. *Journal of Materials Science*, 16(3): 649–659, 1981. ISSN 0022-2461. DOI: 10.1007/BF02402782.

L. Banks-Sills. Application of the finite element method to linear elastic fracture mechanics. *Applied Mechanics Reviews*, 44(10):447–461, October 1991. DOI: 10.1115/1.3119488.

A. Beer. *Entwicklung von Konstruktionsregeln für die Herstellung von gemoldeten Wafern*. Diplomarbeit, Hochschule Regensburg, 2005.

S.J. Bennett, K.L. Devries, and M.L. Williams. Adhesive fracture mechanics. *International Journal of Fracture*, 10(1):33–43, 1974. ISSN 0376-9429. DOI: 10.1007/BF00955077.

J.L. Beuth. Separation of crack extension modes in orthotropic delamination models. *International Journal of Fracture*, 77(4):305–321, 1996. DOI: 10.1007/BF00036249.

- J.J. Bikerman. Theory of peeling through a hookean solid. *J. Appl. Phys.*, 28:1484, 1957. DOI: 10.1063/1.1722682.
- C. Bjerken and C. Persson. A numerical method for calculating stress intensity factors for interface cracks in bimetals. *Engineering Fracture Mechanics*, 68:235–246, 2001. DOI: 10.1016/S0013-7944(00)00098-9.
- W.L. Bradley, R.N. Cohen, and W.S. Johnson. Matrix deformation and fracture in Graphite-Reinforced epoxies. Technical Report ASTM STP 876, American Society for Testing and Materials, Philadelphia, 1985.
- W.A. Brantley. Calculated elastic constants for stress problems associated with semiconductor devices. *Journal of Applied Physics*, 44(1):534, 1973. ISSN 00218979. DOI: 10.1063/1.1661935.
- D. Broek. *Elementary engineering fracture mechanics*. Martinus Nijhoff Publishers, The Hague, 3rd edition, 1982. ISBN 90-247-2580-1.
- M. Brunnbauer, E. Fürgut, G. Beer, and T. Meyer. Embedded wafer level ball grid array (eWLB). In *8th Electronics Packaging Technology Conference (EPTC)*, page 5p, Singapore, 2006a. DOI: 10.1109/EPTC.2006.342681.
- M. Brunnbauer, E. Fürgut, G. Beer, T. Meyer, H. Hedler, J. Belonio, E. Nomura, K. Kiuchi, and K. Kobayashi. An embedded device technology based on a molded reconfigured wafer. In *56th Electronic Components and Technology Conference (ECTC)*, page 5p, San Diego, CA, 2006b. DOI: 10.1109/ECTC.2006.1645702.
- M. Brunnbauer, T. Meyer, G. Ofner, K. Müller, and R. Hagen. Embedded wafer level ball grid array (eWLB). In *33rd IEEE/CPMT International Electronic Manufacturing Technology Symposium (IEMT)*, page 6p, 2008. DOI: 10.1109/IEMT.2008.5507866.
- T.R. Brussat, S.T. Chiu, and S. Mostovoy. *Fracture mechanics for structural adhesive bonds*. Number AFNL-TR- 77-163. Defense Technical Information Center, Air Force Materials Laboratory, Wright-Patterson AFB, Ohio., 1977.
- H.C. Cao and A.G. Evans. An experimental study of the fracture resistance of bimaterial interfaces. *Mechanics of Materials*, 7(4): 295–304, June 1989. DOI: 10.1016/0167-6636(89)90020-3.
- W.C. Carpenter. Extrapolation techniques for determining stress intensity factors. *Engineering Fracture Mechanics*, 18(2):325–332, 1983. DOI: 10.1016/0013-7944(83)90143-1.

S.K. Chan, I.S. Tuba, and W.K. Wilson. On the finite element method in linear fracture mechanics. *Engineering Fracture Mechanics*, 2(1): 1–17, July 1970. ISSN 0013-7944. DOI: 10.1016/0013-7944(70)90026-3.

N. Chandra. Evaluation of interfacial fracture toughness using cohesive zone model. *Composites Part A: Applied Science and Manufacturing*, 33(10):1433–1447, October 2002. ISSN 1359-835X. DOI: 10.1016/S1359-835X(02)00173-2.

N. Chandra and H. Ghonem. Interfacial mechanics of push-out tests: theory and experiments. *Composites Part A: Applied Science and Manufacturing*, 32(3-4):575–584, 2001. DOI: 10.1016/S1359-835X(00)00051-8.

P.G. Charalambides, J. Lund, A.G. Evans, and R.M. McMeeking. A test specimen for determining the fracture resistance of bimaterial interfaces. *Journal of Applied Mechanics, Transactions ASME*, 56: 77–82, 1989. DOI: 10.1115/1.3176069.

G.P. Cherepanov. Crack propagation in continuous media. *Journal of Applied Mathematics and Mechanics*, 31(3):503–512, 1967. DOI: 10.1016/0021-8928(67)90034-2.

M. Comninou. The interface crack. *Journal of Applied Mechanics*, 44(4):631–636, December 1977. DOI: 10.1115/1.3424148.

J.H. Crews and J.R. Reeder. A mixed-mode bending apparatus for delamination testing. NASA technical memorandum NAS 1.15:100662, NASA Langley Research Center, August 1988.

H. Dannenberg. Measurement of adhesion by a blister method. *Journal of Applied Polymer Science*, 5(14):125–134, 1961. ISSN 1097-4628. DOI: 10.1002/app.1961.070051401.

B.D. Davidson and V. Sundararaman. A single leg bending test for interfacial fracture toughness determination. *International Journal of Fracture*, 78(2):193–210, 1996. ISSN 0376-9429. DOI: 10.1007/BF00034525.

B.D. Davidson, R. Krüger, and M. König. Three-dimensional analysis of center-delaminated unidirectional and multidirectional single-leg bending specimens. *Composites Science and Technology*, 54(4): 385–394, 1995. ISSN 0266-3538. DOI: 10.1016/0266-3538(95)00069-0.

B.D. Davidson, L. Yu, S.D. Lundberg, and L.M. Rao. Accuracy assessment of a three-dimensional, crack tip element based approach for predicting delamination growth in stiffened-skin geometries. *International Journal of Fracture*, 132(1):1–32, 2005. ISSN 0376-9429. DOI: 10.1007/s10704-004-8155-y.

- D.A. Dillard and A.V. Pocius, editors. *The Mechanics of Adhesion*. Adhesion Science and Engineering. Elsevier Science B. V., Amsterdam, 1st edition, 2002. ISBN 9780444511409.
- J. Dollhofer, W. Beckert, and B. Lauke. Plasticity aspects of interfacial fracture for polymer/glass specimens. *Theoretical and Applied Fracture Mechanics*, 36(1):1–15, 2001. ISSN 0167-8442. DOI: 10.1016/S0167-8442(01)00051-9.
- M. Dreßler. *Reliability Study of Stud Bump Bonding Flip Chip Assemblies on Molded Interconnect Devices*. PhD thesis, Technische Universität Berlin, February 2010.
- M. Dreßler, K-F. Becker, B. Wunderle, J. Auersperg, and H. Reichl. Application of interfacial fracture mechanics approach for obtaining design rules for flip chip interconnections. *Microsystem Technologies*, 15(1):83–88, 2009. ISSN 0946-7076. DOI: 10.1007/s00542-008-0692-2.
- W.D. van Driel, J.H.J. Janssen, G.Q. Zhang, D.G. Yang, and L.J. Ernst. Packaging induced die Stresses—Effect of chip anisotropy and Time-Dependent behavior of a molding compound. *Journal of Electronic Packaging*, 125(4):520–526, December 2003. DOI: 10.1115/1.1604153.
- W.D. van Driel, D.G. Yang, M. van Kleef, and G.Q. Zhang. Mechanical reliability challenges for mems packages: Capping. In *18th European Symposium Reliability of Electron Devices, Failure Physics and Analysis ESREF*, Bordeaux, France, 8 – 12 October 2007. DOI: 10.1016/j.microrel.2007.07.033.
- D.S. Dugdale. Yielding of steel sheets containing slits. *Journal of the Mechanics and Physics of Solids*, 8:100–104, 1960. DOI: 10.1016/0022-5096(60)90013-2.
- J. Dundurs. Discussion: Edge-bonded dissimilar orthogonal elastic wedges under normal and shear loading. *J. Appl. Mech.*, 36:650–652, 1969. DOI: 10.1115/1.3564739.
- J. Dundurs and A.K. Gautesen. An opportunistic analysis of the interface crack. *International Journal of Fracture*, 36(2):151–159, 1988. DOI: 10.1007/BF00017793.
- L. Durix. *On the Design of a New Test Method to Characterize the Delamination of Thermosetting Polymer Under Thermal Mixed Mode Loading*. PhD thesis, Université de Valenciennes et du Hainaut-Cambrésis, 2010.
- L. Durix, M. Dreßler, D. Coutellier, and B. Wunderle. On the development of a modified button shear specimen to characterize the

mixed mode delamination toughness. *Engineering Fracture Mechanics*, 84:25–40, 2012. DOI: 10.1016/j.engfracmech.2011.12.015.

F. Ercolessi. A molecular dynamics primer. In *Spring College in Computational Physics, ICTP*, Trieste, Italy, 1997.

L.J. Ernst, A. Xiao, B. Wunderle, K.M.B. Jansen, and H. Pape. Interface characterization and failure modeling for semiconductor packages. In *10th Electronics Packaging Technology Conference, EPTC*, pages 808–815, dec 2008. DOI: 10.1109/EPTC.2008.4763531. ISBN: 978-1-4244-2117-6.

T. Fałat. Implementation of cure dependent viscoelastic material models in ANSYS. Technical report, Mechanics and Materials Group, Faculty of Mechanical Engineering, Delft University of Technology, Jul 2008.

J.L. Gardon. Peel adhesion. i. some phenomenological aspects of the test. *Journal of Applied Polymer Science*, 7(2):625–641, 1963. ISSN 00218995. DOI: 10.1002/app.1963.070070219.

B. Gibbesch, G. Elssner, and G. Petzow. Investigation of ti/al2o3 joints with intermediate tantalum and niobium layers. *Biomaterials*, 13(7):455–461, 1992. DOI: 10.1016/0142-9612(92)90166-L.

W. Gill and W. Workmann. Reliability screening procedures for integrated circuits. In T.S. Shilladay and J. Vaccaro, editors, *Physics of Failure in Electronics*, number 5 in RADC Series in Reliability, pages 101–142. June 1967.

N.L. Goldman and J.W. Hutchinson. Fully plastic crack problems: The center-cracked strip under plane strain. *International Journal of Solids and Structures*, 11(5):575–591, 1975. DOI: 10.1016/0020-7683(75)90031-1.

A.A. Griffith. The phenomena of rupture and flow in solids. *Philosophical Transactions of the Royal Society*, 221:163–198, 1920. Series A.

D. Gross and Th. Seelig. *Bruchmechanik. Mit einer Einführung in die Mikromechanik*. X. Springer, Berlin, 4 edition, 2006a.

D. Gross and Th. Seelig. *Fracture Mechanics. With an Introduction to Micromechanics*. XII. Springer, Berlin, 1 edition, 2006b.

S. Hashemi, A.J. Kinloch, and J.G. Williams. Interlaminar fracture of composite materials. In *6th ICCM & 2nd ECCM Conference Proceedings*, volume 3, pages 3.254–3.264., London, July 1987. Elsevier Applied Science.

- M.Y. He and J.W. Hutchinson. Kinking of a crack out of an interface. *Journal of Applied Mechanics*, 56:270–287, 1989. DOI: 10.1115/1.3176078.
- T.K. Hellen. On the method of virtual crack extensions. *International Journal for Numerical Methods in Engineering*, 9(1):187–207, 1975. ISSN 1097-0207. DOI: 10.1002/nme.1620090114.
- G. Hu and A.A.O. Tay. Numerical study of the effects of temperature, moisture and vapour pressure on delamination in a pqfp during solder reflow. In *Electronics Packaging Technology Conference EPTC*, 2004. DOI: 10.1109/EPTC.2004.1396585.
- G. Hu and A.A.O. Tay. Application of modified virtual crack closure method on delamination analysis in a plastic ic package during lead-free solder reflow. In *Electronics Packaging Technology Conference EPTC*, 2005. DOI: 10.1109/EPTC.2005.1614465.
- G. Hu, A.A.O. Tay, L. Jing-En, and M. Yiyi. Numerical and experimental study of interface delamination in flip chip BGA package. *Journal of Electronic Packaging*, 132(1):011006–7, March 2010. DOI: 10.1115/1.4001145.
- J.W. Hutchinson. Crack tip shielding by Micro-Cracking in brittle solids. *Acta Metallurgica*, 35(7):1605–1619, 1987. DOI: 10.1016/0001-6160(87)90108-8.
- J.W. Hutchinson and Z. Suo. Mixed mode cracking in layered materials. *Advances in Applied Mechanics*, 29:63–191, 1992. ISSN 0065-2156. DOI: 10.1115/1.2893779.
- J.W. Hutchinson, M.E. Mear, and J.R. Rice. Crack paralleling an interface between dissimilar media. *Transactions of the ASME*, 54: 828–832, December 1987.
- S.-F. Hwang, J.-H. Yu, B.-J. Lai, and H.-K.Liu. Young’s modulus and interlaminar fracture toughness of SU-8 film on silicon wafer. *Mechanics of Materials*, 40(8):658–664, August 2008. ISSN 0167-6636. DOI: 10.1016/j.mechmat.2008.02.005.
- G.R. Irwin. Onset of fast crack propagation in high strength steel and aluminium alloys. In *Sagamore Research Conference Proceedings*, volume 2, page 289, 1956.
- G.R. Irwin. Analysis of stresses and strains near the end of a crack traversing a plate. *Journal of Applied Mechanics*, 24:361, 1957.
- G.R. Irwin. Linear fracture mechanics, fracture transition, and fracture control. *Engineering Fracture Mechanics*, 1(2):241–257, August 1968. ISSN 0013-7944. DOI: 10.1016/0013-7944(68)90001-5.

G.R. Irwin, J.M. Krafft, P.C. Paris, and A.A. Wells. Basic aspects of crack growth and fracture. NRL Report 6598, Naval Research Laboratory, Washington, D.C., November 1967.

K.M.B. Jansen. Thermomechanical modelling and characterisation of polymers. Lecture Notes WB1433, Delft University of Technology, Mar 2007.

K.M.B. Jansen, L.J. Ernst, and C. Qian. Cure dependent properties of molding compounds. Technical Report TUD-Inf4, Delft University of Technology, 2008.

JEDEC Solid State Technology Association. JESD22-A113F, preconditioning of nonhermetic surface mount devices prior to reliability testing. JEDEC Standard, March 2006.

Z.H. Jin and C.T. Sun. Cohesive zone modeling of interface fracture in elastic bi-materials. *Engineering Fracture Mechanics*, 72:1805–1817, 2005. DOI: 10.1016/j.engfracmech.2004.09.011.

Z.H. Jin and C.T. Sun. A comparison of cohesive zone modeling and classical fracture mechanics based on near tip stress field. *International Journal of Solids and Structures*, 43(5):1047–1060, 2006. DOI: 10.1016/j.ijsolstr.2005.06.074.

A.M. Karlsson. Closure to "discussion: 'on the reference length and mode mixity for a bimaterial interface'". *ASME J. Eng. Mater. Technol.*, 130:p. 045501, 2008. DOI: <http://dx.doi.org/10.1115/1.2975232>.

J. Keller. *Micro- and Nanoscale Characterization of Polymeric Materials by Means of Digital Image Correlation Techniques*. PhD thesis, Brandenburgische Technische Universität Cottbus, 2005.

J. Keller, I. Maus, G. Schlottig, H. Pape, B. Wunderle, and B. Michel. Interface fracture mechanics evaluation by correlation of experiment and simulation. In *Proceedings of the Electronic System-Integration Technology Conference (ESTC)*, September 2010. DOI: 10.1109/ESTC.2010.5642934.

J.H. Kim. Effect of an adhesive interlayer on the fracture of a brittle coating on a supporting substrate. *J. Mater. Res.*, 18(1):222–227, 2003. DOI: 10.1557/JMR.2003.0031.

J.H. Kim. High throughput screening of interfacial adhesion strength in compositional libraries of epoxy films. Contribution of the National Institute of Standards and Technology, in Adhesion Society Extended Abstracts, 2007.

A.J. Kinloch, Y. Wang, J.G. Williams, and P. Yayla. The mixed-mode delamination of fibre composite materials. *Composites Science and Technology*, 47(3):225–237, 1993. ISSN 0266-3538. DOI: 10.1016/0266-3538(93)90031-B.

A.J. Kinloch, C.C. LAU, and J.G. WILLIAMS. The peeling of flexible laminates. *International Journal of Fracture*, 66:45–70, 1994. DOI: 10.1007/BF00012635.

R. Krueger. The virtual crack closure technique: History, approach and applications. Technical report, ICASE and National Aeronautics and Space Administration (NASA), 2002.

R. Krueger. The virtual crack closure technique: History, approach and applications. *Appl Mech Rev*, 57(2):109–143, 2004. DOI: 10.1115/1.1595677.

R. Krueger. Computational fracture mechanics for composites - state of the art and challenges. In *Proceedings of NAFEMS Nordic Seminar: Prediction and Modelling of Failure Using FEA*, Roskilde, Denmark, 2006.

H.P. Kugler, R.G. Stacer, and C. Steimle. Direct measurement of poisson's ratio in elastomers. *Rubber Chem. Tech.*, 63:473–487, 1990. DOI: 10.5254/1.3538267.

Y.-H. Lai, M.D. Rakestraw, and D.A. Dillard. The cracked lap shear specimen revisited—a closed form solution. *International Journal of Solids and Structures*, 33(12):1725–1743, May 1996. ISSN 0020-7683. DOI: 10.1016/0020-7683(95)00124-7.

M. Larisch. Gabo Eplexor Sichtfenster Tür. Technical report, Infineon Technologies AG, Regensburg, October 2010.

K.M. Liechti. On the use of classical interferometry techniques in fracture mechanics. In *Experimental Techniques in Fracture*. 1993.

K.M. Liechti. Delamination mechanics. In *Springer Handbook of Experimental Solid Mechanics*, pages 961–984. December 2008. DOI: 10.1007/978-0-387-30877-7_34.

K.M. Liechti and Y.-S. Chai. Biaxial loading experiments for determining interfacial fracture toughness. *Transaction of the ASME*, 58: 680–687, 1991. DOI: 10.1115/1.2897248.

K.M. Liechti and Y. S. Chai. Asymmetric shielding in interfacial fracture under In-Plane shear. *Journal of Applied Mechanics*, 59(2): 295–304, June 1992. DOI: 10.1115/1.2899520.

M.L. Loke. Molded flip chip package with enhanced mold-die adhesion. Patent, US 2009/0309238 A1, December 2009.

X. Ma, G.Q. Zhang, O. van der Sluis, K.M.B. Jansen, W.D. van Driel, L.J. Ernst, C. Regard, C. Gautier, and H. Frémont. Die attach interface property characterization as function of temperature using cohesive zone modeling method. In *Proceedings of 11th EuroSimE*, 2010. DOI: 10.1109/ESimE.2010.5464533.

B.M. Malyshev and R.L. Salganik. The strength of adhesive joints using the theory of cracks. *International Journal of Fracture*, 1(2): 114–128, June 1965. DOI: 10.1007/BF00186749.

V. Mantić. Discussion: "on the reference length and mode mixity for a bimaterial interface". *J. Eng. Mater. Technol.*, 130(4):045501, 2p, 2008. DOI: <http://dx.doi.org/10.1115/1.2975231>.

S. Mariani, A. Ghisi, R. Martini, A. Corigliano, and B. Simoni. Two-scale vs three-scale FE analyses of shock-induced failure in polysilicon MEMS. In *Proceedings of 11th EuroSimE*, April 2010. DOI: 10.1109/ESimE.2010.5464588.

P.P.L. Matos, R.M. McMeeking, P.G. Charalambides, and M.D. Drory. A method for calculating stress intensities in bimaterial fracture. *International Journal of Fracture*, 40(4):235–254, aug 1989. DOI: 10.1007/BF00963659.

L.L. Mercado, H. Wieser, and T. Hauck. Mold delamination and die fracture analysis of mechatronic packages. In *Proceedings of the 51st ECTC*, pages 903–910, Orlando, FL, USA, 2001. DOI: 10.1109/ECTC.2001.927902.

T. Meyer. Embedded wafer level ball grid array (eWLB). In *SEMI-CON Europa*, 2007.

Y. Miyano, M. Shimbo, and T. Kunio. Viscoelastic analysis of residual stress in quenched thermosetting resin beams. *Experimental Mechanics*, 22(8):310–316, 1982. ISSN 0014-4851. DOI: 10.1007/BF02327249.

I. Mohammed and K.M. Liechti. Cohesive zone modeling of crack nucleation at bimaterial corners. *Journal of the Mechanics and Physics of Solids*, 48(4):735–764, April 2000. ISSN 0022-5096. DOI: 10.1016/S0022-5096(99)00052-6.

S. Mukherjee, C.R. Ananth, and N. Chandra. Evaluation of fracture toughness of mmc interfaces using thin-slice push-out tests. *Scripta Materialia*, 36(11):1333–1338, 1997. DOI: 10.1016/S1359-6462(97)00019-5.

S. Nakamura, Y. Miyano, S. Sugimori, and A. Kaneda. Thermoviscoelastic analysis of residual stresses in a thermosetting resin/metal laminated beam caused by cooling. *JSME International Journal. Series 1, Solid mechanics, strength of materials*, 31(1):126–131, 1988. ISSN 0914-8809.

S. Nakamura, E. Pavlovic, and E.J. Kramer. Fracture energy of epoxy interfaces with layers of different silane coupling agents. *The Journal of Adhesion*, 83(4):351, 2007. ISSN 0021-8464. DOI: 10.1080/00218460701282372.

A. Needleman. A continuum model for void nucleation by inclusion debonding. *Journal of Applied Mechanics*, 54:525–531, 1987. DOI: 10.1115/1.3173064.

A. Needleman. An analysis of decohesion along an imperfect interface. *International Journal of Fracture*, 42:21–40, 1990.

M. Neinaß. Entwurf GABO-Tür mit Sichtfenster zur Rissbeobachtung. Technical report, Fraunhofer IZM, Berlin, June 2008.

J.C. Newman, M.A. James, and U. Zerbst. A review of the ctoa/ctod fracture criterion. *Engineering Fracture Mechanics*, 70(3–4):371–385, 2003. DOI: 10.1016/S0013-7944(02)00125-X.

L.T. Nguyen, R.H.Y. Lo, A.S. Chen, and J.G. Belani. Molding compound trends in a denser packaging world: qualification tests and reliability concerns. *Reliability, IEEE Transactions on*, 42(4):518–535, 1993. ISSN 0018-9529. DOI: 10.1109/24.273570.

H.F. Nied. Mechanics of interface with applications in electronic packaging. *Device and Materials Reliability, IEEE Transactions on*, 3(4):129–143, 2003. ISSN 1530-4388. DOI: 10.1109/TDMR.2003.820623.

A. Nishimura, I. Hirose, and N. Tanaka. A new method for measuring adhesion strength of ic molding compounds. *Journal of Electronic Packaging*, 114(4):407–412, 1992. DOI: 10.1115/1.2905473.

T.K. O'Brien. Mixed-Mode Strain-Energy-Release rate effects on edge delamination of composites. Technical Report ASTM STP 836, ASTM, 1984.

T. Ohori. Liquid Molding Compound T693/R4000 series. Technical report, Nagase Chemtex Corp., April 2010. URL <http://www.nagasechemtex.co.jp/english/LMCEN.pdf>. last accessed Feb. 8th, 2011.

M. Ortiz and A. Pandolfi. Finite-deformation irreversible cohesive elements for three-dimensional crack-propagation analysis. *International*

- Journal for Numerical Methods in Engineering*, 44(9):1267–1282, 1999. DOI: 10.1002/(SICI)1097-0207(19990330).
- N.J. Pagano and R.B. Pipes. Some observations on the interlaminar strength of composite laminates. *Int. J. Mech. Sci.*, 15:679, 1973. DOI: 10.1016/0020-7403(73)90099-4.
- H. Pape, I. Maus, I. Paul, L.J. Ernst, and B. Wunderle. Fracture toughness characterization and modeling of interfaces in micro-electronic packages – a status review. In *Proceedings of the 13th EuroSimE*, 2012.
- M. Patel, C. Qian, K.M.B. Jansen, and L.J. Ernst. Viscoelastic properties of fully cured molding compounds: Elongation, shear, bulk modulus and cure shrinkage. Technical Report TUD-Inf3, Delft University of Technology, 2008.
- K.E. Petersen. Silicon as a mechanical material. *Proceedings of the IEEE*, 70(5):420–457, 1982. DOI: 10.1109/PROC.1982.12331.
- I.S. Raju. Calculation of strain-energy release rates with higher order and singular finite elements. *Eng. Fracture Mech.*, 28:251–274, 1987. DOI: 10.1016/0013-7944(87)90220-7.
- I.S. Raju, J.H. Crews Jr, and M.A. Aminpour. Convergence of strain energy release rate components for Edge-Delaminated composite laminates. *Engineering Fracture Mechanics*, 30(3):383–396, 1988. DOI: 10.1016/0013-7944(88)90196-8.
- K. Ravi-Chandar. Fracture mechanics. In *Handbook of Experimental Solid Mechanics*, pages 125–158. Springer, 2008. DOI: 10.1007/978-0-387-30877-7_5.
- J. Renart, N. Blanco, E. Pajares, J. Costa, S. Lazcano, and G. Santacruz. Side clamped beam (scb) hinge system for delamination tests in beam-type composite specimens. *Composites Science and Technology*, accepted manuscript in press, 2010. ISSN 0266-3538. DOI: 10.1016/j.compscitech.2010.10.005.
- J.R. Rice. A path independent integral and the approximate analysis of strain concentration by notches and cracks. Technical report, Brown University, Division of Engineering and Department of Defense, Advanced Research Projects Agency, Contract SD-86, Material Research Program, Providence, R. I., May 1967.
- J.R. Rice. Elastic fracture mechanics concepts for interfacial cracks. *J. Appl. Mech.*, 55:98–103, 1988. DOI: 10.1115/1.3173668.

- H.A. Richard. Bruchvorhersagen bei überlagerter Normal- und Schubbeanspruchung von Rissen. *VDI-Forschungsheft*, 631/85:1–60, 1985.
- E.J. Ripling, S. Mostovoy, and R.L. Patrick. Application of fracture mechanics to adhesive joints. *ASTM STP360-EB*.
- A. Ritter. *Untersuchung der Grenzflächenhaftung von Halbleiter-Gehäusematerialien*. Master thesis, Hochschule Regensburg, 2011.
- J.E. Ritter, T.J. Lardner, L. Rosenfeld, and M.R. Lin. Measurement of adhesion of thin polymer coatings by indentation. *Journal of Applied Physics*, 66(8):3626, 1989. ISSN 00218979. DOI: 10.1063/1.344071.
- J.E. Ritter, T.J. Lardner, W. Grayeski, G.C. Prakash, and J. Lawrence. Fatigue crack propagation at polymer adhesive interfaces. *J. Adhesion*, 63(4):265–284, 1997. DOI: 10.1080/00218469708017223.
- L.G. Rosenfeld, J.E. Ritter, T.J. Lardner, and M.R. Lin. Use of microindentation technique for determining interfacial fracture energy. *Journal of Applied Physics*, 67(7):3291–3296, 1990. DOI: 10.1063/1.345363.
- A.J. Russell. On the measurement of mode II interlaminar fracture energies. Materials Report MAT-R-82-0, Defence Research Establishment Pacific (DREP), Victoria BC, Canada, December 1982.
- E.F. Rybicki and M.F. Kanninen. A finite element calculation of stress intensity factors by a modified crack closure integral. *Engineering Fracture Mechanics*, 9(4):931–938, 1977. DOI: 10.1016/0013-7944(77)90013-3.
- M.K. Saraswat, K.M.B. Jansen, M.D. Patel, L.J. Ernst, C. Bohm, A. Kessler, H. Preu, and M. Stecher. A characterization method for viscoelastic bulk modulus of molding compounds. In *Proceedings of the 9th EuroSimE*, Freiburg, Germany, 2008. DOI: 10.1109/ESimE.2008.4525098.
- A. Saxena. *Nonlinear Fracture Mechanics for Engineers*. CRC Press, Boca Raton, 1998. ISBN 0849394961.
- G. Schlottig, H. Pape, B. Wunderle, and L.J. Ernst. Induced delamination of silicon-molding compound interfaces. In *Proceedings of the 10th EuroSimE*, 2009a. DOI: 10.1109/ESimE.2009.4938478.
- G. Schlottig, H. Pape, A. Xiao, B. Wunderle, and L.J. Ernst. How to fabricate specimens for Silicon-to-Molding compound interface adhesion measurements. In *Proceedings of the 11th Electronics Packaging Technology Conference (EPTC)*, pages 357–362, 2009b. DOI: 10.1109/EPTC.2009.5416523.

G. Schlottig, I. Maus, H. Walter, K.M.B. Jansen, H. Pape, B. Wunderle, and L.J. Ernst. Interfacial fracture parameters of silicon-to-molding compound. In *Proceedings of the 60th ECTC, Electronic Components and Technology Conference*, pages 1939–45, 2010a. DOI: 10.1109/ECTC.2010.5490689.

G. Schlottig, A. Xiao, H. Pape, B. Wunderle, and L.J. Ernst. Interfacial strength of silicon-to-molding compound changes with thermal residual stress. In *Proceedings of the 11th EuroSimE*, April 2010b. DOI: 10.1109/ESIME.2010.5464554.

G. Schlottig, H. Pape, B. Wunderle, and L.J. Ernst. Establishing the critical fracture properties of the die backside-to-molding compound interface. In *Proceedings of the 61st Electronic Components and Technology Conference (ECTC)*, pages 1090–1096, June 2011. DOI: 10.1109/ECTC.2011.5898646.

H.R. Schubach and A. Ettemeyer. Investigations on aluminum alloys with a 3despi-system. Technical Report Application Report 01-97, Dr. Ettemeyer GmbH & Co., Neu-Ulm, Germany, 1997.

C.F. Shih and R.J. Asaro. Elastic-plastic analysis of cracks on bimaterial interfaces: Part I—small scale yielding. *Journal of Applied Mechanics*, 55(2):299–316, 1988. DOI: 10.1115/1.3173676.

M.H. Shirangi. *Simulation-based Investigation of Interface Delamination in Plastic IC Packages under Temperature and Moisture Loading*. PhD thesis, Technische Universität Berlin, August 2010.

G.C. Sih. Implication of scaling hierarchy associated with nonequilibrium: field and particulate. *Theoretical and Applied Fracture Mechanics*, 37:335–369, 2001. DOI: 10.1016/S0167-8442(01)00080-5.

G.C. Sih. Spatial and temporal scaling affected by system inhomogeneity: atomic, microscopic and macroscopic. In *ecf 16*, 2006. DOI: 10.1007/1-4020-4972-2_15.

G.C. Sih and B. Liu. Mesofracture mechanics: a necessary link. *Theoretical and Applied Fracture Mechanics*, 37:371–395, 2001. DOI: 10.1016/S0167-8442(01)00081-7.

H.K. Singh, K.-T. Wan, J.G. Dillard, D.A. Dillard, P. Reboa, J. Smith, E. Chappell, and A. Sharan. Subcritical delamination in epoxy bonds to silicon and glass adherends: Effect of temperature and preconditioning. *The Journal of Adhesion*, 84(7):619, 2008. ISSN 0021-8464. DOI: 10.1080/00218460802255509.

O. van der Sluis, R.A.B. Engelen, R.B.R. van Silfhout, W.D. van Driel, and M.A.J. van Gils. Efficient damage sensitivity analysis of

advanced cu low- k bond pad structures by means of the area release energy criterion. *Microelectronics Reliability*, 47:1975–1982, 2007. DOI: 10.1016/j.microrel.2007.04.004.

O. van der Sluis, R.A.B. Engelen, P.H.M. Timmermans, and G.Q. Zhang. Numerical analysis of delamination and cracking phenomena in multi-layered flexible electronics. *Microelectronics Reliability*, 49(8):853–860, August 2009a. ISSN 0026-2714. DOI: 10.1016/j.microrel.2009.03.013.

O. van der Sluis, C. A. Yuan, W. D. van Driel, and G. Q. Zhang. Advances in delamination modeling. In *Nanopackaging*, pages 1–31. 2009b. DOI: 10.1007/978-0-387-47325-3_4.

G.J. Spies. The peeling test on redux-bonded joints. *Aircraft Eng.*, 25(3):64–70, 1953. DOI: 10.1108/eb032268.

T. Suga, G. Elssner, and S. Schmauder. Composite parameters and mechanical compatibility of material joints. *Journal of Composite Materials*, 22(10):917, 1988. DOI: 10.1177/002199838802201002.

C.T. Sun and C.J. Jih. On strain energy release rates for interfacial cracks in bi-material media. *Engineering Fracture Mechanics*, 28(1): 13–20, 1987. ISSN 0013-7944. DOI: 10.1016/0013-7944(87)90115-9.

C.T. Sun and Z.H. Jin. Modeling of composite fracture using cohesive zone and bridging models. *Composites Science and Technology*, 66(10): 1297–1302, 2006. DOI: 10.1016/j.compscitech.2005.10.013.

C.T. Sun and W. Qian. The use of finite extension strain energy release rates in fracture of interfacial cracks. *Int. J. Solids Structures*, 34(20):2595–2609, 1997. DOI: 10.1016/S0020-7683(96)00157-6.

Z. Suo. Interfacial fracture. Lecture Notes ES247, Harvard University, April 2010.

Z. Suo and J.W. Hutchinson. Sandwich test specimens for measuring interface crack toughness. *Materials Science and Engineering: A*, 107:135–143, January 1989. ISSN 0921-5093. DOI: 10.1016/0921-5093(89)90382-1.

A. Szekrényes. Prestressed fracture specimen for delamination testing of composites. *International Journal of Fracture*, 139:213–237, 2006. DOI: 10.1007/s10704-006-0043-1.

A. Szekrényes and J. Uj. Over-leg bending test for mixed-mode I/II interlaminar fracture in composite laminates. *International Journal of Damage Mechanics*, 16(1):5–33, January 2007. DOI: 10.1177/1056789507060774.

- A. Tay. Application of fracture mechanics in microelectronics. In *EuroSimE Short Course*, 2006.
- R.E. Taylor, T.H.K. Barron, A. Cezairliyan, P.S. Gaal, T. Hahn, C.Y. Huang, R.K. Kirby, H.A. McKinstry, S.T. McKinstry, A.P. Miiller, B.D. Rothrock, G. Ruffino, C.A. Swenson, and G.K. White. *Thermal Expansion of Solids*, volume I-4 of *CINDAS Data Series on Material Properties*. ASM International, 1998.
- R. Tilgner, P. Alpern, J. Baumann, G. Pfannschmidt, and O. Selig. Changing states of delamination between molding compound and chip surface: a challenge for scanning acoustic microscopy. *Components, Packaging, and Manufacturing Technology, Part B: Advanced Packaging, IEEE Transactions on*, 17(3):442–448, 1994. ISSN 1070-9894. DOI: 10.1109/96.311795.
- M. Toya. On mode i and mode ii energy release rates of an interface crack. *International Journal of Fracture*, 56(4):345–352, 1992. DOI: 10.1007/BF00015864.
- C. Uhlig, O. Kahle, B. Wieneke, and M. Bauer. A new method for the automatic determination of fracture toughness of polymers. *Forum der Forschung*, 5(11):50–53, 2000.
- United States. Final report of a board of investigation convened by order of the secretary of the navy to inquire into the design and methods of construction of welded steel merchant vessels. *Welding Journal*, 26:569–619, 1947.
- P.S. Vanderkley. *Mode I- Mode II Delamination Fracture Toughness of a Unidirectional Graphite/Epoxy Composite*. Master thesis, Texas A&M University, College Station, TX, December 1981.
- D. Vogel, F. Luczak, A. Gollhardt, H. Walter, and B. Michel. Measurement of material properties by a modified microDAC approach. In *Proceedings of MicroMat 2000, 3rd International Micro Materials Conference*, pages 829–832, Berlin, April 2000. ddp goldenbogen.
- D. Vogel, A. Gollhardt, and B. Michel. Micro- and nanomaterials characterization by image correlation methods. *Sensors and Actuators A: Physical*, Volume 99, Issues 1-2, 30:165–171, 2002. DOI: 10.1016/S0924-4247(01)00908-6.
- A.A. Volinsky, N.R. Moody, and W.W. Gerberich. Interfacial toughness measurements for thin films on substrates. *Acta Materialia*, 50: 441–466, 2002. DOI: 10.1016/S1359-6454(01)00354-8.

- O. Volkersen. Die Nietkraftverteilung in zugbeanspruchten Nietverbindungen mit konstanten Laschenquerschnitten. *Luftfahrtforschung*, 15:41–47, 1938.
- J. de Vreugd. *The effect of aging on molding compound properties – aging characterization of molding compounds and its modeling*. PhD thesis, Delft University of Technology, 2011.
- J. de Vreugd, K.M.B. Jansen, A. Xiao, L.J. Ernst, C. Bohm, A. Kessler, H. Preu, and M. Stecher. Advanced viscoelastic material model for predicting warpage of a QFN panel. In *Proceedings 58th ECTC*, 2008. DOI: 10.1109/ECTC.2008.4550196.
- H. Walter. *Morphologie-Zähigkeits-Korrelationen von modifizierten Epoxidharzsystemen mittels bruchmechanischer Prüfmethoden an Miniaturprüfkörpern*. PhD thesis, Martin-Luther-Universität Halle-Wittenberg, 2003.
- H. Walter and S. Hartmann. Determination of thermo-mechanical and fracture properties of one mold compound as a function of temperature. Technical report, Fraunhofer Institute of Reliability and Micro-Integration Berlin, 2010.
- J. Wang, D. Zou, M. Lu, W. Ren, and S. Liu. Evaluation of interfacial fracture toughness of a flip-chip package and a bimaterial system by a combined experimental and numerical method. *Engineering Fracture Mechanics*, 64(6):781–797, December 1999. ISSN 0013-7944. DOI: 10.1016/S0013-7944(99)00078-8.
- Y. Wei and J.W. Hutchinson. Interface strength, work of adhesion and plasticity in the peel test. *International Journal of Fracture*, 93:315–333, 1998. DOI: 10.1023/A:1007545200315.
- A.A. Wells. Critical crack tip opening displacement as fracture criterion. In *Proceedings of the Crack Propagation Symposium*, volume 1, pages 210–221, Cranfield, 1961.
- J.M. Whitney, C.E. Browning, and W. Hoogsteden. A double cantilever beam test for characterizing mode I delamination of composite materials. *Journal of Reinforced Plastics and Composites*, 1(4):297–313, October 1982. DOI: 10.1177/073168448200100402.
- J. Widodo, M. Damayanti, S.G. Mhaisalkar, W. Lu, S. Ong, T. Sritharan, K.Y. Zeng, and L.C. Hsia. Adhesion study of tetra methyl cyclo tetra siloxanes (TMCTS) and tri methyl silane (3MS)-based low-k films. *Microelectronic Engineering*, 81(1):35–43, July 2005. ISSN 0167-9317. DOI: 10.1016/j.mee.2004.11.017.

S. Wiese. *Verformung und Schädigung von Werkstoffen der Aufbau- und Verbindungstechnik*. Springer, Heidelberg, 1st edition, 2010. ISBN 978-3-642-05462-4. DOI: 10.1007/978-3-642-05463-1.

M.L. Williams. The stresses around a fault or crack in dissimilar media. *Bulletin of the Seismology Society of America*, 49:199–204, 1959.

O. Wittler. *Bruchmechanische Analyse von viskoelastischen Werkstoffen in elektronischen Bauteilen*. PhD thesis, Technische Universität Berlin, 2004.

O. Wittler, P. Sprafke, H. Walter, A. Gollhardt, D. Vogel, and B. Michel. Time and temperature dependent mechanical characterisation of polymers for microsystems applications. In *Materials Week*, München, September 25–28 2000.

B. Wunderle. *Thermo-Mechanical Reliability of Flip-Chip Assemblies with Heat-Spreaders*. PhD thesis, Technische Universität Berlin, 2003.

B. Wunderle, E. Dermizaki, O. Hölck, J. Bauer, H. Walter, Q Shaik, K Rätzke, F Faupel, and B. Michel. Molecular dynamics simulation and mechanical characterisation for the establishment of Structure-Property correlations for epoxy resins in microelectronics packaging applications. In *Proceedings of the 10th EuroSimE*, Delft, NL, 2009. DOI: 10.1109/ESimE.2009.4938455.

B. Wunderle, M. Schulz, J. Keller, D. May, I. Maus, H. Pape, and B. Michel. Advanced Mixed-Mode bending test: A rapid, inexpensive and accurate method for Fracture-Mechanical interface characterisation. In *Proceedings of the 13th EuroSimE*, 2012. DOI: 10.1109/ESimE.2012.6191698.

A. Xiao, L.G. Wang, W.D. van Driel, O. van der Sluis, D.G. Yang, L.J. Ernst, and G.Q. Zhang. Thin film interface fracture properties at scales relevant to microelectronics. In *Proceedings of the 8th EuroSimE*, pages 350–355, London, Apr 2007. DOI: 10.1109/ESimE.2007.360011.

A. Xiao, H. Pape, B. Wunderle, K.M.B. Jansen, and L.J. Ernst. Interfacial fracture properties and failure modeling for microelectronics. In *58th Electronic Components and Technology Conference, ECTC*, pages 1724–1730, Orlando, FL, 2008a. DOI: 10.1109/ECTC.2008.4550213.

A. Xiao, G. Schlottig, H. Pape, B. Wunderle, K.M.B. Jansen, and L.J. Ernst. Mixed mode interface characterization considering thermal residual stress. In *International Conference on*

Electronic Packaging Technology and High Density Packaging, ICEPT, pages 937–943, Shanghai, Peoples R China, jul 2008b. DOI: 10.1109/ICEPT.2008.4607131.

A. Xiao, G. Schlottig, H. Pape, B. Wunderle, K.M.B. Jansen, and L.J. Ernst. Delamination and combined compound cracking of EMC-Copper interfaces. In *60th Electronic Components and Technology Conference, ECTC*, pages 114–120, 2010. DOI: 10.1109/ECTC.2010.5490893.

S. Yurenka. Peel testing of adhesive bonded metal. *Journal of Applied Polymer Science*, 6(20):136–144, 1962. ISSN 00218995. DOI: 10.1002/app.1962.070062004.

R. Yuuki and S.-B. Cho. Efficient boundary element analysis of stress intensity factors for interface cracks in dissimilar materials. *Engineering Fracture Mechanics*, 34:179–188, 1989. DOI: 10.1016/0013-7944(89)90251-8.

A.T. Zehnder. Lecture notes on fracture mechanics. Department of Theoretical and Applied Mechanics, Cornell University, Ithaca, NY, June 2009.

Z. Zhang. *Thermomechanical Reliability of Microelectronics*. PhD thesis, Harvard School of Engineering and Applied Sciences, Cambridge, MA, April 2007.

W. Zhao and G. Jin. An experimental study on measurement of Poisson’s ratio with digital correlation method. *J. Appl. Poly. Sci.*, 60:1083–1088, 1996. DOI: 10.1002/(SICI)1097-4628(19960523)60:8<1083::AID-APP1>3.0.CO;2-H.

X.W. Zhou, N.R. Moody, R.E. Jones, J.A. Zimmerman, and E.D. Reedy. Molecular-dynamics-based cohesive zone law for brittle interfacial fracture under mixed loading conditions: Effects of elastic constant mismatch. *Acta Materialia*, 57(16):4671–4686, September 2009. DOI: 10.1016/j.actamat.2009.06.023.

]Bruchmechanik

Index

- 4PB, *see* Four Point Bending
- aDCB, *see* Double Cantilever Beam
- Advanced Mixed Mode Bending (AMB), 38
- AFM, *see* atomic force microscopy
- AMB, *see* Advanced Mixed Mode Bending
- Arcan Specimen, *see* Compact Tension Shear
- ARE, *see* area release energy
- area release energy (ARE), 16
- atomic force microscopy (AFM), 36, 56, 57
- bake out, 66
- Blister Specimen, 38
- blister test, 39
- BN, *see* Brazil Nut
- Brazil Nut (BN), 38, 39
- Brazilian Disk, cracked b.d., 39
- CCD, *see* charge-coupled device
- CDM, *see* continuum damage mechanics
- Center Crack Beam, symmetric (sCCB), 38
- charge-coupled device (CCD), 72
- clamping, c. of the specimen, 42
- CLS, *see* Cracked-Lap Shear
- coefficient of thermal expansion (CTE), 78, 96
- cohesive zone (CZ), 15, 16
- Compact Tension Shear (CTS), 39
- Cone Test, 38
- continuum damage mechanics (CDM), 15
- correlation, deformation analysis by c. (DAC), 70
- correlation, image c., 70
- crack opening interferometry, 70
- crack surface displacement extrapolation (CSDE), 28, 92, 93
- crack tip opening displacement (CTOD), 28
- crack tip recognition, 70
- Cracked-Lap Shear (CLS), 38
- criterion
- failure c., 15, 16
 - fracture c., 15, 16
- CSDE, *see* crack surface displacement extrapolation
- CTE, *see* coefficient of thermal expansion
- CTOD, *see* crack tip opening displacement
- CTS, *see* Compact Tension Shear
- DAC, *see* correlation
- DCB, *see* Double Cantilever Beam
- deviation
- ERR from polyn. fit, 86
- dicing, 59
- Digital Image Correlation, 70
- digital object identifier (DOI), 133
- dilatometer, 54
- DMA, *see* Dynamic Mechanical Analyzer
- DOI, *see* digital object identifier
- Double Cantilever Beam (DCB), 38, 39
- dryback, 65, 66
- Dundurs parameters, 21, 100
- dye and pry, *see* staining
- Dynamic Mechanical Analyzer (DMA), 54, 75
- EBSD, *see* electron backscatter
- Edge-Delamination Tension (EDT), 38
- EDT, *see* Edge-Delamination Tension
- electron backscatter diffraction (EBSD), 80
- embedded wafer level ballgrid array (eWLB), 48
- EMC, *see* epoxy molding compound
- End Notch Flexure (ENF), 38, 39
- energy release rate (ERR), 18
- deviations, 86, 96
 - results, 81
- ENF, *see* End Notch Flexure
- Eplexor, 36, 73
- epoxy molding compound (EMC), 16
- ERR, *see* energy release rate
- eWLB, *see* embedded wafer level
- fabrication, 45, 48
- FEDc, *see* Free-Edge Delamination Coupon
- filler, 54
- Fixed Ratio Mixed Mode (FRMM), 38
- flank exposure, 48, 49, 58
- force tendency, 18
- Four Point Bending (4PB), 38, 39, 61
- fracture
- brittle f., 35
 - random f., 30, 31
 - subcritical f., 17
- fracture mechanics, linear elastic f.m.(LEFM), 16
- fracture mode mix, 23
- fracture modes, 19
- fracture toughness, 19, 22
- Free-Edge Delamination Coupon(FEDc), 38

- Free-Edge Delamination, modified (mEDT), 38
- FRMM, *see* Fixed Ratio Mixed Mode
- gold, 56
- grinding, 52
- inlay, 49, 59
- integral, J-int., 27
- kerf, 53
- lap shear, 39
- LEFM, *see* fracture mechanics
- length
 - characteristic l., 21
 - reference l., 21, 25, 26
 - reference l. chosen, 81, 91
 - reference l. impact on G_c , 85, 89
- load angle, 22
- load lip, 42, 47, 58, 60
- load transfer, parasitic l.t., 48
- loss modulus, 75
- manufacturing, 45, 48
- MD, *see* molecular dynamics
- mEDT, *see* Free-Edge Delamination
- mesh, 70
- Microtester 5948, 36
- Mixed Mode Bending (MMB), 38, 39
- Mixed Mode Bending, modified (mMMB), 38
- Mixed Mode Flexure (MMF), 38
- MMB, *see* Mixed Mode Bending
- MMF, *see* Mixed Mode Flexure
- mMMB, *see* Mixed Mode Bending
- mode mix, 20, 22, 23
 - interfacial, **25**
 - virtual modes, 86, 91
- mold flow channels, 53
- molding
 - cavity, 51, 53
 - compound, 54
 - compression m., 48, 67
 - pressure, 51
 - temperature, 49, 51
 - transfer m., 48, 49
- molecular dynamics (MD), 16
- OLB, *see* Over-Leg Bending
- oscillation, 21
- oscillation zone, 26
 - size of o., 26
- oscillatory index, 21
- Over-Leg Bending (OLB), 38
- Peel Test, 38, 39
- physical aging, 66
- pick & place, 49
- pitch, 53
- plunger, 49
- PMC, *see* post mold cure
- Poisson's ratio, 76
- polytetrafluoroethylene (PTFE), 57
- post mold cure (PMC), 49, 51
- pre-crack, 16, 32, **54**, 56
 - by bending, 54
 - by gold, 56
 - by PTFE, 56
 - by release agent, 56
 - in CT specimens, 56
 - in interface specimens, 56
 - layer thickness, 56
- Pressure Volume Temperature measurements (PVT), 54
- PTFE, *see* polytetrafluoroethylene
- PVT, *see* Pressure Volume
- Q800, 36
- re-juvenation, 65, 66
- reference length, *see* length, 26
- residual stresses, 16, 23, 31, 47, 51, **79**
- roughness, 54
- SAM, *see* scanning acoustic microscopy
- Sandwich Strip Blister Specimens(SSBS), 38
- SBS, *see* Short Beam Shear
- scanning acoustic microscopy (SAM), 70
- SCB, *see* Side Clamped Beam
- sCCB, *see* Center Crack Beam
- Short Beam Shear (SBS), 38
- Side Clamped Beam (SCB), 38
- silicon, 53
 - s. oxide, 53
 - s. placement, 52
- Single Leg Bending (SLB), 38
- singularity, crack tip s., 20
- SLB, *see* Single Leg Bending
- specimens
 - demands on s., 45
 - design of the s., 45, 47, 59
 - dimensions of the s., 47
 - fabrication of s., 45
 - materials used in the s., 53
 - molding of s., 48
 - preparation of s., 48
- sprue, 49, 53
- SSBS, *see* Sandwich Strip Blister Specimens
- staining, crack tip s., 65, 66, 70
- storage modulus, 75
- stress intensity factor, 18
 - of classical type, 25
- TBSS, *see* Triangle Button Shear Specimen
- thermal expansion, *see* coefficient of t.e.
- Thermo Mechanical Analyzer (TMA), 54
- thermoset, 54
- TMA, *see* Thermo Mechanical Analyzer
- tolerance, t. in the MMC, 44
- Triangle Button Shear Specimen (TBSS), 38
- Variable Mixed Mode (vMM), 38
- VCCT, *see* virtual crack closure technique
- virtual crack closure technique (VCCT), 27
- virtual modes, 86, 91
- visco-elasticity, 75
 - impact on $G_c(\psi)$, 96
- vMM, *see* Variable Mixed Mode
- wafer, 53
- x-ray diffractometry, 80